APPLICATION OF HCRSV PROTEIN CAGE

FOR ANTICANCER DRUG DELIVERY

REN YUPENG

(B. Sc., CHINA PHARMACEUTICAL UNIVERSITY)

A THESIS SUBMITTED FOR THE DEGREE

OF DOCTOR OF PHILOSOPHY

DEPARTMENT OF PHARMACY
NATIONAL UNIVERSITY OF SINGAPORE

2007

ACKNOWLEDGEMENTS

I could never thank my supervisor, Associate Professor Lim Lee Yong, enough. When I was discouraged, hesitant and disappointed, she gave me guidance, encouragement and help. I thank her for her invaluable guidance, generosity, untiring counsel and enormous support.

Deep gratitude is also expressed to Professor Wong Sek Man. During my Ph.D project, Prof Wong had given me an enormous amount of help. I am very grateful for his instruction not only on scientific techniques but also on ways to solve problems.

Sincere appreciation is also due to A/P Go Mei Lin, A/P Ho Chi Lui, Ms. Ng Sek Eng, Ms Dyah Nanik Irawati, Ms Napsiah Bte Suyod, Mr Chong Ping Lee, and Madam Loy for their technical help and support.

I would like to thank the Department of Pharmacy, National University of Singapore for granting me the graduate scholarship that enabled me to pursue this study, and for providing the premises and equipment for me to conduct the experiments.

I would like to thank my friends, Lai Peng, Zeng Shuan, Mo Yun, Huang Min, Siok Lam, Han Yi, Wei Qiang, Wen Xia, Da Hai, Chun Xia, Keng Chuang, Chun Yin, Hai He, Xiao Xin, Luo Qiong, Shi Shu, and Wei Min for their friendship and discussion on life.

I am deeply indebted to my family. I thank my parents and sister for their love and encouragement when I faced difficulties. Special appreciation is due to my wife, Li Cheng. She has been a great source of support, providing a happy family life for me during my Ph.D study, and for standing with me during the many difficult periods.

Content

Summary

Certain icosahedral plant viruses are capable of undergoing capsid disassembly under specific chemical environments. Coat proteins (CP) isolated from the disassembled mix could be reassembled *in vitro* into uniformly sized and precisely structured virus-like protein cages (PC). The PC could be an attractive platform for drug delivery as its cavity could serve as a carrier of exogenous materials, while the amino acids in the CP could be chemically functionalized. To date, however, plant viruses have not been applied to the development of targeting anticancer drug delivery systems. The hypothesis for this project was that PC derived from the *Hibiscus Chlorotic Ringspot* virus (HCRSV) could be developed into a targeting anticancer drug delivery system. The HCRSV is a member of the genus *Carmovirus* in the *Tombusviridae* family of plant viruses. It is an icosahedral virus of 30 nm diameter, and has a 4 kb genomic RNA enclosed within a capsid of 180 CP subunits. The *in vitro* capsid disassembly and CP reassembly of HCRSV have not been evaluated. Neither has it been applied as a drug delivery platform.

HCRSV was successfully cultured in kenaf leaves under controlled environment and efficiently purified by serial centrifugation on sucrose gradients to give reproducible yields of 4 to 5 mg of purified HCRSV per 100 g of leaves. This method provided a stable source of HCRSV for subsequent experimentation. The HCRSV capsids were disassembled by incubation with 8 M of urea or by dialysis against a Tris buffer of pH 8 in the absence of Ca^{2+}. CP isolated from the disassembled mix showed much lower $OD_{260\ nm}/OD_{280\ nm}$ (about 0.6) than the native HCRSV (about 1.5), indicating a successful removal of the viral RNA. The purified CP was reassembled into empty PC by dialysis

against a sodium acetate buffer of pH 5 in the presence of Ca^{2+}. Circular dichroism analysis did not register any changes in the CP conformational structure following capsid disassembly and PC reassembly. Particle size measurement, together with transmission electron microscopy (TEM), showed the reassembled PC to be comparable in size and morphology to the native HCRSV. However, the dialysis method produced PC of more uniform size and better defined morphology than the urea incubation method, and was used to produce subsequent batches of PC.

The HCRSV-derived PC had the capacity to accommodate guest molecules in its cavity. Analysis by sucrose gradient ultracentrifugation and gel electrophoresis showed the loading efficiency to be dependent on electrostatic interactions between the PC and the cargo. The positively charged Arg and Lys moieties located at the N-terminal of the CP could have made the inner cavity of the PC attractive for the binding of negatively charged compounds, as demonstrated by the successful loading of polystyrenesulfonic acid (PSA) and polyacrylic acid (PAA). In contrast, neutral FITC-dextran molecules with mw ranging from 4 to 150 kDa could not be encapsulated. Even with the polyacids, only samples with mw no less than 13 kDa were successfully encapsulated. The failure to load PSA below the threshold mw has been attributed to the rapid leaching of these molecules through the surface cavities of the PC upon dilution. Cargo loading had to be initiated with PC reassembly, as the preformed PC could not be used for the loading of the polyacids. PSA (≥13 kDa)- and PAA-loaded PC, despite differences in the mw and acid type of their cargoes, were comparable in size, morphology and protein conformation to each other and to the native HCRSV with its RNA load.

To impart a capability to target cancer tissues that over-express the folic acid receptor, the native HCRSV was conjugated with folic acid by a 2-step carbodiimide method. The conjugated folic acid did not affect the disassembly of the HCRSV, nor the subsequent reassembly of the folic acid-conjugated CP into fPC. Folic acid conjugation efficiency was 1.9%, which translated to about 360 folic acid molecules per fPC. The PSA- and PAA-loaded fPC were comparable in size, morphology and conformational structure to the corresponding polyacid-loaded PC without folic acid conjugation.

Doxorubicin, the model anticancer drug used for the project, did not satisfy the twin requisites of possessing a negative charge and mw above the specified threshold, for loading into the PC. To overcome these barriers, a novel method named "polyacid association" was established. This method involved the simultaneous encapsulation of doxorubicin with PSA (200 kDa), the PSA aiding in the retention of doxorubicin within the PC and fPC through the formation of a semi-stable complex by electrostatic interactions. The resultant systems, denoted as PC-Dox and fPC-Dox, were homogenously sized and shaped, and were similar in morphology and size to the native HCRSV. Drug encapsulation efficiency for both samples was within the acceptable range of 49 – 59%, with each PC containing about 900 entrapped doxorubicin molecules. The encapsulated drug in PC-Dox and fPC-Dox was readily released upon dilution, with both samples exhibiting a sustained drug release profile at simulated physiological condition. About 40% of the drug load was released within the initial 4 h, followed by a slower release of the remaining drug load from the PC over the next 20 h.

The efficacy of PC-Dox and fPC-Dox was evaluated *in vitro* using representative cell culture models. The cancer cell models were OVCAR-3 (human ovarian epithelial

adenocarcinoma) and CNE-1 (human nasopharyngeal carcinoma), while CCL-186 (human diploid fibroblast) was used as a normal cell model. Folic acid uptake data confirmed the over-expression of folic acid receptors in OVCAR-3 and CNE-1 cells cultured in folic acid-deficient RPMI-1640 medium. CCL-186 cells did not over-express the folic acid receptor when cultured with the normal RPMI-1640 medium. MTT assay data suggested that the HCRSV and PSA at concentrations equivalent to those applied in the PC-Dox and fPC-Dox formulations were non-cytotoxic towards the 3 cell lines.

Data obtained from fluorescence spectroscopy, confocal microscopy and flow cytometry were in agreement that the fPC-Dox could effectively enhance doxorubicin uptake in the OVCAR-3 and CNE-1 cells. The enhanced drug uptake was correlated with higher cytotoxicity as evaluated by the MTT assay. In comparison, the cancer cell uptake of PC-Dox was 2- to 3-fold lower. Cellular uptake and cytotoxicity of PC-Dox were comparable to doxorubicin in solution, suggesting that doxorubicin encapsulation within the PC could not by itself increase drug efficacy in the cancer cell models. This is reasonable considering the current lack of evidence to support the cytoinvasive and cytotoxicity properties of plant viruses, including the HCRSV, in animal cells. PC-Dox could, however, be useful in clinical applications where sustained drug release and/or protection against cytotoxic drugs are desired. The enhanced uptake of fPC-Dox in the OVCAR-3 and CNE-1 cells was inhibited by excess co-administratered folic acid, supporting the role of the folic acid receptor in mediating its uptake. It also accounted for the failure of fPC-Dox to show enhanced uptake in the folic acid receptor-deficient CCL-186 cells. This selectivity of action suggests that the fPC-Dox has the potential to be

applied as a targeting platform for anticancer drug delivery, and that it should be further evaluated to realize this potential.

List of Tables

Dox with 1 mM folic acid (IV). Analysis by one-way ANOVA indicated that the $IC50_{doxorubicin}$ of fPC-Dox was significantly lower than those of the other formulations for the OVCAR-3 and CNE-1 cells. PC-Dox and fPC-Dox did not decrease the $IC50_{doxorubicin}$ compared with free doxorubicin in the CCL-186 cells. (* $P < 0.05$ compared with other formulations, $n = 3$)

List of figures

List of Abbreviations

AAV	Adeno-associated virus
Ad	Adenoviruses
AIDS	Acquired Immunodeficiency Syndrome
ATCC	American Type Culture Collection
AUC	area under the plasma concentration-time curve
BCA	bicinchoninic acid
CarMV	Carnation mottle virus
CCMV	Cowpea chlorotic mottle virus
CD	circular dichroism
CP	coat protein
CPMV	Cowpea mosaic virus
CSLM	confocal scanning laser microscopy
DMSO	dimethylsulfoxide
DTT	dithiothreitol
EBV	Epstein-Barr virus
EDAC	(1-ethyl-3-[3-dimethylaminopropyl] carbodiimide hydrochloride)
EDTA	ethylenediaminetetraacetic acid
ELISA	enzyme-linked immunosorbent assay
FBS	fetal bovine serum
FD	FITC-dextran
FIV	feline immunodeficiency virus
fPC- PSA	fPC loaded with polystyrenesulfonic acid
fPC	folic acid-conjugated protein coat
fPC-Dox	folic acid-conjugated protein coat loaded with doxorubicin
fPC-PAA	fPC loaded with polyacrylic acid
FR	folic acid receptor
gRNA	genomic RNA
HCRSV	Hibiscus chlorotic ringspot virus
HER2	human epidermal growth factor receptor 2
HIV	Human immunodeficiency virus
HIV-1	Human immunodeficiency virus type 1
HPV	Human papilloma virus
MTT	3-(4,5-dimethylthiazol-2-yl)-2,5-diphenyltertrazolium bromide
MV	measles virus
mw	molecule weight
NHS	N-hydroxysuccinimide
NPC	Nasopharyngeal carcinoma
ORF	open reading frames
PAA	polyacrylic acid

PAHs	polyaromatic hydrocarbons
PBS	phosphate buffered saline
PC	protein cage
PC-Dox	doxorubicin-loaded protein cage
PC-FD	protein cages loaded with FD
PC-PAA	protein cages loaded with PAA
PC-PSA	protein cages loaded with PSA
PCS	photon correlation spectroscopy
PEG	polyethylene glycol
PMSF	phenyl methanesulfonyl fluoride
PSA	polystyrenesulfonic acid
PSMA	prostate-specific membrane antigen
PTA	phosphotungstic acid
RES	reticuloendothelial system
RES	reticuloendothelial system
SARS-CoV	SARS-associated coronavirus
SDS	sodium lauryl sulfate
sgRNA	subgenomic RNA
SIV	simian immunodeficiency virus
SUV	small unilamellar vesicles
TCV	Turnip crinkle virus
TEM	transmission electron microscope
TMV	Tobacco mosaic virus
TPP	tripolyphosphate acid
Trp	tryptophan
Tyr	tyrosine
VLP	virus-like particles
WGA	wheat germ agglutinin
WHO	World Health Organization

List of publications and conference presentations

Ren Y, Wong SM, Lim LY. Folic acid-conjugated protein cages of a plant virus: a novel delivery platform for doxorubicin. *Bioconjugate Chemistry*. 2007; Apr 4; [Epub ahead of print]

Ren Y, Wong SM, Lim LY. In vitro reassembled plant virus-like particles for loading of polyacids. *Journal of General Virology*. 2006; 87:2749-54

Ren Y, Wong SM, Lim LY. *In vitro* reassembled virus-like particles for drug delivery. American Association of Pharmaceutical Scientists Annual Meeting**,** 6-10 November 2005, Nashville, USA

Ren Y, Wong SM, Lim LY. Producing of empty HCRSV-like particle - a potential platforms for drug delivery. Japan-Singapore Symposium on Nanoscience and Nanotechnology, 1-4 November 2004, National University of Singapore, Singapore

Ren Y, Wong SM, Lim LY. Hibiscus Chlorotic Ringspot Virus for drug delivery: cytotoxicity and cytoinvasive evaluation. *Pharmaceutical Sciences World Congress* 2004, 29 May – 3 June 2004, Kyoto, Japan.

Chapter 1

Introduction

1.1 Cancer

1.1.1 Introduction

Cancer, also termed as malignant tumor or neoplasm, includes more than 100 diseases. The defining characteristic of cancer is the presence of abnormal cells that multiply very rapidly, growing beyond their usual boundaries to invade adjoining tissues and spreading to other organs. The latter process, which is referred to as metastasis, is usually the cause of death in cancer patients.

Cancer has surpassed heart disease as the leading cause of death in the world [Jemal et al., 2006]. In 2005, 7.6 million people died of cancer, accounting for 13% of the total global death. About 22 million people worldwide are cancer patients, and an alarming 10 million people are added to this number yearly from both developing and developed countries. According to the World Health Organization (WHO), worldwide cancer rates are set to increase by as much as 50% by the year 2020 unless further preventative measures are put into practice [http://www.who.int/cancer/en/, date of access: 06/11/2006]. WHO estimates cancer will claim 9 million lives in 2015 and 11.4 million in 2030 [http://www.who.int/mediacentre/factsheets/fs297/en/index.html, date of access: 06/11/2006].

1.1.2 Treatment

Common modalities for treating cancer include surgery, radiotherapy and chemotherapy. Often, a combination of therapies is required to optimize outcome. For

example, radiation therapy or chemotherapy may be performed before, during or after surgical excision of the cancer tissue. The main objectives of cancer treatment are to rid the body of tumor cells and prevent their spread to other tissues, as well as to prolong and improve the quality of life for the patient. Some cancers, such as breast cancer, cervical cancer and colorectal cancer, have good prognosis if diagnosed in the early stages.

Unlike surgery and radiotherapy, which are used only to treat localized cancer, chemotherapy can be applied to cancers that have spread to other tissues or organs. Cancer chemotherapy employs chemicals that target rapidly dividing cells, and it has the advantage of reaching cancer cells that are inaccessible by surgery or radiotherapy. For these reasons, chemotherapy is especially suited for the treatment of advanced cancer [Bonetti et al., 2006; Vergnenegre et al., 2005].

Cancer chemotherapeutic agents can be divided into different groups based on their mechanisms of action. Alkylating agents, e.g. chlorambucil [Torabian et al., 2006] and hexamethylmelamine [Keldsen et al., 2003], prevent cell replication by bonding with the electronegative DNA [Walters, 2006; Lawley, 1995]. Antimetabolites, such as the antifolates [Bajetta et al., 2003], purine analogs [Fazzi et al., 2003] and pyrimidine analogs [Temmink et al., 2006], are structurally related to endogenous compounds, and they work by competing for specific enzymes that participate in nucleic acid production. A more selective anticancer agent is the monoclonal antibody, designed to bind with a membrane protein that is overexpressed in cancer cells. An example is trastuzumab, which targets the extracellular domain of the human epidermal growth factor receptor 2 (HER2), a tyrosine kinase that regulates cell growth and is overexpressed in many cancer

cells, including breast cancer cells [Vogel et al., 2002], gastric cancer cells [Fujimoto-Ouchi et al., 2006] and uterine papillary serous cancer cells [Villella et al., 2006]. The antitumor activity of trastuzumab arises from its ability to diminish cell receptor signaling [Baselga et al., 2001], cause the G1 arrest of cell proliferation [Lane et al., 2001], induce apoptosis [Chang et al., 2003], and/or provoke an immune response [Cooley et al., 1999]. Cytotoxic antibiotics, on the other hand, prevent cell reproduction by blocking the synthesis and repair of DNA or RNA [Swift et al., 2006]. They are amongst the most widely prescribed anticancer agents, examples of which include doxorubicin, mitoxantrone and bleomycin [Muggia and Green, 1991]. Doxorubicin is used as the model anticancer agent in this project.

Doxorubicin (Figure 1-1) is indicated for the treatment of breast cancer [Wong e al., 2006], soft tissue sarcoma [Di Filippo et al., 2003] and ovarian cancer [Cunningham et al., 1994]. It interferes with cell reproduction in several ways. Firstly, doxorubicin blocks DNA synthesis by direct binding, via intercalation between base pairs on the DNA helix [Capranico et al., 1986]. Secondly, it inhibits DNA repair by inactivating topoisomerase II [Burden and Osheroff, 1998]. Thirdly, doxorubicin generates .OH radicals that cleave the doxorubicin-nucleic acid complex, leading to cell death [Feinstein et al., 1993]. Like most cancer chemotherapeutic agents, doxorubicin is highly potent, yet non-selective in its action. In targeting rapidly dividing cells, it destroys not only cancer cells but also normal cells with high turnover rates, such as those in the bone marrow, skin, hair follicles, oral and gastrointestinal mucosae. Consequently, treatment with doxorubicin is associated with many serious adverse effects, including a suppressed immune system, severe nausea and vomiting, diarrhea or constipation, hair loss, sore mouth, ulcers and

poor sense of taste [Burish and Tope, 1992; Wujcik, 1992]. As the adverse effects of doxorubicin are believed to be alleviated by delivering the drug specifically to the cancer cells, doxorubicin is often employed as a model drug in the development of targeting drug delivery platforms [Kalra and Campbell, 2006; Sun et al., 2006; Nasongkla et al., 2006].

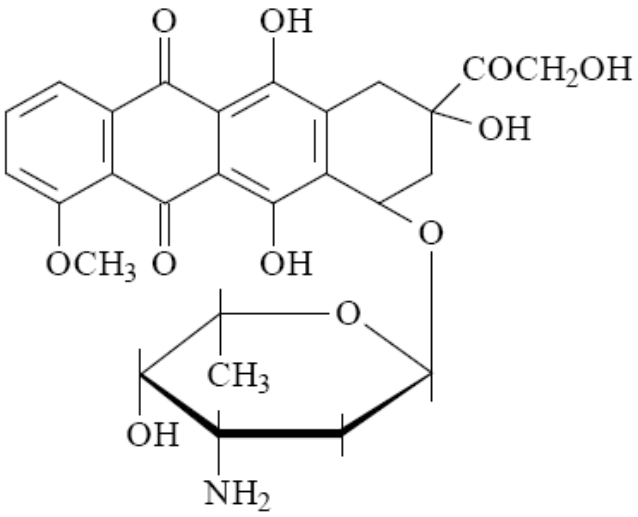

Figure 1-1 Chemical structure of doxorubicin.

1.2 Targeted drug delivery systems

1.2.1 Rationale

Most therapeutic drugs provide little, if any, targeting specificity. Yet, for drugs with a narrow therapeutic window, such as the highly cytotoxic anticancer agents, targeted delivery has the potential to significantly improve clinical outcome. A drug that is

delivered specifically to its therapeutic site would have enhanced uptake and absorption by the target tissue and reduced adverse effects from inappropriate disposition at other sites [Xu et al., 2006; O'Brien et al., 2004]. Proof of concept has been illustrated in a phase III clinical trial of a liposomal formulation of doxorubicin, which passively targets the drug to the cancer cells and significantly reduces its cardiotoxic effects [O'Brien et al., 2004]**.** Targeted delivery systems have also been designed to resolve problems associated with the physicochemical properties of the drug, for example, by improving drug stability against degradation [Kleemann et al., 2005] or increasing drug aqueous solubility [Mo and Lim, 2005].

1.2.2 Targeting strategies

Drugs may be delivered to a specified tissue by passive targeting and/or active targeting. Passive targeting relies on the natural distribution pattern of the drug or delivery system. When applied to cancer chemotherapy, drug uptake and accumulation by tumor cells are dependent on factors such as increased permeability of intratumoral vessels aided by lack of lymphatic drainage in tumor tissues [Dvorak et al., 1988], electrostatic interactions between the drug carrier and plasma membrane [Kohler et al., 2006], and phagocytosis of the drug carrier by the immune system [Falo et al., 1995]. Active targeting, on the other hand, is more selective as it is designed specifically to detect molecules unique to cancer cells.

A wide variety of ligands has been explored for the active targeting of cancer chemotherapeutic agents. A novel strategy exploits the advantage of aptamers, which are

short, synthetic, single-stranded DNA or RNA molecules that bind with high affinity to specific proteins [Chu et al., 2006; Bagalkot et al., 2006]. An example is the conjugation of doxorubicin with 2'-fluoropyrimidine RNA aptamer to target prostate cancer cells that overexpress the prostate-specific membrane antigen [Bagalkot et al., 2006]. Conjugation with a monoclonal antibody may also enhance the targeting efficiency of a delivery system. Immunoliposomes of doxorubicin, constructed using the Fab' fragment from the humanized anti-EGFR monoclonal antibodies, have been shown to exhibit significantly higher cytotoxicity towards the EGFR-overexpressing colorectal cancer cells compared to conventional liposomal doxorubicin [Mamot et al., 2006].

Small molecules have also been used as ligands for targeting drug delivery systems to cancer cells. A well-known example is folic acid (Figure 1-2). Folic acid is a vitamin essential for the synthesis of adenine and thymine, two nucleic acids that make up genomic materials. Folic acid is also necessary for the metabolism of the essential amino acid, methionine [Stanger, 2002]. Cellular uptake of folic acid is by the transmembrane folic acid receptor (FR), which consists of three well-characterized isoforms (α, β and γ), with 70–80% similarity in amino acid identity [Shen et al., 1994]. The affinity factors for FR α, β and γ are 0.1, 1 and 0.4 nM, respectively [Kamen and Caston, 1986; Costa and Rothenberg, 1996; Shen et al., 1995].

The principle for using folic acid as a cancer-targeting ligand is based on the differential expression of FR on normal and cancer cells. Although certain normal cells, such as the renal tubular cells, express a significant level of FR [Weitman et al., 1992], most normal epithelia express low levels of FR. In contrast, FR expression is greatly

elevated in malignant cancer cells of epithelial origin, such as cancer cells of the ovary, uterus, endometrium, brain, kidney, head and neck, and mesothelium [Toffoli et al., 1997; Ross et al., 1994]. The upregulated FR expression in malignant cells could approach two orders of magnitude compared to normal cells in the same tissue (Figure 1-3) [Ross et al., 1994; Lu and Low, 2002]. FR expression has been shown to increase with the stage of cancers [Toffoli et al., 1997], and is correlated with a stronger resistance to chemotherapy [Toffoli et al., 1998]. Thus, folate-targeted therapeutics can be a potential remedy for advanced cancers that are resistant to standard chemotherapy. Targeting is also possible because of the differential distribution of FR in normal and cancer cells. FR on normal epithelial cells is located on the apical (externally-facing) membrane, which limits its access from the serosal side. Thus, FR in the renal tubular cells, which aid in the re-absorption of folates from urine, are located in the luminal membrane [Weitman et al., 1992], while FR in the blood brain barrier are concentrated on the membrane facing the brain tissue and function to retain the vitamin within the cerebrospinal fluid [Patrick et al., 1997]. By comparison, FR distribution in malignant epithelial cells is not limited to the apical membrane because of the lack of polarization of these cells. Consequently, cancer cells with overexpressed FR are susceptible to folic acid-conjugated drug delivery systems circulating in the blood [Toffoli et al., 1997; Ross et al., 1994] while normal tissues with elevated FR expression are not [Weitman et al., 1992; Patrick et al., 1997; Lu and Low, 2002]. Proof of concept of the folic acid-mediated targeting systems has been obtained with the delivery of drugs and liposomes to a variety of cancer cells [Leamon and Low, 1991; Drummond et al., 2000].

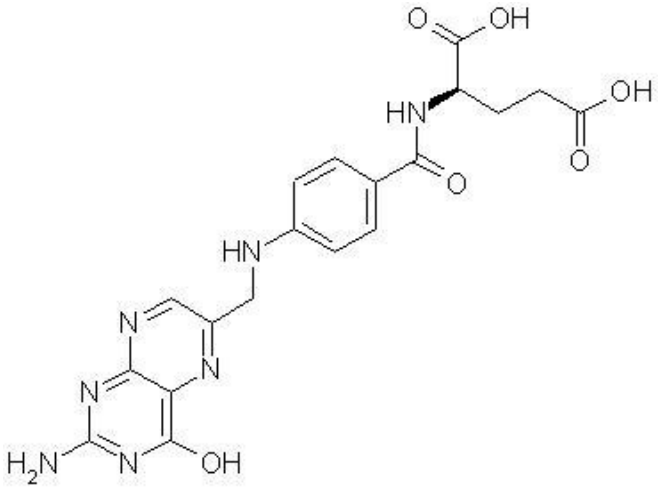

Figure 1-2. Chemical structure of folic acid

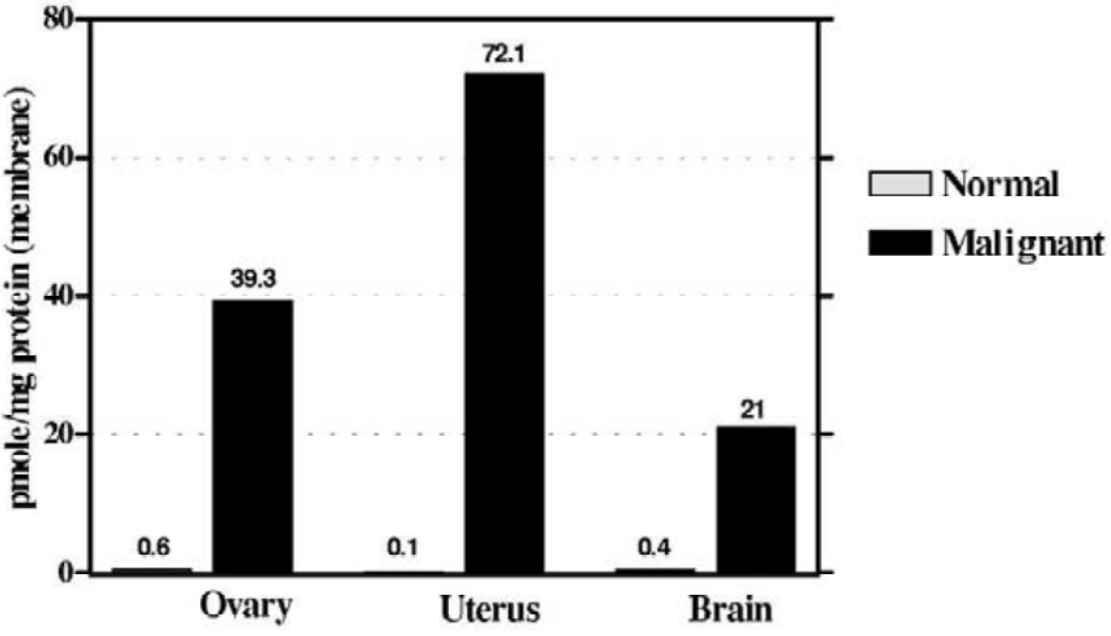

Figure 1-3 Comparison of the FR expression between normal and malignant human tissues [Ross et al., 1994].

1.3 Nanoscale drug delivery systems

1.3.1 Rationale

Nanoscale systems can be defined as colloidal structures in the size range of 10 to 1000 nm [Quintanar-Guerrero et al., 1998]. Most nanoscale drug delivery systems are prepared from macromolecular materials called carrier molecules, and the drug cargo is dissolved, entrapped, adsorbed, dispersed or covalently linked to the carrier molecules [Zamboni, 2005; Jain, 2005]

Nanoscale drug delivery systems have many advantages over conventional pharmaceutical dosage forms. Drugs have been incorporated into polymer nanoparticles to overcome intractable solubility e.g. the loading of paclitaxel in PLGA nanoparticles allowed the poorly water-soluble drug to be administered in an aqueous medium [Mo and Lim, 2005]. Peptide drugs encapsulated in nanoscale systems may exhibit stronger resistance to chemical and enzymatic degradation [Ma et al., 2005], resulting in prolonged action [Luo et al., 2006]. The delivery of 5-aminolevulinic acid (ALA) via liposomes smaller than 63.5 nm was statistically ($p < 0.05$) more efficient than the administration of ALA alone [Kosobe et al., 2005]. Nanoscale delivery systems may also be designed to provide a specific controlled drug release profile [Allen et al., 2006; Ishida et al., 2006], or to direct a drug to specific tissues [Hattori and Maitani, 2005]. Many of these benefits are also seen in microscale drug delivery systems; however, the reduction of the delivery system to the nanoscale can be helpful in promoting its circulation half-life, targeting capacity and cellular uptake rate. When injected subcutaneously into mice, PEG-distearoylphosphatidylethanolamine liposomes with diameter of 80 to 90 nm were

found to translocate with ease from the site of injection into the bloodstream while similar but larger vesicles (656 nm) remained at the site of injection [Allen, 1993]. Liposomes with diameter of 400 nm were 3 times more efficient than those of 1200 nm diameter in targeting the bone marrow in the mongrel dog model [Schettini et al., 2006]. Another study showed gold nanoparticles with diameter in the range of 14 to 100 nm to be the most efficiently taken up by the HeLa cells, with nanoparticles of 50 nm diameter having the highest uptake rate [Chithrani et al., 2006].

1.3.2 Classification

Nanoscale drug delivery systems may be classified into several major categories. As it is not practical to describe all the categories in this thesis, only 3 major systems, namely the micelles, liposomes and polymer nanoparticles are described. Micellar systems, which are prepared by self-assembly of amphiphilic block copolymers in aqueous media [Liu et al., 2006; Wei et al., 2006], present with a hydrophobic core that can accommodate drugs at concentrations exceeding their solubility in water. Surrounding the core are the hydrophilic regions of the polymers, which form hydrogen bonds with water and serve to protect the encapsulated drug from hydrolysis and enzymatic degradation. The hydrophilic palisade also enables the micelles to evade recognition by the reticuloendothelial system (RES), thereby prolonging their circulation time. Micellar systems are highly versatile, as the chemical composition, molecular weight (mw) and block length ratios of the copolymers can readily be changed to control the size, morphology and functionality of the micelles. An example of a micellar system

is NK105, a formulation produced with polyethylene glycol (PEG) as the hydrophilic segment and modified polyaspartate as the hydrophobic segment. The area under the plasma concentration-time curve (AUC) of paclitaxel incorporated into NK105 was 90-fold higher than free paclitaxel when administered by subcutaneous injection into nude mice implanted with the human colonic cancer cell line, HT-29 [Hamaguchi et al., 2005]. Besides anticancer drugs, inorganic materials, such as superparamagnetic iron oxide for MRI imaging, have also been loaded into micelles [Nasongkla et al., 2006] for targeted delivery to tumor endothelial cells.

Liposomes are vesicles consisting of one or more lipid bilayers with aqueous cores. Lipids, such as phospholipids [Ickenstein, et al., 2006] or cholesterol [Lee et al., 2005], were used to construct the hydrophobic membrane of liposomes. Drugs can be encapsulated within the liposomal core [Chen et al., 2004], although amphiphilic or lipophilic molecules e.g. gold nanoparticles [Park et al., 2006] and anthrax protective antigens [Sloat and Cui, 2006], are incorporated within the phospholipid bilayers. Drugs encapsulated in liposomes can be protected from chemical and enzymatic degradation. A highly successful formulation is that of doxorubicin encapsulated within PEGylated liposomes. Developed by Johnson & Johnson, this formulation has been approved by the U.S.A Food Drug Administration (FDA) in 2005 for the treatment of ovarian cancer. Doxorubicin is encapsulated within the aqueous core of the liposomes via a salt gradient [Lasic et al., 1992] and the conjugated PEG reduces liposomal uptake by the RES [Gabizon et al., 1993]. The resultant system improves clinical outcome by increasing the tumor uptake of doxorubicin while at the same time reducing its cardiotoxicity [Papahadjopoulos et al., 1991].

Solid polymeric nanoparticles in the size range of 10 to 400 nm have also been widely synthesized for biomedical applications. Nanoparticles produced from biodegradable polymers, e. g. chitosan [Huang et al., 2005] and poly(lactide-co-glycolide) [Mo and Lim, 2005], are particularly popular for drug delivery. Polymer nanoparticles have been applied to deliver both large molecules, e.g. peptide [Ma et al., 2002] and gene [Huang et al., 2005], and small molecules, e.g. anticancer agents [Bertin et al., 2005; Mo and Lim, 2005], to a target organ. Polymer nanoparticles can be formulated using one or a combination of a wide variety of biocompatible polymers, and further functionalized after preparation by chemical manipulation. When conjugated with a targeting ligand, e.g. a small molecule such as folic acid [Kim et al., 2005] or a macromolecule, such as wheat germ agglutinin (WGA) [Mo and Lim, 2005], polymer nanoparticles could direct the drug cargo to specific tumor sites. PEGylation, on the other hand, enables the polymer nanoparticles to evade clearance by the RES, thereby prolonging their circulation half-life and increasing drug bioavailability [Craparo et al., 2006].

1.4 Virus-based drug delivery systems

1.4.1 General properties of viruses

Viruses straddle between living and non-living materials. They are omnipresent and can be found residing in all living species, including plants, animals, bacteria and fungi. Viruses may be considered to be mere assembles of macromolecules that are as alive as a rock, yet they can rapidly multiply and infect increasing number of cells upon contact

with the right host. To reproduce, viruses release their genomic materials into the host cell, either by fusing their coat protein with the host cell membrane [Henderson and Hope, 2006], or by direct injection, leaving the empty viral protein shell outside the host cell [Jiang et al., 2006]. New viral genomic materials and proteins are subsequently synthesized with the aid of the host enzymes, assembled into infective viral particles, called virions, and released to infect other cells. Viruses tend to infect only their natural host species, although cross-species transfer is not uncommon. In recent years, certain animal viruses, such as the hantavirus [Deutz et al., 2003] and SARS-associated coronavirus [Peiris et al., 2003], have crossed species to cause new diseases in human [Louz et al., 2005]. Plant viruses, however, are generally not equipped to infect animal cells although they may be capable of infecting a number of related plants.

1.4.2 Virus Structure

1.4.2.1 Components

Viruses are generally composed of genomic materials enclosed within a protein shell known as the capsid [Johnson and Speir, 1997]. Viruses may be grouped into DNA viruses (e.g. hypovirus, atadenovirus) or RNA viruses (e.g. influenzavirus and carmovirus) depending on the type of genomic materials they carry. Most viruses have their genomic information encoded in a single stranded RNA. Positive-stranded viruses, e.g. Hibiscus latent Singapore virus, Broad bean mottle virus and Cowpea chlorotic mottle virus, use the RNA as a messenger RNA for direct synthesis of viral proteins (translation) [Dzianott

and Bujarski, 1991], while negative-stranded viruses, such as the simian virus, have genomes which are complementary to the mRNA and carry RNA polymerase to synthesize the mRNA [Arimilli et al., 2006]. The protein cage (PC) of virus, also named capsid, which protects the nucleic acid from enzyme digestion and aids in viral penetration of host cell, is made up of repeating copies of structural units known as coat proteins [Crick and Watson, 1956]. The capsid, together with the enclosed genomic materials, is called the nucleocapsid, which is equivalent to the virion for many plant viruses**.** Most animal viruses, e.g. the human immunodeficiency virus [Zhu et al., 2006], also have an envelope structure surrounding the capsid [Szakonyi et al., 2006]. The envelope of phospholipids and glycoprotein further protects the virus from chemical and enzymatic degradation. Plant viruses, on the other hand, do not often possess an envelope structure [Ke et al., 2004].

1.4.2.2 Architecture

There are predominantly two kinds of shape found amongst viruses: rods and spheres [Klug and Caspar, 1960; Johnson and Speir, 1997]. The Tobacco mosaic virus (TMV) is an example of a rod-shaped virus (Figure 1-4). Viewed under a transmission electron microscope (TEM), the TMV presents with a straight rod protein shell that has a length of about 300nm [Choi and Rao, 2000]. The rod-like capsid comprises of protein subunits arranged in a helix model [Klug and Caspar, 1960].

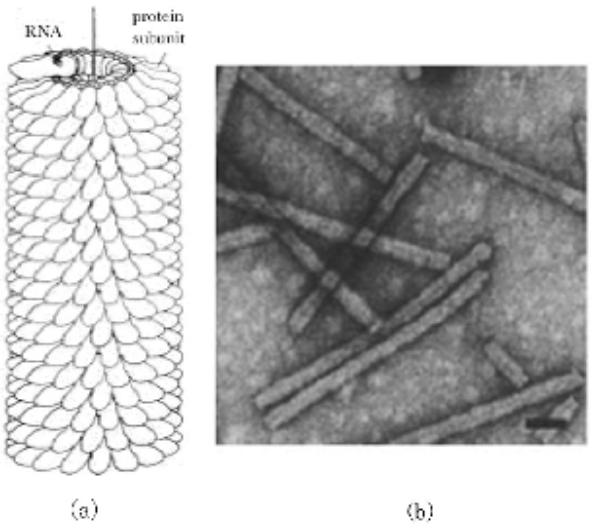

Figure 1-4. The rod shape of Tobacco mosaic virus . (a) Schematic structure showing the arrangement of helical protein subunits in the capsid [Klug and Caspar, 1960]. (b) TEM micrograph of TMV. Bar = 50 nm [Choi and Rao, 2000].

Most plant and animal viruses, however, appear as spherical particles under an electron microscope. The spherical structure is actually an icosahedron, also known as a cubic symmetrical polygon [Crick and Watson, 1956]. Examples of icosahedral viruses are the *Human immunodeficiency virus* (HIV) [Fuller et al., 1997], *Cowpea chlorotic mottle virus* (CCMV) [Speir et al., 1995], *Cowpea mosaic virus* (CPMV) [Chatterji et al., 2002] and *Hibiscus chlorotic ringspot virus* (HCRSV) [Doan et al., 2003]**.** An icosahedron is a highly symmetrical structure with 12 vertices and 20 facets, each facet being an equilateral triangle (Figure 1-5, a). As shown in Figure 1-5 b, the edges of the triangles have 2-fold axes of symmetry and there are fifteen of such axes in each icosahedron. In addition, there are ten 3-fold axes of symmetry extending through each facet, and six 5-fold axes of symmetry passing through the vertices of the triangles. The

template shown in Figure 1-5 c provides the construction blueprint of an icosahedron. Besides hexamers (6 equilateral triangles), the incorporation of pentamers (5 equilateral triangles) is necessary, for the convex pentamers introduced curvature into an array of hexamers, which would otherwise form a flat or planar sheet. Twelve pentamers are required to form the icosahedron structure. Viruses adopt the icosahedral symmetry because the quasi-equivalent structure appears to be an economical way to evolve into larger volume [Harrison, 2001]. It has been shown that the construction of 20 subunits of triangles into an icosahedron is an optimal method for producing a shell of equivalently bonded identical structures with minimum free energy [Crick and Watson, 1956].

However, it is difficult to maintain the integrity of an icosahedron structure made up with only 20 subunits. Even an icosahedral structure with 60 coat proteins is not common amongst viruses, a rare example being phi X174 [Leodevico et al., 1994]. Most viruses have complex icosahedral structures comprising more than 60 subunits [Olson et al., 1992]. The number of subunits in an icosahedral viral capsid is calculated in multiples of 60, the multiple being designated as the triangulation or T number. The T value is calculated using the flat template (Figure 1-5 d), and the value is deduced from the distance between the hexamers, or pentamers when folded to the icosahedron. T values of 1, 3, 4, 7, 9, 12 or higher have been obtained. T=1 gives the simplest icosahedral structure that is made up of 60 subunits and in which the pentamers are located side by side. Most viral structures have T=3 or 180 subunits, the final assembly of which resembles a football (Figure 1-5 e) [Speir et al., 1995; Chatterji et al., 2002; Doan et al., 2003].

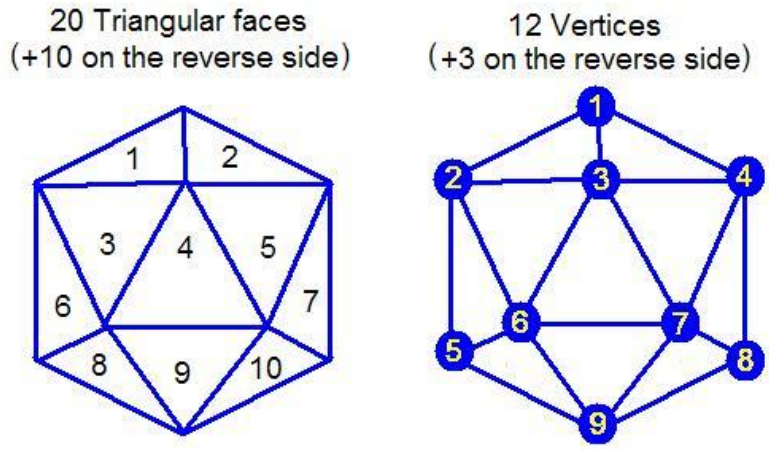

(a)

Related by 2-fold, 3-fold and 5-fold axes of symmetry

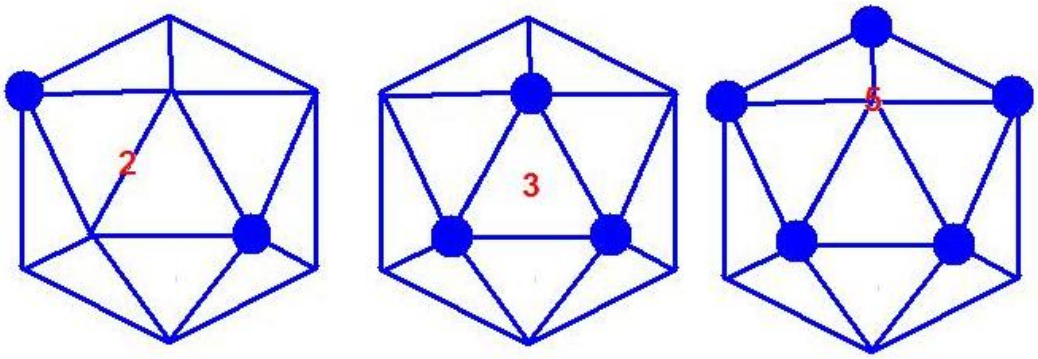

(b)

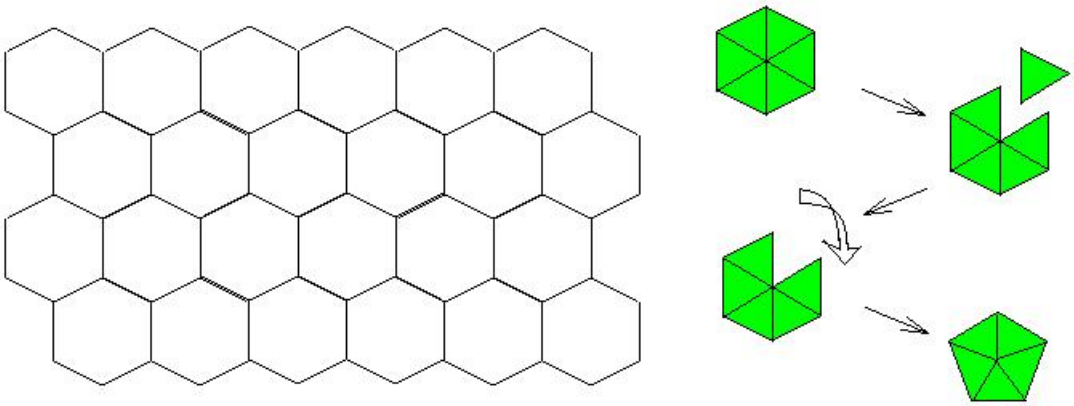

(c)

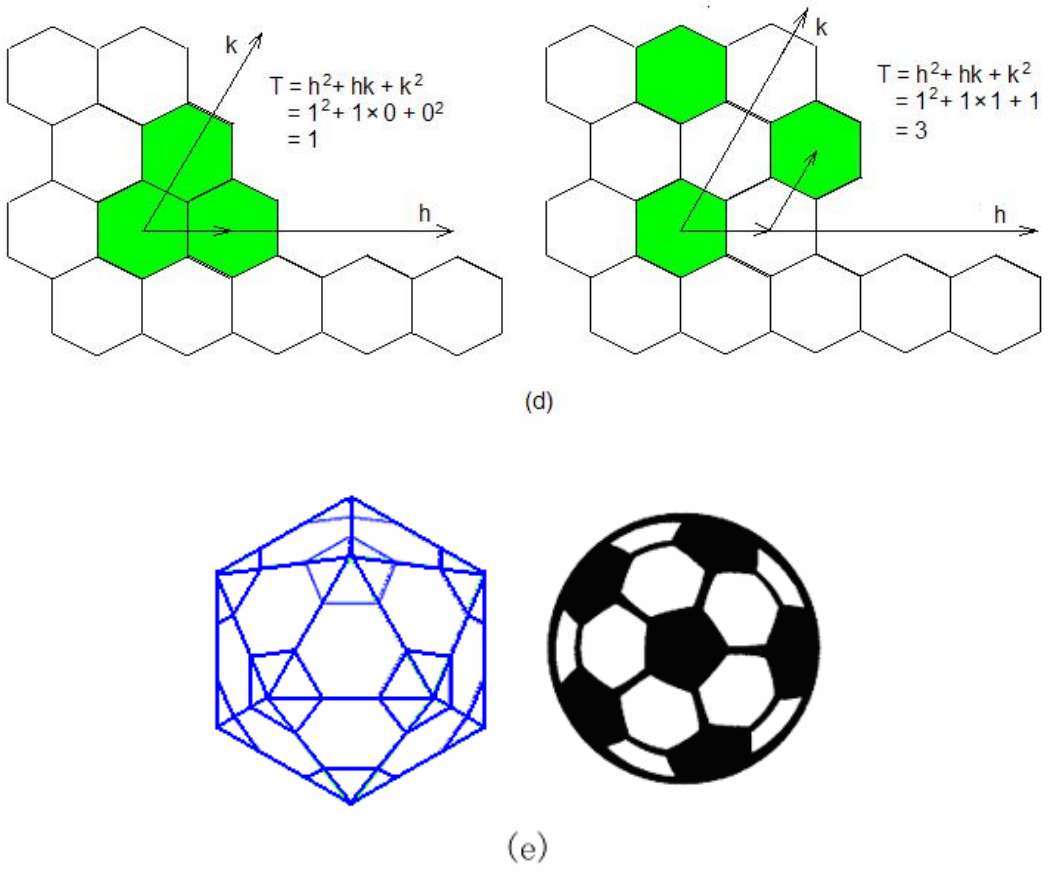

Figure 1-5. Structure of an icosahedron virus. (a) The 20 facets and 12 vertices. (b) The 2-fold, 3-fold and 5-fold axes of symmetry. (c) Introduction of pentamers induces curvature in a planar sheet of hexamers that allow for the formation of an icosahedron. (d) Calculation of T value for the icosahedral structures. To form icosahedral structure, the green color hexamers shall be replaced by pentamers. (e) Schematic representation of an icosahedral structure with T = 3.

The CCMV and CPMV are well-characterized examples of icosahedral viruses with T value of 3 and a protein cage of diameter 28 nm comprising of 180 units of coat protein. The icosahedral virus is stable enough to maintain its integrity even under harsh

conditions, e.g. at pH values ranging from 3.5 to 9 for 1 h [Wang et al., 2002] or when subjected to chemical modifications, such as PEG conjugation [Raja et al., 2003]. However, a high pH (>7.0) and low ionic strength (I = 0.1) may result in swelling of the virus, causing 2 nm-openings along the 3-fold axes of symmetry [Fox et al., 1998]. The assembly of the coat proteins of CCMV into the stable icosahedral structure does not require a host cell, and has been shown to occur *in vitro* in the presence of divalent cations or low pH [Fox et al., 1998; Douglas and Young, 1998]. These properties render the CCMV to be an interesting nanoscale platform to explore for drug delivery [Douglas and Young, 2006].

1.4.3 Pharmaceutical applications

The majority of viruses are uniform nanoscale assembly of biomacromolecules [Crick and Watson, 1956]. This monodispersity in size, coupled with their cytoinvasive capability and the potential to manipulate viruses into carrying a cargo other than their natural genomic materials, have made viral particles highly attractive vectors for gene delivery. For example, the transfection efficiency of pHCMV-β-galactosidase plasmids was at least 4-fold higher when delivered by the Herpes simplex virus than by liposomes [Rouse et al., 2000].

Animal viruses have been widely studied as vectors for gene delivery as their inherent cytoinvasive property offers a distinct advantage over non-viral nanoscale gene delivery platforms [Zhang and Godbey, 2006]. Gene delivery by animal viral vectors, such as the

Adeno-associated viruses (AAV), Adenoviruses (Ad) and Retroviruses, has been well documented. The AAV has the advantages of being a non-pathogenic human virus [Hermonat and Muzyczka 1984] that can infect both dividing and non-dividing cells [Kearns et al., 1996]. However, the application of AAV as a gene vector has been limited by the costly and labor-intensive purification processes [Zhang et al., 2001] as well as by the size limitation of the capsid, which cannot accommodate a therapeutic gene larger than 4.7 kb [Dong et al., 1996]. Ad-based systems are able to carry a larger gene cargo as the native virus has a double-stranded DNA genome of 36 kb [Mah et al., 2002]. Ad-based systems are highly efficient in infecting both dividing and non-dividing cells [St George, 2003], but they tend to elicit a host immune response [Crystal et al., 1994].

Viruses in the *Retroviridae* family are enveloped, single-stranded RNA-containing viruses [Mah et al., 2002]. Retroviral-mediated gene therapy showed efficacy in *ex vivo* gene transfer [Miller et al., 1990; Scharfmann et al., 1991; Mah et al., 2002] but it was difficult to engraft the gene-transferred cells back into the hosts [Mah et al., 2002]. The *Retrovirus* family also includes the Lentiviruses, well-known members of which are the Human immunodeficiency virus type 1 (HIV-1), Simian immunodeficiency viruses (SIV) and Feline immunodeficiency virus (FIV) [Poeschla et al., 1998; Mah et al., 2002]. Although lentiviral-based vectors can efficiently transfer and integrate exogenous genomic material into non-proliferating cells [Naldini et al., 1996; Kafri et al., 1997; Miyoshi et al., 1999], safety is a major concern as they may revert to the extremely harmful wild-type viruses, especially the HIV-1 based vectors [Mah et al., 2002].

A safer alternative to using intact viral capsid as vectors is to use virosomes, which are artificially reconstituted micro- or nano-systems e.g. liposomes conjugated with viral

proteins or envelops [Westerfeld et al., 2006]. Virosomes lack infectivity but possess the viral functions of interacting and fusing with cell membrane, They have been shown to be highly efficient in delivering therapeutic materials as diverse as doxorubicin [Waelti et al., 2002], malaria-antigens [Westerfeld et al., 2006] and small interfering RNA [de Jonge et al., 2006] .

Compared with animal viruses, plant viruses have rarely been used for biomedical applications. An underlying reason may be the significant differences between plant and animal viruses in their structure, and the mechanisms of infection and transmission. Thus, it is necessary to consider the characteristics of plant viruses to explore whether different strategies are required to utilize plant viruses for drug delivery.

1.4.4 Plant viruses for biomedical applications

1.4.4.1 Mechanisms of Infection and Transmission of Plant viruses

There are fundamental differences in the infection and transmission mechanisms between plant and animal viruses. The coat protein of an animal virus can target specific membrane receptor on the host cell that permits entry of its genomic materials into the cell [Zhang and Godbey, 2006]. This major mechanism of animal virus transduction is exploited in gene delivery. On the other hand, no plant virus to date has been found to gain entry into host cells by interacting with a specific cellular receptor. Plants are protected by layers of wax and pectin, and the cytoplasmic membranes of plant cells are surrounded by a thick overlying cellulose wall [Gamble, 2003]. Successful infection by

plant viruses therefore necessitates some form of mechanical damage to the cell wall followed by opportunistic penetration by the viruses. For example, the widely used vegetative propagation/grafting technique often introduces injury that allows viruses to spread to new plants [Crescenzi et al., 2004]. In the laboratory, the infection of plants with viruses is carried out by simulating such mechanical injury, usually by rubbing virus-containing solutions on plant leaves, the injury to the leaves creating the opportunity for viral entry into the plant [Lee et al., 2003]. Plant viruses may also infect new host through vectors, such as bacteria, fungi, nematodes, arthropods, mites and insects [McPherson, 2006].

Once they have infected a host plant, plant viruses are observed to spread to all other parts and to cause systemic symptoms involving the whole plant [Pacha and Ahlquist, 1992; Zhou et al., 2006]. However, the transmission of plant viruses between cells occurs by a different mechanism from that of animal viruses, which infect new cells via specific receptors. It is believed that the spreading of plant viruses in the host is either by direct cell-to-cell contact or by the vascular system [Scholthof, 2005]. Some plant viruses exploit the plasmodesmata to aid transmission. The plasmodesmata is a channel in the cell wall that allows neighbouring cells to communicate with each other and exchange materials, but is too small to permit the entry of exogenous particles or genomic materials [Wolf et al., 1989; Martens et al., 2006]. To overcome this barrier, plant viruses have evolved specialized proteins to modify the plasmodesmata. An example is the TMV, which expresses a 30 kDa-protein from a sub-genomic mRNA, which can dilate the host plasmodesmata, the increased permibility permitting the virus to move between plant cells [Beachy and Heinlein, 2000; Citovsky, 1999]. Similarly, the CPMV expresses a

special protein that forms tubular structures in the plasmodesmata to allow for its transfer from cell to cell [Wellink et al., 1993].

1.4.4.2 Potential as drug delivery platforms

The protein cages of plant viruses can undergo conformational changes, including swelling, disassembly and reassembly, under different conditions [Bancroft et al., 1968; Bancroft and Hiebert, 1967; Hiebert and Bancroft, 1969; Hiebert et al., 1968]. Plant viral capsids can be disassembled to allow for the removal of native viral RNA, then reassembled to produce empty viral protein cages for drug loading. Several methods have been explored for this purpose, including dialysis against a medium of high pH (> 7.5) or exposure to heat (55 ^{o}C) [Mutombo et al., 1993], high pressure (2400 × 10^5 Pa, 50 min, 25 ^{o}C) [LeimkuÈhler, 1994; Michels et al., 1999] or alkaline pH (>pH 11, 30 min, 30 ^{o}C) [Kaper, 1964], or subjection to freezing and thawing cycles [Michels et al., 1999]**.** Among these methods, the dialysis of a viral solution against a buffer of high pH is most often employed. For some plant viruses, capsid disassembly will occur when dialyzed against a buffer of pH 7.5 or higher [Fox et al., 1998]. Following the disassembly of the capsid, the viral RNA will be released. It can then be separated from the protein coats by centrifugation before the coat proteins are reassembled into empty capsids at lower pH [Douglas and Young, 1998].

The capability to disassemble, then resemble the plant viruses *in vitro* offers opportunities for the development of drug delivery platforms. In fact, under appropriate

in vitro conditions, the purified coat proteins and viral RNA can be reassembled into a virion, which is not only similar to the native virus when viewed under an electron microscope, and has been shown to retain infectivity [Zhao et al., 1995]. Removal of the viral genomic materials prior to reassembly will cause the formation of empty protein cages [Bancroft et al., 1968], which often have identical structures to the native viruses [Fox et al., 1998]. These protein cages offer nanoscaled cavities, which may be used to encapsulate drug molecules for delivery.

In addition, the viral protein cage can be made to undergo reversible conformational changes under specific conditions that cause the opening or closure of pores on the cage surface. One of the most widely studied plant viruses in this regard is the CCMV, a 28 nm icosahedral plant virus with T = 3 and 180 coat proteins. CCMV particles were stable at pH 5.0, but their diameter could increase by approximately 10% when the pH was increased to 7.0 at low ionic strength (I = 0.1) [Zhao et al., 1995]. This swelling was caused by a radial expansion at the 3-fold axes of symmetry, and was accompanied by the appearance of 2-nm apertures at each of the axes [fox et al., 1998; Speir et al., 1995]. Calcium ions were important for the stability of the capsids**.** Swelling occurs only in the absence of Ca^{2+}, the swelling phenomenon being readily reversible by lowering the pH and resupplying the viral particles with Ca^{2+}. The chemical switches offered by these pores provide unique molecular gating mechanisms to control the containment and release of entrapped materials [Fox et al., 1998; Zhao et al., 1995], and create opportunities for the development of controlled release drug delivery platforms.

A review of the literature indicates that some materials could be loaded into empty protein cages derived from plant viruses. Again, the most widely studied example is the protein cage obtained from the CCMV, which has been used to load materials ranging from ions to polymers and metal nanoparticles. Charged species, e.g. ions, were loaded into CCMV protein cages by utilizing the pH-dependent gating mechanism. For example, the aqueous soluble tungstate ions (WO_2^{-4}) were loaded into the protein cages by co-incubation at pH 6.5. Swelling of the CCMV protein cage at this pH caused the opening of apertures on its surface, which enabled the tungstate ions to diffuse into its interior. When pH of the medium was subsequently lowered to 5.0, the precursor tungstate ions (WO_2^{-4}) were converted to the paratungstate polyanions ($H_2W_{12}O_{10}^{-42}$), which being less water-soluble, would precipitate out as nanosized crystals. At the same time, the lowering of pH reversed the conformational change in the virus protein cage, and the closure of apertures on the surface of the cages ensured the successful encapsulation of nanosized tungstate crystals within the protein cage. Likewise, anionic polymers e.g. poly-anetholesulfonic acid, could be encapsulated into the CCMV protein cages by a similar mechanism. The resultant polymer-loaded viral protein cages could be isolated from the empty ones by gradient centrifugation. When imaged under the TEM, the polymer-loaded viral protein cages appeared as uniformly sized particles whose shape was no different from that of the native virus [Douglas and Young, 1998]. More recently, gold nanoparticles (16 nm diameter) have also been successfully loaded into the CCMV protein cages [Chen et al., 2006].

Electrostatic interaction appears to be critical for the loading of materials into the CCMV. The native CCMV coat proteins have highly basic N-termini, made up of

positively charged Arg and Lys that project into the interior of the viral capsid. The positive charges facilitate the encapsulation of anionic RNA viral genome, and the interaction between coat proteins and RNA is believed to be important for the initiation of resembly into viral capsids [Douglas and Young, 2002]. These positively charged N-termini could be exploited for the loading of negatively charged exogenous material, such as the WO_2^{-4} ions, but they would hinder the loading of positively charged materials. Genetic manipulation to change the amino acid sequence of the N-terminus of CCMV to provide an anionic interior surface has been attempted [Douglas and Young, 2002], the mutated coat proteins being reassembled into protein cages with no significant change in architecture compared to the native virus. The mutated protein cages of CCMV have been used successfully to encapsulate nanosized ferric ions [Douglas and Young, 2002]. The encapsulation of uncharged gold nanoparticles required a different approach. The gold nanoparticles were conjugated with carboxylated terminated thiolalkylated tetraethylene glycol functionality, which allowed them to mimick the electrostatic behaviour of the native nucleic acid to bring about initiation of the PC reassembly [Chen et al., 2006]. The resultant system was a nanostructure that was virus-like with a gold core.

Researchers have also used plant viral protein cages as a template for compound conjugation. The protein cages provide several reactive groups e.g. Lys and Cys amino acids, on their surface, and they exhibit considerable stability, being able to retain their chemical and conformational structures under a variety of conditions. For example, the plant virus CPMV could retain its integrity at temperatures of up to 60 ^{o}C, or in the presence of small amounts of organic solvents, such as DMSO, as well as in a wide pH range of 3.5 to 9 [Raja et al., 2003]. Plant virus protein cages can be reacted with both

hydrophobic and hydrophilic molecules, including metal, polymer as well as protein/peptide, to produce novel nanosized compounds [Wang et al., 2002].

The protein cage of the CPMV has been the most widely applied amongst plant viruses as a potential nanoscaled scaffold for compound conjugation. CPMV has served as a nanoscaled template for conjugation with gold nanoparticles [Soto et al., 2005; Wang et al. 2002]. Site-specific mutations were performed to insert the amino acid, Cys, between positions 98 and 99 in the coat protein of CPMV for the conjugation. Colloidal gold nanoparticles with diameter of 2 to 5 nm were attached to the surface of the protein cage by reaction with the sulfhydryl groups of the Cys. The result was a three-dimensioned pattern with specific inter-gold particle distances [Blum et al., 2005].

Besides inorganic gold nanoparticles, organic polymers could also be conjugated onto the coat protein of plant viruses. For example, the surface of the CPMV protein cage has been modified with poly(ethylene glycol) (mw 2000 and 5000) by N-hydroxysuccinimide ester-mediated reaction [Raja et al., 2003]. The CPMV retained its stability during the reaction process, which required exposure to a high pH (pH 8.4) for a prolonged period of 4 h. The hydrophilic PEG-linked CPMV protein cage had the same size and morphology as the native virus particles but provoked a poorer immune response in the female mice.than the native virus. Entire proteins, e.g. Intron 8 protein, T4 lysozyme and LRR-internalin B, were also been reported to be chemically linked to the protein cage of the CPMV [Chatterji et al., 2004], the protein molecules preserving their biological activity after conjugation. The capacity to chemically modify the surface of plant virus protein cage to provide specific functionalities would significantly widen the potential of these

cages as drug delivery platforms, including the possibility of developing the protein cages as targeting drug delivery systems.

Several research groups have further explored the feasibility of using plant virus protein cages for foreign peptide expression. The icosahedral structure of the cages appears to be sufficiently robust not to be disrupted by the insertion of bioactive peptides [Lico et al., 2006; Shadwick and Doran, 2006]. Novel vaccines have been generated by introducing antigens onto the coat proteins of the CPMV [Langeveld et al., 2001] and TMV [McCormick et al., 2006] through genetic engineering. Chimaeric virus particles of CPMV expressing the peptide of the canine parvovirus were shown capable of eliciting high titres of the peptide-specific antibody when injected into dogs, the levels being sufficient to protect the dogs from a canine parvovirus challenge [Langeveld et al., 2001]. In another study, a peptide from the outer-membrane protein of *Pseudomonas aeruginosa* was expressed on the coat protein of TMV. Upon administration to mice, the engineered plant virus protein cage was able to generate high titres of antibody to protect the mice from the bacterial infection [Staczek et al., 2000]. A distinct advantage of these chimaeric plant virus platforms compared with animal virus platforms is their safety profile, as plant viruses have no infectivity towards the animal recipients [Nicholas et al., 2002].

Other bioactive functional peptides have been expressed on the surface of plant virus protein cages to impart novel functions. CPMV was used as a platform to display a heterogeneous functional peptide, a sequence derived from the binding site of CD46 to the measles virus. The peptide was expressed on all 180 copies of the coat protein in each CPMV protein cage, which provides a clustering of the peptide on the surface at high

concentration. As a result, the expressed peptide was able to inhibit the measles virus (MV) infection in mice and showed a-100 fold higher efficacy at inhibiting MV infection *in vitro* compared to the original CD46 peptide [Khor et al., 2002].

To summarize, plant virus protein cages present with specific properties that made them attractive carriers for drug delivery. They are uniformly sized, robust nanostructures that are precise in chemical and conformational structures. Yet they lend themselves to physical and chemical manipulation that not only allowed exogenous material to be encapsulated within the cages, but also to be conjugated onto the protein cage surface. Specific functions, e.g. targeting capability, may also be imparted by the conjugation of appropriate chemical species to the protein cage surface. In this project, the feasibility of producing a nanoscale targeted drug delivery platform using the *Hibiscus chlorotic ringspot virus* (HCRSV) was explored. Although the structure of the HCRSV has been widely studied, this virus has not been evaluated in depth for pharmaceutical applications.

1.5 Hibiscus chlorotic ringspot virus

1.5.1 Taxonomy

The *Hibiscus chlorotic ringspot virus* (HCRSV) [Huang et al., 2000] is a monopartite virus that was first described in a hibiscus cultivar imported to the United States from El Salvador. The virus infects the kenaf (*Hibiscus cannabinus*), a woody plant of interest to the woodpulp industry in the United States [Johnson, 2001], and is found worldwide where the hibiscus is cultivated [Waterworth et al., 1976], including Singapore [Wong

and Chng, 1992]. It induces chlorotic ringspots on naturally infected hibiscus leaves and causes local lesions on infected kenaf.

The HCRSV is a single-stranded RNA virus belonging to the *Tombusviridae* family of plant viruses [Liang et al., 2002]. Based on virion morphology, genome organization, physicochemical properties and amino acid sequence, the virus is classified in the genus *Carmovirus*, which also includes the *Carnation mottle virus* (CarMV) [Guilley et al., 1985], *Turnip crinkle virus* (TCV) [Carrington et al., 1989], *Melon necrotic spot virus* [Riviere and Rochon, 1990], *Cardamine chlorotic fleck virus* [Skotnichi et al., 1993], *Saguaro cactus virus* [Weng and Xiong, 1997], *Galinsoga mosaic virus* [Ciuffreda and Rubino, 1998], *Japanese iris necrotic ring virus* [Takemoto and Kanehira, 2000] and *Pelargonium flower break virus* [Berthome and Kusiak, 1998].

1.5.2 Structure of HCRSV

The genomic RNA (gRNA) of HCRSV is 3911 nucleotides long (Figure 1-6) and has the potential to encode seven major open reading frames (ORF) [Huang et al., 2000; Koh et al., 2002] or two subgenomic RNAs (sgRNAs) of 1.7 and 1.5 kb [Huang et al., 2000; Liang et al., 2002]. The gRNA could potentially encode seven viral proteins. Two 5'-proximal ORF may encode proteins with molecular weight (mw) of 28 and 81 kDa, which are believed to form the putative viral RNA-dependent RNA polymerase [Liang et al., 2002]. Two centrally located small ORFs encode two proteins required for viral

movement [Hacker et al., 1992; Li, et al., 1998]. The coat protein (CP) is encoded by p38 from the 3'-proximal open reading frames.

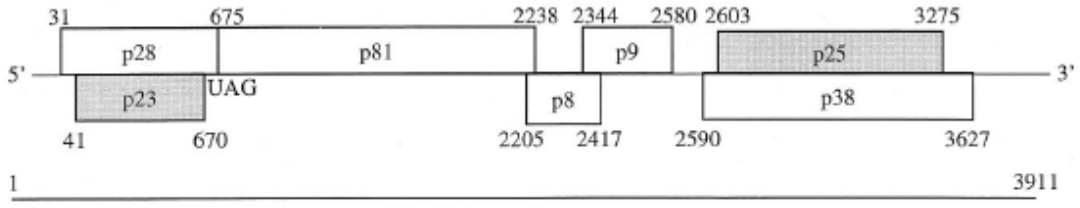

Figure 1-6. The genomic RNA and corresponding open reading frames of HCRSV [Huang et al., 2000].

RNA binding domain	MLQKNDPAVQRAFNAHLPWAIKLKNDGWAALSKGQKRAANR YAGGTRPVTSQIKLSTLKVTAPVAASMRTRNPGANIRTAGKSVT VVHCEFVGNIARQT
Shell-forming domain	GSGLLVVERTINPSNVLSFPWLSVLAAGYEKYRVSSLSLRYSPT CATTTEGKVILAFDKDAADASPTSKSDMYNHDGAVGVSPWDS AMLQIPCDNVDRFINDSSSSDPKLVDFGKVVVANYGQSEGDVD VIGELFLQYSITLKIPQGMATPTQSGVGIS
Protruding domain	SVGPSLFRVQLRDDTHVFTCNGTGRFLFFFNSTVDATSTIAGME VKQKSSTDDKGETTIMELLATESGGTIAILAATGTLTWWACRN

Table 1-1. Amino acid sequence of the HCRSV coat protein, which is composed of three domains: RNA binding domain, shell-forming domain and protruding domain.

The 38-kDa CP of HCRSV is composed of 345 amino acids (Table 1-1), consisting of 3 domains. The internal RNA binding domain (R) may bind with the encapsulated viral RNA. The shell-forming domain (S) is the construct of the PC. As is common of viruses in the *Tombusviridae* family, the CP of HCRSV has a protruding domain (P) that is accessible for ligand conjugation (Figure 1-7). Both the shell-forming domain and the protruding domain contain an 8-stranded β–sandwich fold [Doan et al., 2003].

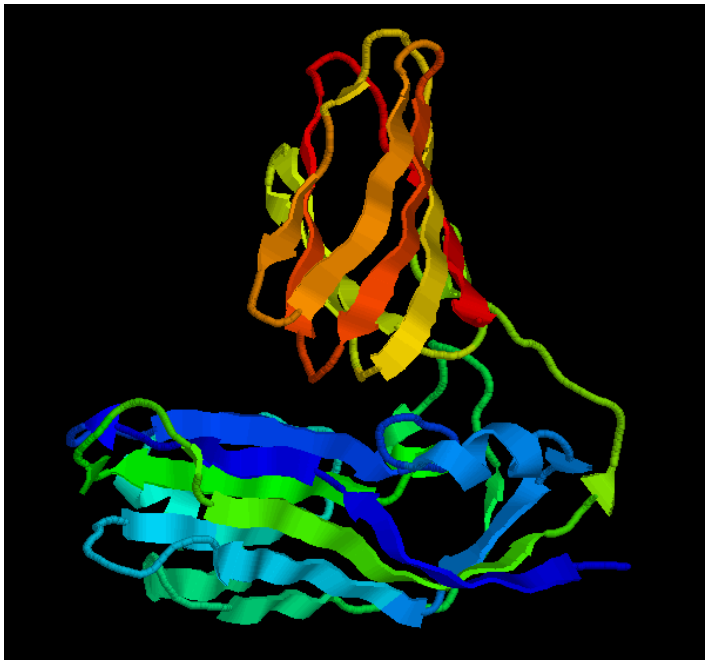

Figure 1-7. Conformational structure of the HCRSV coat protein, which contains two β-sheets: the one in the P domain is shown in red-yellow color, and the other in the S domain is shown in blue-green color. The structure was modeled by SWISS-MODEL [http://www.expasy.ch/swissmod/]

The HCRSV virus particle contains 180 copies of the CP, forming a 30-nm diameter icosahedral protein cage (PC) with T = 3 symmetry. The HCRSV particle has been crystallized and its structure determined at the atomic resolution of 4.5 A° [Doan et al., 2003]. Observed by cryo-electron microscopy, the HCRSV PC has 90 dimers of protruding domains (Figure 1-8), again a characteristic arrangement of the *Tombusviridae* family of viruses. The S domains form fivefold and sixfold rings around the fivefold and threefold axes, respectively, with a depression or hole in the centre [Doan et al., 2003, Lee et al., 2003].

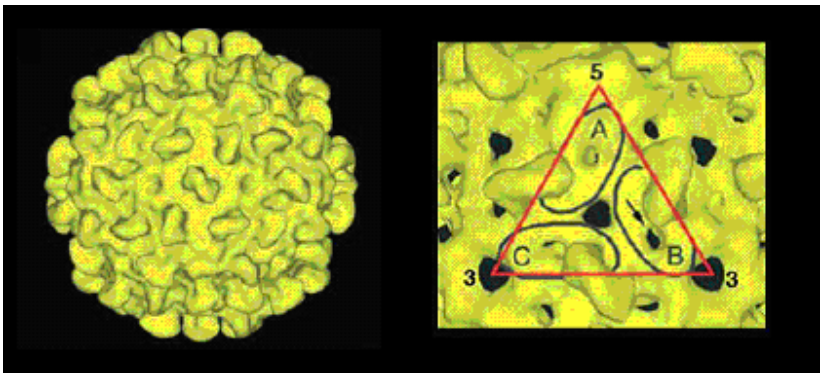

(a) (b)

Figure 1-8. Structure of the HCRSV virus protein cage. The coat protein is arranged in T = 3 icosahedral model. (a) view down from a 2-fold axis of symmetry, (b) closeup view down from a 3- fold axis of symmetry [Doan et al., 2003]

1.6 Statement of purpose

Chemotherapeutic agents remain a mainstay of treatment for cancer, a leading cause of death for human beings. Treatment outcomes for patients who are being treated with these potent, highly toxic drugs would be significantly improved if the drug delivery could be targeted specifically to the tumor cells. Targeted delivery would not only increase efficacy as a result of drug concentration in the target cells, but would reduce undesirable side effects by sparing normal cells from the cytotoxic effects of the drugs.

Plant virus-based systems, in particular, the icosahedral plant virus protein cages constructed from T × 60 coat proteins, could be an attractive novel platform to develop a targeted delivery system for anticancer drugs. These virus protein cages are nanoscale in dimension, highly uniform in size and composition, and adequately robust under relatively harsh processing conditions of pH and ionic strength. More importantly, the virus protein cages readily lend themselves to physical and chemical manipulations without sacrificing structural integrity. The native virus capsid can be disassembled *in vitro* to remove the native RNA genomic materials, then reassembled into empty protein cages that are similar in morphology to the native viruses. Under appropriate conditions, guest molecules, e.g. drugs, could be successfully loaded and retained within the protein cage. Alternatively, these molecules could be chemically conjugated onto the surface of the protein cage, or the coat proteins could be genetically engineered to express exogenous peptides. These manipulations would allow the development of drug delivery systems with specific functionalities e.g. a capability to target cancer cells. Another

reason for developing plant virus-derived delivery systems was their potentially lower pathogenicity and immunogenicity compared with animal virus-based systems.

To date however, there is a scarcity of research on plant virus-derived systems for the delivery of anticancer drugs, although a variety of other types of compounds, ranging from inorganic metals to organic polymers and peptides have been successfully conjugated on or encapsulated into plant virus protein cages. Moreover, the research has tended to focus on a couple of plant viruses, namely the CCMV and CPMV. Although the HCRSV is a common icosahedral plant virus in Singapore, its structure having been well established by local researchers [Doan et al., 2003], this virus had not been investigated for its potential as a drug delivery platform. This project was therefore initiated to evaluate the feasibility of using the HCRSV PC as a template for targeted drug delivery. The hypothesis for the project was that the purified coat proteins of HCRSV could be reassembled into protein cages *in vitro* to load an anticancer agent, and its surface could be modified to impart cancer-targeting functionality. Doxorubicin was used as the model anticancer agent and folic acid the targeting ligand.

Various studies were conducted in this project to test the hypothesis. The objectives of these studies were as follows:

(1) Preparation of purified empty protein cages of HCRSV for the loading of guest molecules. The study included the development of methodologies to disassemble the capsid of HCRSV to remove the native RNA, followed by reassembly of the purified coat proteins into empty protein cages. Methods were developed to characterize the HCRSV

coat protein and protein cages at different stages of processing, in order to provide a fundamental understanding of the HCRSV protein cage.

(2) Evaluation of the mechanisms for loading guest molecules into the reassembled protein cages derived from the HCRSV.

(3) Development and characterization of doxorubicin-loaded HCRSV protein cages whose surface had been conjugated with folic acid molecules.

(4) In vitro evaluation of the efficacy of the doxorubicin-loaded folic acid-conjugated HCRSV based drug delivery systems using human ovarian carcinoma and human nasopharyngeal carcinoma cell models.

Chapter 2

Preparation and characterization of empty protein cages (PC) derived from HCRSV

2.1 Introduction

The primary purpose of this project was to develop a nano-sized drug delivery system based on the protein cage (PC) of a plant virus, the HCRSV, which belongs to the family of *Tombusviridae*, genus *Carmovirus* [Doan et al., 2003; Huang et al., 2000]. The HCRSV PC is an icosahedral structure comprising of 180 identical coat proteins (CP). The 38-kDa CP of HCRSV would be the most important "raw material" for this project as it constituted the building block for the construction of the drug delivery platform. However, neither HCRSV nor its CP was commercially available. Thus, for this project to be viable, a stable HCRSV virus resource from which a purified form of the virus could be harvested had to be established. In addition, methods had to be developed to remove the 3.9 kb RNA from the viral capsid, and to reassemble the purified CP into empty cages that were comparable in structure to the HCRSV capsids. This section describes the development of methods to prepare and evaluate the empty HCRSV PC.

The kenaf, a plant crop of major interest to the wood pulp industry [Johnson, 2001], was chosen as the host of HCRSV because it thrived in the warm and humid environment of Singapore. Nevertheless, care had to be exercised in the cultivation of HCRSV in the kenaf. Conditions that adversely affected the growth of the host, such as extreme temperature and humidity, inadequate sunlight, strong winds, and insects that fed on the kenaf leaves, would lower HCRSV yield. Insects could also contaminate the HCRSV source by transmitting other viruses to the kenaf, as could infection of the plant by viruses in the soil. Contamination of the HCRSV source was of particular concern as failure to detect and isolate the contaminant would result in erroneous data [Doan et al.,

2003]. For these reasons, it was critical at the outset to establish standard operation protocols for the culture of the host plant culture and for virus transfection in order to ensure a stable and reliable HCRSV source.

Having established the HCRSV source, methods were developed to isolate the virus from its host, and subsequently to produce empty PC from the purified viruses. Isolation and purification of the HCRSV were achieved by a series of centrifugation processes, including centrifugation on sucrose gradient, as these had previously been established to be effective for the purification of a large quantity of HCRSV [Lee et al., 2003]. Novel methods, however, had to be developed to produce the empty PC from the HCRSV. This was because preliminary experiments have shown that the published methods, including dialysis against a medium of high pH (7.5) [Fox et al., 1998; Zhao et al., 1995], exposure to heat (55 ^{o}C) [Mutombo et al., 1993], incubation at alkaline pH (> pH 11, 30 min, 30 ^{o}C) [Kaper, 1964], and freezing and thawing cycles [Michels et al., 1999], could not effectively remove the RNA from the HCRSV without destroying its CP. In this project, methods involving the use of urea and dialysis were optimized to produce empty PC from the HCRSV.

In vitro cytotoxicity studies were included as safety was a major concern for any novel drug delivery system. The MTT assay, which is a quantitative colorimetric method developed for measuring the mitochondrial dehydrogenase activity in viable cells, was employed for the *in vitro* cytotoxicity studies against the CCL-186, OVCAR-3 and CNE-1 cell lines. The CCL-186 cells [Nichols et al., 1977] were derived from human normal lung fibroblasts, and were used in this project to represent normal human cells. The

OVCAR-3 [Hamilton et al., 1983] and CNE-1 [Zhang et al., 2005] cell lines, respectively developed from human ovarian carcinoma and human nasopharyngeal carcinoma, were used as representative models of human cancer cells.

2.2 Materials

CH_3COONa, NaCl, NaOH, $CaCl_2$, phenyl methanesulfonyl fluoride (PMSF), methanol, sodium lauryl sulfate (SDS), 3-(4,5-dimethylthiazol-2-yl)-2,5-diphenyltertrazolium bromide (MTT) and carborundum powder were from BDH Ltd (Poole, England); penicillin G, streptomycin, $NaHCO_3$, sucrose, Triton X-100, $(NH_4)_2SO_4$ and dialysis tube (mw cutoff 12 400) were from the Sigma Chemical Co. (Steinheim, Germany); fetal bovine serum (FBS), trypsin-EDTA and phosphate buffered saline (PBS, 14.4 g/L Na_2HPO_4, 2.4 g/L KH_2PO_4, pH 7.4) were from Gibco BRL Life Technologies (Grand Island, NY, USA); Tris (base) was from J.T. Baker (NJ, USA); ethylenediaminetetraacetic acid (EDTA), dithiothreitol (DTT) and urea were from Bio-Rad (CA, USA); β-mercaptoethanol was from Merck (Darmstadt, Germany) and agarose was from Biowhittaker Molecular Applications (ME, USA).

Hibiscus chlorotic ringspot virus (HCRSV) was obtained from the infected leaves of kenaf grown in the laboratory of Dr. SM Wong, National University of Singapore [Huang et al., 2000]. The human normal lung fibroblast cell line, CCL-186 (passage 15 to 25) and human ovarian carcinoma cell line, OVCAR-3 (passage 22 to 32), were obtained from the American Type Culture Collection (ATCC, Manassas, VA, USA), while the human nasopharyngeal carcinoma cell line, CNE-1 (passage p + 10 to p + 20), was obtained

from the National Cancer Centre of Singapore. The culture medium for OVCAR-3 and CNE-1 cell lines was folic acid-deficient RPMI 1640 medium, and that for the CCL-186 cells was normal RPMI 1640 medium. All culture media were supplemented with 10% of FBS, 0.1 g/L of streptomycin and 0.1 g/L of penicillin.

The following buffers were used: extraction buffer (0.2 M NaOAc, 50 mM NaCl, 5 mM EDTA, 20 mM $CaCl_2$, pH 5.4), re-suspension buffer (50 mM NaOAc, 50 mM NaCl, 5 mM EDTA, 20 mM $CaCl_2$, pH 5.4), storage buffer (10 mM NaOAc, 50 mM NaCl, 5 mM $CaCl_2$, pH 5.4) and buffer A (50 mM NaOAc, 50 mM NaCl, 2 mM EDTA, 20 mM $CaCl_2$, pH 5.0).

2.3 Methods

2.3.1 Cultivation of HCRSV

J. Arthur Bower's Seed and Potting Compost (William Sinclair Horticulture Ltd., Lincoln, UK) was used for the plant culture. The seeds of kenaf (*Hibiscus cannabinus*) [Johnson, 2001] were cultured in the wetted earth in a culture room maintained at 20 to 25 ºC with 18 h of light per day. After germination, the kenaf plants were transferred to pots at a density of 2 to 3 plants per pot. When the plants had developed 4 to 5 leaves, usually after 2 to 3 weeks, they were placed in a dark environment for one day before infection with the HCRSV virus.

HCRSV was obtained from an infected H. rosa-sinensis plant exhibiting chlorotic leaf spots tested positive for HCRSV by an enzyme-linked immunosorbent assay (ELISA) [Lee et al., 2003]. About 2 g of the infected leaves were ground with 10 ml of ice-cold phosphate buffered saline (PBS, 137 mM NaCl, 10 mM phosphate, 2.7 mM KCl, pH 7.4) in a mortar to produce a homogeneous slurry to which carborundum powder was added. The carborundum powder served to facilitate virus infection by inducing mechanical lesions when the slurry was rubbed onto the leaves of the kenaf plant using cotton sticks. Two leaves per plant were inoculated, care being taken to limit the mechanical damage to the leaves. After 5 min incubation, the leaves were rinsed with distilled water to remove traces of salts and the kenaf plants were kept in the dark overnight. The plants were subsequently cultured in a controlled environment of 25 ºC with 18 h of light per day for one month. During culture, the plants were protected with gauze to prevent potential contamination transmitted via insects. Kenaf leaves with chlorotic spots were then collected and stored at -80 ºC (Forma -86C ULT Freezer, Thermo Electron Corporation, MA, USA) until use.

2.3.1.2 Purification of HCRSV

HCRSV was purified by sequential steps of extraction, sedimentation and resuspension [Lee et al., 2003]. All procedures were carried out at 4 ºC unless otherwise stated. Kenaf leaves exhibiting chlorotic spots were homogenized in a Waring Blender (Waring Products, Inc., CT, USA) with 2 to 3 volumes (w/v) of extraction buffer containing 0.1% of β-mercaptoethanol. The slurry was centrifuged at 12 000 *g* for 15 min

using a JA14 rotor (Beckman Coulter Inc., Fullerton,CA, USA) and the supernatant was collected on ice. The pellet containing the plant debris was re-extracted with one volume of extraction buffer containing 0.1% β-mercaptoethanol and centrifuged at 12 000 *g* for 15 min to maximize the virus yield. The pooled supernatants were incubated for 2h on ice with one volume of saturated $(NH_4)_2SO_4$ solution to sediment the virus, which was subsequently pelleted by centrifugation at 12 000 *g* for 20 min.

The HCRSV pellet was re-suspended overnight at 4 ºC in the re-suspension buffer supplemented with 0.1% of β-mercaptoethanol and 1% of Triton-X100. After centrifugation at 12 000 *g* for 15 min, the supernatant was collected and put on a layer of 10% sucrose cushion. The viruses were collected as a pellet following ultracentrifugation at 100 000 *g* for 3 h using a SW41 rotor (Beckman Coulter Inc., Fullerton,CA, USA). The pellet was re-suspended in a small volume (0.5 to 1 ml) of re-suspension buffer overnight at 4 ºC to obtain the crude virus suspension. Sucrose dissolved in the re-suspension buffer to concentrations of 10%, 20%, 30% and 40% were layered in centrifuge tubes using a syringe device (Figure 2-1) to prepare the sucrose gradients. These were stored at 4 ºC overnight before use. The crude virus suspension was centrifuged at 12 000 *g* for 3 min to remove insoluble debris, and the supernatant was ultracentrifuged on the sucrose gradient at 100 000 *g* at 4 ºC for 3 h using the SW41 rotor. The virus band in the sucrose gradient was visible under a beam of light in a dark room. The virus band was aspirated with a pipette, diluted with 3 to 4-fold its volume of re-suspension buffer and centrifuged at 100 000 *g*, 4 ºC for 3 h to sediment the virus. The supernatant was discarded and the virus pellet was re-suspended in 0.5 ml of the storage buffer. The virus dispersion was stored at 4 ºC until use.

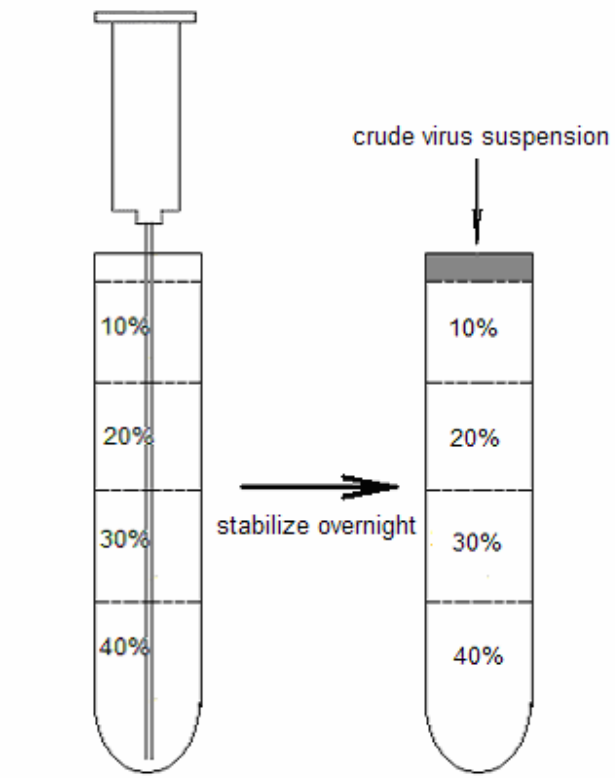

Figure 2-1. Preparation of a 10%-40% sucrose gradient for HCRSV virus purification. Layering of the sucrose solutions was achieved by using a syringe and needle, positioned near the bottom of a centrifugation tube, to introduce each sucrose solution in consecutive order of increasing concentration into a centrifuge tube (Left). After overnight stabilization of the sucrose gradient, the crude virus suspension was loaded on the top layer of the gradient (Right). The sample was then purified by ultracentrifugation.

2.3.4 MTT assay

The determination of cell viability following exposure is a common assay to evaluate the *in vitro* cytotoxicity of biomedical materials. The MTT assay is one of several methods established for measuring cell viability. It is a sensitive, quantitative and reliable

colorimetric assay that is used not only for measuring cell viability, but also cell proliferation and activation [Smith et al., 2005; Mosmann, 1983]. The MTT assay is based on the ability of mitochondrial dehydrogenase enzymes in living cells to convert the water-soluble 3-(4,5-dimethylthiazol-2-yl)-2,5-diphenyl tetrazolium bromide (MTT) into a dark blue, water-insoluble formazan product. The intracellular formazan may be extracted and solubilized with an appropriate solvent, and the optical density of the resultant solution is directly proportional to cell viability for a wide variety of cell lines [Mosmann, 1983; Gerlier and Thomasset, 1986; Grailer et al., 1988].

In this study, test samples for the MTT assay were prepared in the following manner. HCRSV dispersion was sterilized by filtration through a 0.22 μm membrane (Millipore Corporation, MA, USA), then diluted with the cell culture medium to concentrations ranging from 1 mg/ml to 10 ng/ml. SDS and dextran were similarly dissolved in cell culture medium to 0.1% w/v and used as positive and negative controls, respectively. The CCL-186, OVCAR-3 and CNE-1 cells were separately seeded onto 96-well plates at the respective densities of 5 000, 20 000 and 5 000 cells/well. After 24h incubation at 37 ºC under 5% CO_2/95% air atmosphere in a water-jacketed autoflow CO_2 incubator (NuAire, MN, USA), the culture medium was replaced with 200 μl of test or control sample. Controls also included untreated cells, which were incubated with 200 μl of the culture medium. After incubation for the designated period of 4 h or 3 days, the samples were replaced with 100 μl of MTT solution (1 mg/ml in PBS, pH 7.4) and the cells were incubated in the CO_2 incubator for another 4 h. The MTT solution was removed and 100 μl of DMSO was added to each well to solubilize the formazan product, which was quantified by measuring the optical density of the resultant solution in a microplate

reader (TECAN fluorimeter, MA, USA) at λ_{590nm}. Cell viability was expressed as the percentage of absorbance in sample wells relative to that in control culture medium wells. Experiments were performed in eight replicate wells for each test and control sample.

2.3.2 Viral RNA removal and PC reassembly

2.3.2.1 Protein denaturation using urea

Urea has a strong capacity to denature protein [da Poian et al., 1995]. At sufficiently high concentrations, which might range from 1 M [da Poian et al., 1995] to 8 M [Michels et al., 1999], urea could induce the unfolding of viral CP to disrupt the integrity of the capsid, thus allowing for the separation of native RNA from the viral CP [Shirley et al., 1995; Michels et al., 1999]. The purified CP could refold and assemble into viral-like capsids by dialysis against an appropriate medium following the removal of urea [Michels et al., 1999].

To remove the viral RNA from the HCRSV, about 0.1 ml of HCRSV dispersion (10 mg/ml in re-suspension buffer) was incubated with 1 ml of urea solution (8 M urea, 1 M NaCl and 0.01 M Na_2HPO_4, pH 7.2) at room temperature for 10 min [Michels et al., 1999]. The solution was centrifuged at 25 000 *g* for 30 min at 4 °C to separate the viral RNA (pellet) from the unfolded CP (supernatant). To reassemble the CP into viral-like PC, the supernatant was dialyzed against buffer A for 12 h at 4 °C. The precipitate was isolated by centrifugation at 12 000 g for 15 min at 4 °C.

2.3.2.2 Dialysis

Dialysis against a buffer of high pH is another method reported to aid in the removal of RNA from the capsid of viruses. The RNA of CCMV was isolated from its CP following the disassembly of the viral capsids upon dialysis against a Tris buffer (50 mM, 1 mM EDTA, 1 mM DTT, 0.5 mM PMSF, 0.5 M $CaCl_2$, pH 7.5) [Zhao et al., 1995; Fox et al., 1998]. For this reason, the method of dialysis was also explored for the removal of RNA from the HCRSV capsids.

In our experiments, 0.1 ml of HCRSV dispersion (10 mg/ml in re-suspension buffer) was dialyzed for 12 h against one of 6 buffers (Table 2-1) to determine the effects of Ca^{2+} and pH on the efficiency of viral RNA removal. Samples dialyzed against buffers containing $CaCl_2$ (Buffers 1 - 3) were subsequently centrifuged at 25 000 *g* at 4 °C for 30 min, and the supernatants were collected for optical density measurement at 260 nm (OD_{260nm}) and 280 nm (OD_{280nm}) (Beckman Du 640B spectrometer, CA, USA). Samples that had been dialyzed against buffers without $CaCl_2$ (Buffers 4 - 6) were subsequently mixed with a 5.5 M $CaCl_2$ solution at a volume ratio of 10:1 to achieve final $CaCl_2$ concentration of 0.5 M. The mixtures were incubated at 4 °C for 30 min before they were processed by centrifugation and subjected to optical density measurement as described for samples dialyzed against Buffers 1 – 3. The supernatants, which represented purified CP solutions, were dialyzed against buffer A for 12 h at 4 °C to initiate the reassembly of the CP into empty PC.

	pH 7.0	pH 7.5	pH 8.0
0.5 M $CaCl_2$	Buffer 1	Buffer 2	Buffer 3
No $CaCl_2$	Buffer 4	Buffer 5	Buffer 6

Table 2-1. Buffers used for the removal of HCRSV viral RNA via the dialysis method. All buffers contained 50 mM Tris, 5 mM EDTA, 2 mM DTT and 0.2 mM PMSF, but were adjusted to different pH using 1 M NaOH or HCl solutions. In addition, Buffers 1 – 3 contained 0.5 M $CaCl_2$ while Buffers 4 – 6 were prepared in the absence of $CaCl_2$.

2.3.3 Characterization of HCRSV and CP

2.3.3.1 Ultraviolet (UV) spectroscopy

The concentration of HCRSV was evaluated by optical density measurement at 260 nm (OD_{260nm}) using an extinction co-efficient of e_{260nm} = 5.0 [Morris and Carrington, 1988; Lee et al., 2003]. The following equations were used to calculate the concentration and yield of HCRSV. The purity of HCRSV was monitored by the ratio of OD_{260nm}/OD_{280nm}.

$$\text{Viral Concentration (mg/ml)} = \frac{OD_{260nm} \times \text{dilution factor}}{5.0 \text{ (extinction coefficient)}}$$

$$\text{Yield (mg/100g)} = \frac{\text{Viral Concentration (mg/ml)} \times \text{volume (ml)} \times 100}{\text{Weight of leaves (g)}}$$

UV spectroscopy also provided a reliable, convenient and sensitive method to confirm efficient viral RNA removal from the capsids [Michels et al., 1999; Douglas and Young, 1998]. Viral RNA and proteins have different UV spectra as the former has strong optical absorption at 260 nm [De Mey et al., 2006], while the CP has maximum absorption at 280 nm due to the presence of the amino acids, tryptophan (Trp) and tyrosine (Tyr), in its sequence [Mach et al., 1992]. The $OD_{260\ nm}/OD_{280\ nm}$ ratio is a useful index to measure virus purity because a virus in whose structure the relative amounts of RNA and CP have been determined will have a defined $OD_{260\ nm}/OD_{280\ nm}$ ratio. Changes to this ratio would indicate contamination and impurity [Michels et al., 1999]. In addition, the extinction co-efficient of the viral RNA at 260 nm is much higher than that of the CP at 280 nm [De Mey et al., 2006] and the virion would have a UV spectrum showing maximum absorption at 260 nm due to the predominance of the RNA optical absorption [Lee et al., 2003]. Only when the viral RNA has been removed by more than 95% would the CP and viral RNA have comparable optical absorption at the respective wavelengths, and the $OD_{260\ nm}/OD_{280nm}$ will decrease to below 1. Samples with $OD_{260\ nm}/OD_{280\ nm}$ ratios lower than 0.9 may therefore be regarded as containing very little, if any, residual RNA or intact virions [Michels et al., 1999].

In our study, the efficiency of RNA removal from the HCRSV was determined by evaluating the UV spectra and $OD_{260\ nm}/OD_{280nm}$ ratios of the respective supernatants. Since there were 6 Trp and 7 Tyr units in the sequence of the HCRSV CP, the extinction coefficient (e) of the CP at 280 nm was taken to be 36 200 ml/mmol [Mach et al., 1992]. This value was used to determine the concentration of the purified CP in the supernatants.

2.3.3.2 Native gel electrophoresis

Native agarose gel electrophoresis [Newman et al., 2003] was used to analyze the electrostatic property of the HCRSV virions and CP. The CP and in *vitro* reassembled empty PC produced by the dialysis method, as well as the native HCRSV, were mixed with a loading buffer (60% sucrose solution) to give concentrations of about 1 mg/ml. About 10 μl of samples were loaded onto 1% agarose gel and subjected to electrophoresis at 5 V/cm for 1 h (Bio-Rad Sub-Cell electrophoresis system, CA, USA). The protein was stained with coomassie blue (0.0025%) followed by destaining overnight with a destaining buffer (5% acetic acid, 5% methanol).

2.3.3.3 Circular Dichroism (CD) spectroscopy

CD experiments were performed to study the conformational structure of the HCRSV CP. Samples including the native HCRSV, purified CP and *in vitro* reassembled PC were diluted in the re-suspension buffer to a final concentration of 0.1 mg/ml at ambient temperature. Analysis was performed in a CD spectrometer (Jasco J-815 spectropolarimeter, Tokyo, Japan) using a quartz cell with a 1 mm path length. Spectra were recorded with a 1.0 nm bandwidth and resolution of 0.1 nm over the wavelength range of 190 to 260 nm. The final spectra was averaged from 3 scans and subtracted from the solvent spectra. CD values were expressed as the mean residue ellipticity (θ).

2.3.3.4 Transmission Electron Microscopy (TEM)

The size and morphology of native HCRSV and reassembled PC were observed under a transmission electron microscope (TEM). Samples were diluted to 0.1 mg/ml with re-suspension buffer, and about 10 μl of dispersion was placed on a copper grid [Lee et al., 2003]. The samples were stained with 10 μl of 1% PTA solution, with excess PTA removed after 30 s by blotting. The grid was allowed to dry at ambient temperature before observation under a TEM (CM10; Philips Electronic Instruments, NJ, USA).

2.3.3.5 Zeta size and zeta potential analysis

Photon correlation spectroscopy (PCS), also referred to as dynamic light scattering and quasi-elastic light scattering [Goll and Stock, 1977; Huang et al., 2004], has been widely applied to measure the size of nanosized structures. It is applicable to particles of 1 to 5 000 nm which exhibit Brownian movement in a liquid. The pace of movement can be detected by analyzing the time dependency of the fluctuations in light intensity scattered from the particles when they are illuminated with a laser beam. The speed of movement is inversely proportional to particle size; the smaller the particles, the faster in movement or diffusion. Particle size of native HCRSV and PC was determined using a particle size analyzer based on the PCS principle (Zetasizer 3000HSA, Malvern Instruments Ltd., Worcestershire, England). Samples were diluted to about 0.1 mg/ml with distilled water and measured at room temperature.

Zeta potential can be determined by the electrophoretic mobility of charged particles. The surface charge may provide information on the stability of the particles since a

higher zeta potential [Yang et al., 2007] suggests stronger electrostatic repulsive forces between particles, and a lower risk of the particles aggregating. In this experiment, the zeta potentials of native HCRSV and the empty PC were determined by laser doppler velocimetry using the same particle size analyzer (Zetasizer 3000HSA) equipped with an electrophoresis cell. Samples were diluted to about 0.1 mg/ml with distilled water and measured at room temperature.

2.4 Results and discussion

2.4.1 Culture of plant and virus

The kenaf grew well under the specified controlled environment, taking about 2 to 3 weeks to grow to the stage of 4 to 5 leaves per plant. During plant growth, the temperature and lighting of the environment were tightly regulated, and all plants were protected from insects, unclean earth and strong winds. Kenaf with 4-5 leaves were inoculated with HCRSV by rubbing the leaves of the plant with a dispersion containing the virus and carborundum powder. Successful transfection was marked by the appearance of chlorotic ringspots, a classic symptom of plants infected with the HCRSV [Liang et al., 2002], on both the inoculated as well as new leaves about 10 days later (Figure 2-1). A previous study based on the ELISA assay has shown the HCRSV virus titre in the infected kenaf to fluctuate cyclically, reaching peak titres every 15 days [Lee et al., 2003]. Since 15 days were too short a period for the kenaf to grow an adequate number of leaves, HCRSV extraction was carried out on Day 30. Harvested leaves were either used at once or stored in a -80 °C freezer until use.

Figure 2-2 Kenaf leaves infected with the hibiscus chlorotic ringspot virus showing the characteristic chlorotic ringspots.

2.4.2 Purification and yield of HCRSV

HCRSV was successfully extracted and purified by a series of centrifugation and washing processes. The extraction buffer (pH 5.4) contained 20 mM of Ca^{2+} to stabilize the extracted virus particles [Lee et al., 2003]. Proteins, including the HCRSV, was isolated by precipitation with $(NH_4)_2SO_4$, followed by centrifugation. The pellet, resuspended in a sodium acetate buffer containing 1% of Triton, was ultracentrifuged on a 10% sucrose cushion to selectively sediment materials of high density. Impurities of lower density that could not penetrate the 10% sucrose cushion were discarded. The sample was further fractionated by subsequent ultracentrifugation on a 10 to 40% sucrose

gradient. HCRSV, as a RNA-containing capsid, was concentrated in the central portion of the sucrose gradient, and was clearly visible as a milky band when observed under a strong beam of light in a dark room.

The sucrose gradient was divided into 31 fractions for collection, and the HCRSV content in each fraction was determined by measuring the optical density of the CP at 260 nm (OD_{260nm}). As shown in Figure 2-2, the OD_{260nm} increased gradually from fraction 9 to reach a peak value in fraction 13 before declining to baseline level at fraction 22. This suggests that the HCRSV was concentrated in fractions 9 to 23 of the sucrose gradient. For subsequent batches of HCRSV, the virus band after collection was diluted with 3 to 4-fold its volume of resuspension buffer to bring the sucrose content to below 10% before it was ultracentrifuged to pellet the purified virus particles.

HCRSV yield was 4.6 ± 2.1 mg/100g leaves (n = 4), significantly lower than the reported yield of 50 – 70 mg/100 g leaves [Lee et al., 2003]. Even for subsequent batches of culture, in which there were overt symptoms of viral infection, the HCRSV yield from the kenaf leaves was no higher than 10 mg/ml. While the viral yield could be affected by a host of environmental factors, contamination by a virus that could not be separated from HCRSV by sucrose gradient ultracentrifugatin appeared to be the main contributing factor for the high yield of HCRSV reported in earlier studies [Doan et al., 2003; Lee et al., 2003].

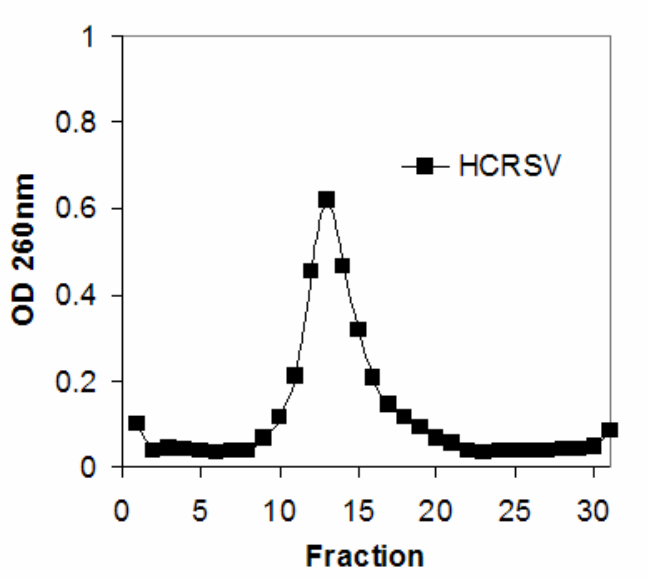

Figure 2-3. Isolation of HCRSV by sucrose gradient ultracentrifugation. The sucrose gradient after ultracentrifugation was divided into 31 fractions for analysis, the top fraction denoted as Fraction 1. HCRSV content was determined from OD_{260nm} measurement. Peak HCRSV concentration was found in Fraction 13.

Purity of virus yield was borne out by the $OD_{260\ nm}/OD_{280\ nm}$ ratio, a useful index for detecting contamination in a batch of virus. Each virus species has a $OD_{260\ nm}/OD_{280\ nm}$ ratio specific to the relative amounts of RNA and CP in its structure, and the ratio is altered in the presence of another virus with a different RNA : protein content. In our experiments, the purified HCRSV had consistent $OD_{260\ nm}/OD_{280\ nm}$ ratios of 1.55 ± 0.01 (n = 4). While the $OD_{260\ nm}/OD_{280\ nm}$ ratio for purified HCRSV was not known with certainty, this value was considerably lower than the $OD_{260\ nm}/OD_{280\ nm}$ ratio of 1.74 previously reported for the HCRSV suspected to be contaminated with another virus [Lee et al., 2003; Doan et al., 2003].

2.4.3 Cytotoxicity of HCRSV

In vitro cytotoxicity of HCRSV in the concentration range of 1 ng/ml to 1 mg/ml was evaluated by the MTT assay. Three human cell lines were employed, the CNE-1 and OVCAR-3 representing cancer cells, and the CCL-186, normal cells. Dextran and SDS at 0.1% w/v served as negative and positive controls, respectively. Cell viability was not significantly reduced for all 3 cell lines following incubation for up to 3 days with the HCRSV at all the concentrations evaluated, suggesting that the plant virus was not cytotoxic against any of the human cell lines studied (Figure 2-4). These results are in agreement with the general consensus that plant virus generally lacks the ability to enter, multiply and transfect animal cells. The HCRSV-derived PC may therefore be regarded as a potentially safe platform for drug delivery in animals and humans.

2.4.4 RNA removal and reassembly of PC

Urea, a strong reagent which can unfold and destroy the conformational structures of most proteins, has been used to promote the disassembly of virus particles [Michels et al., 1999]. Protein denaturation was applied in this study by incubating the HCRSV with 8 M of urea. The native RNA was discarded via centrifugation, and the purified CP was reassembled into viral-like particles by dialysis against a sodium acetate buffer. Successful RNA removal was reflected in a much lower mean $OD_{260\ nm}/OD_{280\ nm}$ ratio of 0.7 ± 0.1 ($n = 3$) obtained for the resultant dispersion. The $OD_{260\ nm}/OD_{280\ nm}$ values correlated with those obtained in another study that employed urea to separate the RNA from the CP of the *Turnip yellow mosaic virus* [Michels et al., 1999].

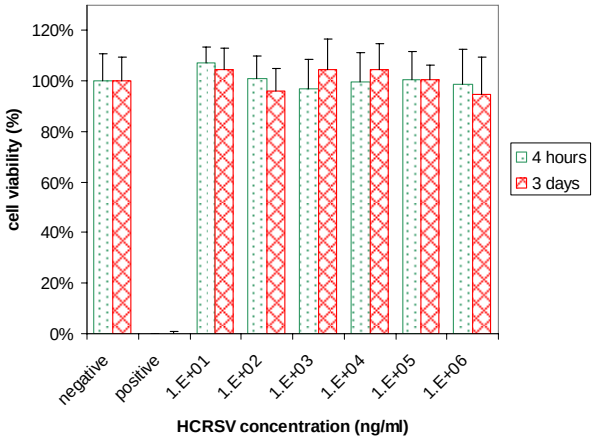

(a)

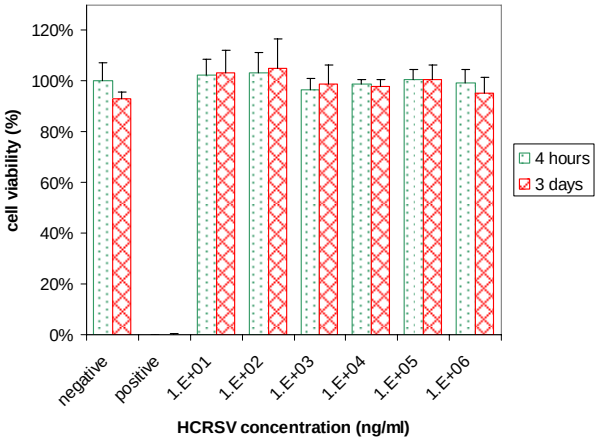

(b)

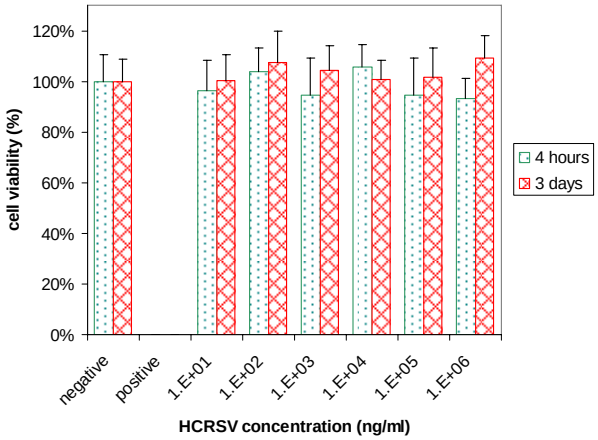

(c)

Figure 2-4 Cell viability of (a) CCL-186, (b) OVCAR-3 and (c) CNE-1 cells as measured by the MTT assay following incubation for 4h and 3 days with HCRSV of different concentrations. Negative control (negative) was dextran; positive control (positive) was SDS.

Urea was, however, a strong reagent that could destroy the conformation of the HCRSV CP. By comparison, dialysis offered milder processing conditions. Dialysis of HCRSV was initially conducted against a Tris buffer of pH 7.5 (50 mM, 1 mM EDTA, 1 mM DTT, 0.5 mM PMSF, 0.5 M $CaCl_2$), as this buffer has been reported to be effective for the removal of the CCMV RNA from its capsids [Zhao et al., 1995; Fox et al., 1998]. However, the dialysis did not produce a change in the OD_{260nm}/OD_{280nm} ratio for the HCRSV dispersion, which retained a value of 1.5 after treatment, indicating that the RNA was not efficiently removed. A survey of the literature suggested that pH and Ca^{2+} were important factors. Plant viruses could be made to swell at pH higher than 6.5 [Douglas and Young, 1998] but capsid disassembly might require higher pH [Fox et al., 1998]. Ca^{2+} was necessary for the reassembly of CP into capsids, but the swelling and disassembly of virus particles may require an absence of Ca^{2+} [Fox et al., 1998; Morgunova et al., 1993]. On this basis, Tris buffers having pH of 7 – 8, with and without 0.5 M $CaCl_2$, were prepared for the dialysis of the HCRSV (Table 2-1). The effectiveness of each buffer was determined by measuring the OD_{260nm}/OD_{280nm} ratio of the dispersion obtained after the CP had been isolated from the RNA, and reassembled by dialysis against a sodium acetate buffer (Table 2-3). Of the 6 buffers employed, the most effective was buffer 6 (pH 8.0, without $CaCl_2$), which resulted in the lowest OD_{260nm}/OD_{280nm} value of 0.6. Further evidence was obtained by adding $CaCl_2$ to the dialyzate as Ca^{2+} could neutralize and precipitate the freed viral RNA. Precipitation was observed upon the addition of 0.5 M of $CaCl_2$ to samples dialyzed against buffer 6, but not in those dialyzed against the other 5 buffers. The collective results suggested that HCRSV capsid

disassembly occurred in the absence of Ca^{2+} at a pH higher than that reported for the disassembly of CCMV.

	pH 7.0	pH 7.5	pH 8.0
With 0.5 M $CaCl_2$	1.5	1.5	1.6
No $CaCl_2$	1.5	1.6	0.6

Table 2-3. OD_{260nm}/OD_{280nm} values of HCRSV dispersions obtained by dialysis against different Tris buffers, followed by RNA removal by centrifugation and coat protein reassembly by dialysis against a sodium acetate buffer. Tris buffers having pH in the range of 7.0 to 8.0 were prepared in the presence or absence of 0.5 M $CaCl_2$.

2.4.5 UV spectroscopy

The UV spectra of purified CP obtained by urea incubation and dialysis are shown in Figure 2-4 b and c. Compared with the UV spectrum of native HCRSV (Figure 2-5 a), the spectra for the CP showed a shift in the absorption peak from 260 to 280 nm, which reflected a change from RNA- to protein-dominated UV absorption in the sample. This shift, together with the low OD_{260nm}/OD_{280nm} values (0.6 - 0.7), was taken as evidence that the viral RNA was successfully removed from the HCRSV following urea incubation or dialysis against a Tris buffer (pH 8, no Ca^{2+}).

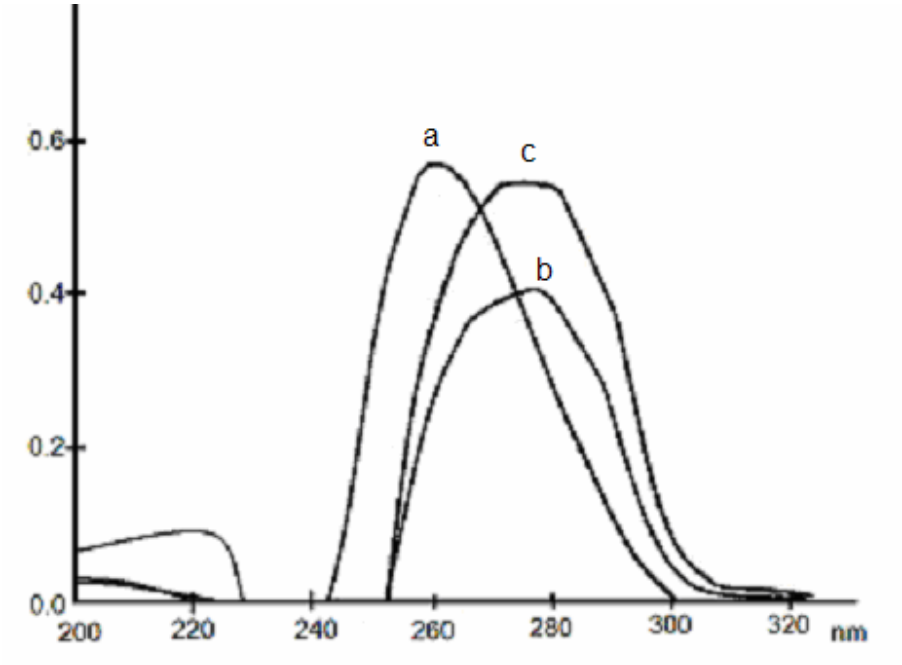

Figure 2-5 UV spectra of (a) HCRSV, (b) coat protein purified by urea incubation method and (c) coat protein purified by dialysis against a pH 8.0 Tris buffer devoid of $CaCl_2$.

2.4.6 Native gel electrophoresis

Native agarose gel electrophoresis has been used to analyze the conformational structure of proteins and viruses [Kim et al., 2000; Newman et al., 2003] because it does not employ protein denaturation reagents, and can thus reflect the size as well as electrostatic properties of these samples. Figure 2-5 shows the results of native gel electrophoresis of HCRSV, the purified CP and reassembled empty PC obtained from HCRSV by the dialysis method.

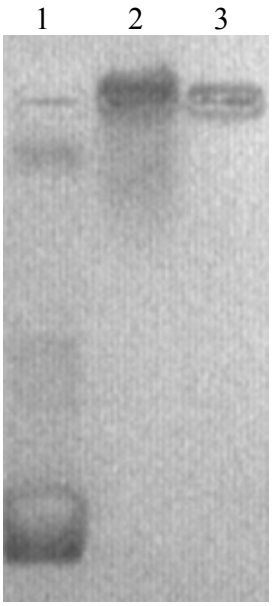

Figure 2-6. Native agarose gel electrophoresis of HCRSV (line 1), CP produced by dialysis method (line 2) and *in vitro* reassembled empty PC produced by the dialysis method (line 3).

Following gel electrophoresis, the HCRSV migrated in the direction of the anode, suggesting a net negative charge, while the reassembled empty PC remained at the site of application, which was indicative of neutrality under the electrophoresis pH of 7.5. Analyses by other techniques (sections 2.4.7 to 2.4.9) had suggested that the PC resembled the HCRSV in size, morphology and protein conformation. Thus, the differences in net charge between the two species could be attributed to the lack of a viral RNA in the PC sample, as the phosphate acid groups of the viral RNA would contribute negative charges to the capsid [Schaldach et al., 2005]. On this basis, it was not surprising that the purified CP also remained at the site of application following gel electrophoresis. There was, however, evidence of some migration, which might be attributed to the smaller size of the CP. By comparison, the reassembled PC would be a

large moiety comprising of 180 copies of the CP if it truly resembled the native HCRSV capsid. These data indirectly confirmed the successful removal of viral RNA from the HCRSV by the dialysis method.

2.4.7 Circular dichroism (CD) spectrum

Circular dichroism (CD) is observed when an optically active compound absorbs left- and right-handed circularly polarized light at different extents. It is a rapid and convenient method for characterizing the secondary structures of peptides and proteins. CD signals in the far UV region (180 ~ 260 nm) reflect peptide bond absorption, which is useful for predicting the secondary structures of proteins and peptides [Greenfield, 1996; Maruyama et al., 1986]. A typical CD spectrum for a protein bearing the β-sheet conformation is a characteristic valley at 215 nm.

Each HCRSV CP contains two β-sheets. One is in the shell-forming domain and the other is in the protruding domain [Doan et al., 2003]. The native conformational structure of the CP is, however, susceptible to harsh processing conditions, and the loss of conformational structure can result in a failure of the CP to reassemble into virions. For this reason, CD experiments were carried out to determine whether the native conformational structure of the HCRSV CP was maintained after the processes of purification, extraction, disassembly and reassembly.

As shown in Figure 2-6, the HCRSV showed a typical minimum at 215 nm, suggesting the existence of β-sheet structure. The purified CP, whether obtained by urea incubation or dialysis, also showed a minimum, though of lesser intensity, around the

same wavelength. Similarly, a valley at 215 nm was observed in the CD spectrum of the empty PC reassembled from CP obtained by dialysis. Collectively, the data indicated that the processes of extraction, purification and reassembly did not destroy the protein conformational structure of the HCRSV CP and PC.

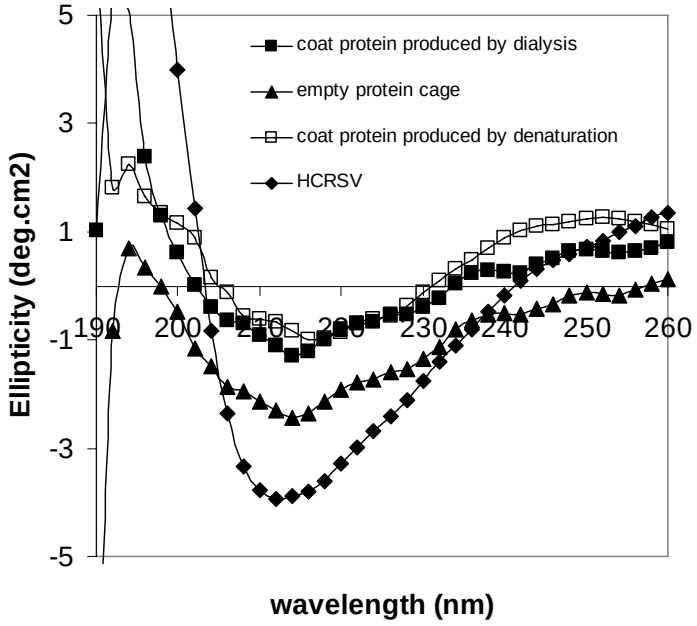

Figure 2-7. CD spectra of HCRSV virions, coat proteins obtained by dialysis and urea incubation, as well as empty PC reassembled from coat protein obtained by the dialysis method.

2.4.8 Morphology of HCRSV and reassembled PC

Viewed under the TEM, the purified HCRSV appeared as uniformly sized spherical particles with diameter of about 30 nm (Figure 2-7a), which corresponded well with the description of HCRSV reported in another study [Doan et al., 2003]. Figures 2-7 b and c

show the TEM micrographs of PC reassembled from purified HCRSV CP obtained by urea incubation and dialysis, respectively. Both PC appeared as spherical particles with comparable diameter and morphology as the native HCRSV, suggesting that the CP could reassemble *in vitro* into empty PC that resembled the native HCRSV. This capacity for *in vitro* reassembly was similar to that observed for the CCMV CP [Douglas and Young, 1998]. A comparison of Figures 2-7 b and c indicated that the CP produced by the dialysis method yielded better quality PC, in terms of size uniformity and well-defined morphology, than the CP produced by urea incubation. For this reason, the dialysis method was used to prepare subsequent batches of HCRSV-derived PC for further experimentation.

2.4.9 Zeta size and zeta potential

The HCRSV virion and empty PC had similar mean sizes of about 50 nm when measured by the zeta sizer. These values, which reflected the hydrodynamic volumes of the particles, were larger than those observed under the TEM. While size analysis by the TEM was dependent on the electron cloud density of the samples, the hydrodynamic volume included the adsorbed layer of counterions and water molecules, and would tend to yield larger values. The zeta potential of HCRSV was around -2.5 mV, the negative charge corresponding with the gel electrophoresis results. In contrast, the reassembled empty PC derived from HCRSV had zeta potential of $+1.4 \pm 0.1$ mV, the positive charge reflecting the absence of RNA in the particles. Thus, the zeta potential values provided yet additional evidence that the viral RNA was successfully removed from the capsids.

The zeta size, on the other hand, indicated that the CP had reassembled into empty PC that were of comparable size to the native HCRSV.

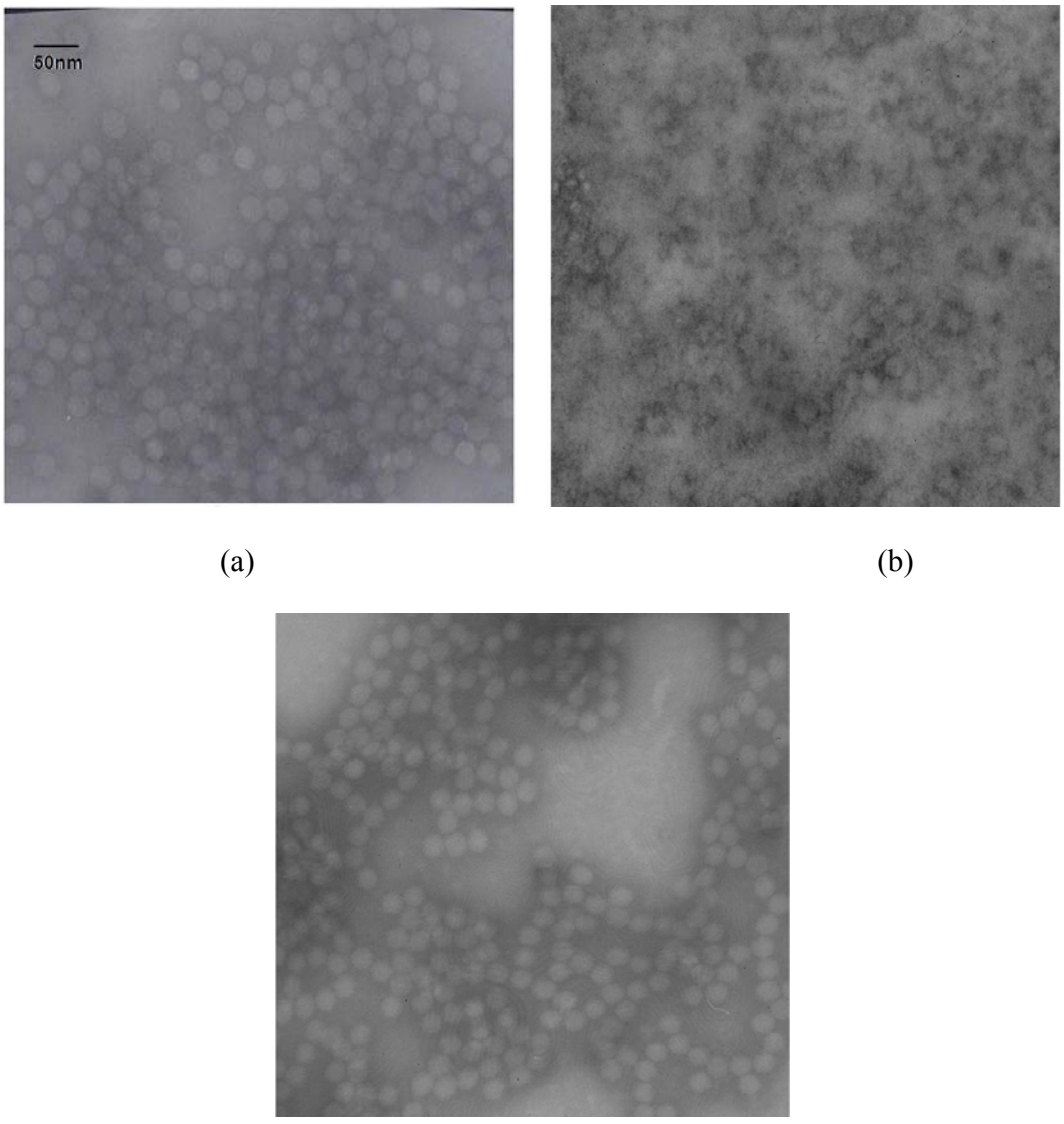

(a) (b)

(c)

Figure 2-8. TEM photos of (a) native HCRSV, (b) empty PC reassembled from coat protein produced by urea incubation method and (c) empty PC reassembled from coat protein produced by dialysis method.

	HCRSV	Empty PC
Diameter (nm)	44 ± 2	46 ± 8
Zeta Potential (mV)	-2.4 ± 0.2	1.4 ± 0.1

Table 2-4. Mean size and zeta potential of native HCRSV and empty PC prepared by the dialysis method (Mean ± SD, n = 3).

2.5 Conclusion

HCRSV was successfully cultured in kenaf leaves and efficiently purified by serial centrifugations on sucrose gradients to give a reproducible yield of 4 to 5 mg of purified HCRSV per 100 g of leaves It was therefore possible to obtain a stable source of HCRSV for subsequent experimentation using the kenaf culture. MTT assay suggested that the HCRSV was not cytotoxic against the human derived CCL-186, OVCAR-3 and CNE-1 cells following incubation for up to 3 days at concentrations as high as 1 mg/ml.

HCRSV RNA was successfully isolated from the CP either by incubation with 8 M of urea or dialysis against a Tris buffer of pH 8 in the absence of Ca^{2+}. The purified CP could reassemble into empty PC by dialysis against a sodium acetate buffer of pH 5 in the presence of Ca^{2+}. The empty PC were comparable to the native HCRSV in size, morphology, and protein conformation. However, PC assembled from CP obtained by the milder dialysis method were more uniform in size and better defined in morphology than those derived from CP obtained by urea incubation. Thus, the dialysis method was deemed to be an appropriate method for producing subsequent batches of HCRSV-derived CP and PC.

Chapter 3

Preparation and characterization of HCRSV-derived PC for drug delivery

3.1 Introduction

Plant viruses may be induced to undergo conformational changes, such as swelling or disassembly, under a specific environment. For instance, viruses that are stable at low pH, such as the *tomato bushy stunt virus* [Perez et al., 2000], CCMV [Tama and Brooks, 2002] and TCV [Sorger et al., 1986], have been shown to undergo radial expansion at high pH. The swelling creates pores or openings on the surface of the viruses and, in some cases, may result in the disassembly of the virus particles [Fox et al., 1998]. The CP that are isolated from the disassembled virus particles can subsequently be made to reassemble *in vitro* to form empty PC [Bancroft et al., 1968] that are identical in structure to the capsids of the native viruses [Fox et al., 1998]. The empty PC of CCMV so assembled have been shown to be capable of encapsulating a host of guest ions and molecules, such as the paratungstate ion ($H_2W_{12}O_{10}^{-42}$), decavanadate ion ($V_{10}O_6^{-28}$), polyanetholesulfonic acid [Douglas and Young, 1999] and gold [Chen et al., 2006]. The guest compounds did not appear to significantly alter the morphology and size of the PC, which retained similar dimensions to the native virus. Empty plant virus-derived PC may therefore have the potential to provide constrained environments for drug delivery. The monodispersity of these particles, along with their nanosized dimensions, adds to their advantages for drug delivery applications.

The model virus in this project, the HCRSV, is a member of the genus *Carmovirus* in the *Tombusviridae* family of plant viruses [Huang et al., 2000; Liang et al., 2002]. The native virus is 30 nm in diameter [Lee et al., 2003], has a 4 kb genomic RNA and a capsid comprising of 180 CP subunits, each of which has mw approximately 37 kDa [Ke

et al., 2004; Lee , et al., 2003]. Preliminary experiments (Chapter 2) had shown it was possible to separate the RNA from the CP, and to subsequently reassemble the CP *in vitro* into empty HCRSV-like PC. This chapter explores the feasibility of encapsulating guest compounds into the nanosized inner cavity of the HCRSV-derived PC. Different types of guest compounds were used to evaluate the effect of charge, mw and chemical group on the loading capability of the PC. FITC-dextrans (FD, mw of 4, 10, 75 and 150 kDa) were used as neutral guest molecules (Figure 3-1, a) while polystyrenesulfonic acid (PSA), a strong acid with multiple sulfonic acid groups (mw range of 1.4 to 990 kDa, Figure 3-1, b), served as negatively charged molecules. Polyacrylic acid (PAA), a weak acid with multiple carboxylic acid groups (Figure 3-1, c), was also used in order to evaluate the effect of different acid groups on the loading capacity of the HCRSV-derived PC.

As the ultimate objective of this project was to formulate a targeting system for anticancer drug delivery, this chapter also explored the feasibility of conjugating the folic acid molecule as a targeting ligand for the HCRSV-derived PC. Folic acid was conjugated onto the CP of native HCRSV particles by a 2-step carbodiimide crosslinking reaction before RNA removal. The experiments in this chapter evaluated the effects of folic acid conjugation on the capacity of the HCRSV-derived PC to load PSA and PAA.

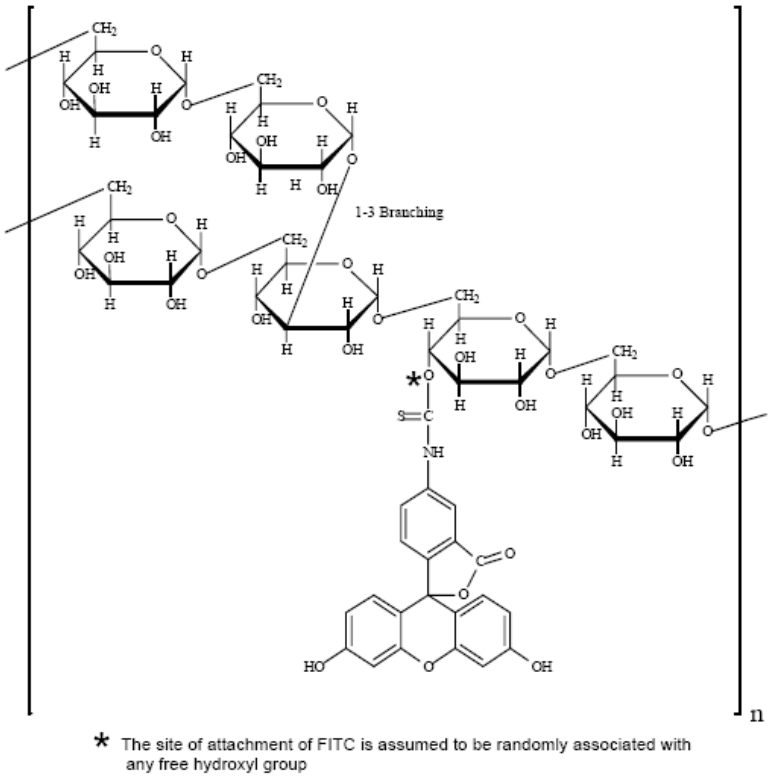

(a)

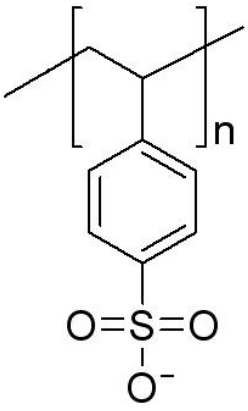

(b)

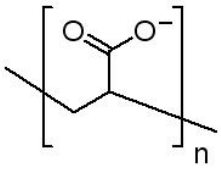

(c)

Figure 3-1. Structures of guest molecules used for the evaluation of the loading capacity of HCRSV-derived protein cages. (a) FITC-dextran (FD), (b) polystyrenesulfonic acid (PSA) and (c) polyacrylic acid (PAA).

3.2 Materials

Methanol was from BDH Ltd (Poole, England). Polystyrenesulfonic acid (PSA) (mw of 1.4, 4.3, 13, 75, 200 and 990 kDa), polyacrylic acid (PAA) (mw of 450 kDa), FITC-dextran (FD) (mw of 4, 10, 75 and 150 kDa), 1-Ethyl-3-[3-dimethylaminopropyl] carbodiimide hydrochloride (EDAC) and N-hydroxysuccinimide (NHS) were from Sigma Chemical Co. Buffer solutions included buffer A (50 mM NaOAc, 50 mM NaCl, 2 mM EDTA, 20 mM $CaCl_2$, pH 5.0), buffer B (Tris buffer made up with 50 mM of Tris, 2 mM of DTT, 0.2 mM of PMSF, and 5 mM of EDTA, pH 8.0) and buffer C (Tris buffer made up with 50 mM of Tris, 2 mM of DTT, 0.2 mM of PMSF, 5 mM of EDTA, and 1 M of NaCl, pH 8.0). All other materials and buffer solutions were the same as those listed in section 2.2.

3.3 Methods

For simplicity of description, HCRSV-derived PC loaded with FD, PSA and PAA are denoted as PC-FD, PC-PSA and PC-PAA, respectively. The mw of the cargoes in kDa are placed before their names, e.g. PC loaded with PSA of 13 kDa is denoted as PC-13PSA. Folic acid-conjugated PC is denoted as fPC, and the related products are known as fPC-PSA and fPC-PAA.

3.3.1 Preparation of PC loaded with guest molecules

The HCRSV CP was purified by the dialysis method as described in section 2.3.2.2. In brief, the HCRSV solution was dialyzed against the Ca^{2+}-free buffer B overnight, and

incubated with 0.5 M of $CaCl_2$ for 30 min at 4 °C. The viral RNA was removed by centrifugation at 25 000 *g*, 4 °C for 30 min and the CP in the supernatant was used for loading guest molecules. Loading was effected by dialyzing the CP solution (0.5 ml) against buffer C for 4 h, followed by incubation of the CP (1 mg/ml) with FD (2:1 w/w), PSA (3:1 w/w) or PAA (3:1 w/w) in buffer C for 8 h at 4 ^{o}C. The resultant samples were dialyzed against 500 ml of buffer A for 15 h at 4°C to reassemble the CP into PC.

3.3.2 Preparation of fPC loaded with guest molecules

The carbodiimide coupling method involving EDAC and NHS was used to conjugate the folic acid onto the HCRSV capsids [Reddy et al., 2001; Drabick et al., 1998; Stella et al., 2000; Zhang et al., 2004; Bharali et al., 2005]. EDAC is a zero-length crosslinking agent widely employed for the coupling of carboxyl groups to primary amines (Figure 3-2). EDAC has been used in diverse applications, such as peptide synthesis and the attachment of haptens to carrier proteins to form immunogens [Drabick et al., 1998]. In these reactions, the amine-reactive O-acylisourea intermediate is highly susceptible to hydrolysis. To extend the half-life of the intermediate in aqueous solutions, NHS is often added to convert the intermediate to an amine-reactive sulfo-NHS ester. The latter possesses sufficient stability to permit the crosslinking reaction to proceed, the two-step procedure significantly increasing the efficiency of EDAC-mediated coupling reactions [Zhang et al., 2004; Grabarek and Gergely, 1990; Staros et al., 1986].

For this project, 5 mg of folic acid, 50 mg of EDAC and 50 mg of NHS were dissolved in 50 ml of bicarbonate buffer (50 mM $NaHCO_3$, pH 6) at ambient temperature.

The reaction mixture was incubated with 5 mg of HCRSV at 4 ^{o}C for 8 h, then concentrated to about 0.5 ml by ultrafiltration (Amicon Ultra-15 filter device, mw cut-off 10 000, Millipore, MA, USA) and washed thrice with 10 ml of resuspension buffer (section 2.2) to remove the unreacted materials. Dialysis against a Tris buffer (pH 8, without Ca^{2+}), as described in section 2.3.2.2, was employed to remove the viral RNA and purify the CP. The conjugated folic acid in a sample was quantified based on $OD_{360\ nm}$ measurements using an extinction coefficient of 5312 $mol^{-1}cm^{-1}$ (Beckman Du 640B spectrometer, CA, USA) [Stella et al., 2000; Zhang et al., 2004; Shinoda et al., 1998; Dube et al., 2002]. The conjugation efficiency was defined as the weight ratio of folic acid to CP, the protein content of a sample being determined by the biscinchoninic acid assay (BCA) according to the manufacturer's directions (Section 3.3.3.2 B) [Smith et al., 1985]. Reassembly of the purified folic-acid conjugated CP into PC, with simultaneous loading of FD, PSA and PAA, were also conducted using methods similar to those described in section 3.3.1 for the unconjugated CP.

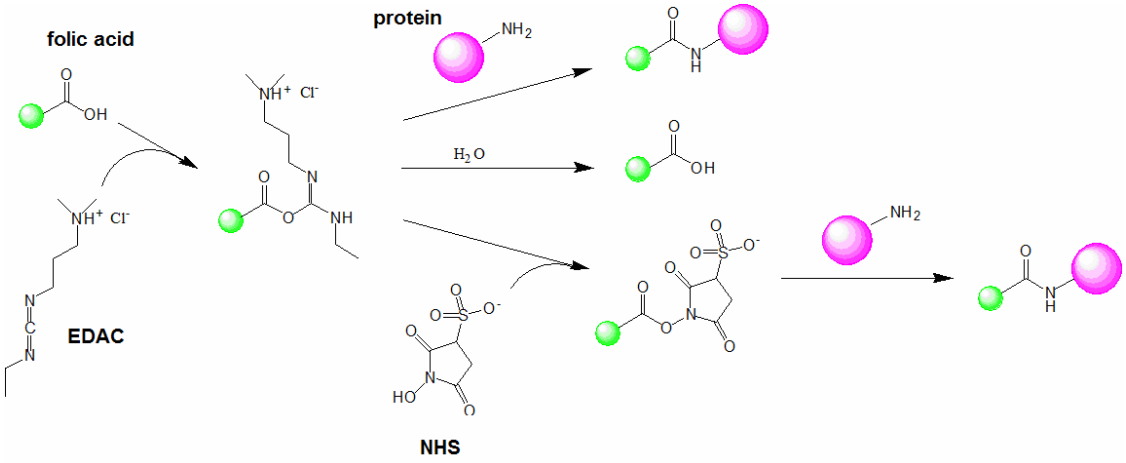

Figure 3-2. Reaction scheme for folic acid conjugation to HCRSV particles by the two-step carbodiimide method.

3.3.3 Characterization

3.3.3.1 Sucrose gradient centrifugation

Sucrose gradient centrifugation was used as the technique for determining whether the guest molecules had been successfully loaded into the PC and fPC. The samples were put on 10-40% sucrose gradients (9 cm in height) and centrifuged for 3 h at 27 000 rpm, 4 °C using the SW41 rotor. Control samples, which consisted of 1 mg/ml of FD, PSA, HCRSV, CP, empty PC or mixtures of empty PC and polyacid in buffer A, were similarly subjected to the sucrose gradient separation. Fractions of the sucrose gradient were collected and analyzed. FD samples were assayed by measuring the fluorescence of each fraction at $\lambda_{ex\ 485\ nm}$ and $\lambda_{em\ 535\ nm}$ (TECAN SpectraFluor). The optical density of HCRSV and PSA samples was determined at 260 nm and 262 nm, respectively, while those of CP, empty PC and PAA were determined at 280 nm (Beckman Du 640B spectrophotometer). Fractions that tested positive for the respective cargo were collected and diluted with up to 4 times their volume with buffer A. The solutions were concentrated to 0.5 ml by ultrafiltration before being used for further analysis.

3.3.3.2 Loading efficiency

The dual wavelength method and BCA-UV method were used to quantify the amount of PSA loaded in the PC. The loading efficiency was calculated on the basis of loaded PSA weight to CP weight in the system. These methods were, however, not applied to the calculation of the loading efficiency of fPC-PSA because of interferences among the UV spectra of folic acid, PSA and CP.

(A) Dual wavelength method

PSA loaded in the PC was quantified by dual-wavelength UV spectroscopy [Szabo and Maguire, 1993] on the basis that PSA showed maximum absorption at 262 nm while the PC had maximum absorption at 280 nm. PC-PSA samples were purified by sucrose gradient centrifugation, and the optical density of pooled sucrose gradient fractions containing the PC-PSA was measured at these two wavelengths. The respective optical density was expressed in the form of equations (3-1) and (3-2).

$$OD_{262\ nm} = OD_{262\ nm,\ PSA} + OD_{262nm,\ PC} \quad (3\text{-}1)$$

$$OD_{280\ nm} = OD_{280\ nm,\ PSA} + OD_{280\ nm,\ PC} \quad (3\text{-}2)$$

From the spectra of pure PSA and purified PC, equations (3-3) and (3-4) were obtained.

$$OD_{262\ nm,\ PSA} = 5.0 \times OD_{280\ nm,\ PSA} \quad (3\text{-}3)$$

$$OD_{262\ nm,\ PC} = 0.66 \times OD_{280\ nm,\ PC} \quad (3\text{-}4)$$

The 4 equations were rearranged to give equations (3-5) and (3-6), from which the absorption of PSA at 262nm and that of PC at 280nm were calculated.

$$OD_{262\ nm,\ PSA} = 5.0 \times (OD_{262\ nm} - 0.66 \times OD_{280\ nm}) / 4.34 \quad (3\text{-}5)$$

$$OD_{280\ nm,\ PC} = OD_{280\ nm} - (OD_{262\ nm} - 0.66 \times OD_{280\ nm}) / 4.34 \quad (3\text{-}6)$$

Calibration plots of PSA (concentration vs $OD_{262\ nm,\ PSA}$) were obtained over the concentration range of 0.02 mg/ml to 0.2 mg/ml. Standard solutions were prepared by dissolving PSA in buffer A that contained PC at 5 times the weight of PSA. The concentration of PC in test samples was calculated by using equation (3-7)

$$C_{PC\ (mg/ml)} = OD_{280\ nm,\ PC} \times 36971 / e \quad (3\text{-}7)$$

where the extinction coefficiency (e) was calculated as 41760 ml/mmol based on its amino acid sequence [Mach et al., 1992]. PSA loading efficiency was calculated as the percent weight of loaded PSA relative to the weight of PC, and this was transformed into the number of PSA molecules loaded in each PC (n) by using the equations (3-8) and (3-9).

$$\text{Loading efficiency (\%)} = C_{PSA} / C_{PC} \times 100\% \quad (3\text{-}8)$$

$$n = \text{Loading efficiency} \times 36\,971 \times 180 / mw_{PSA} \quad (3\text{-}9)$$

(B) BCA-UV method

In the BCA-UV method, the concentration of PC was quantified using the BCA protein assay kit according to the manufacturer's instructions [Smith et al., 1985]. The principle underlying the assay is illustrated as follows:

1. Protein (peptide bonds) + Cu^{2+} ——→ tetradentate-Cu^{1+} complex

2. Cu^{1+} complex + BCA ——→ BCA-Cu^{1+} complex

A working solution was prepared by mixing 25 parts of solution A (sodium carbonate, sodium bicarbonate and sodium tartrate in 0.2 N NaOH), 24 parts of solution B (4% BCA in water) and 1 part of solution C (4% cupric sulfate pentahydrate in water). The calibration curve was obtained by incubating 1 ml of working solution with 1 ml of CP solution (concentration ranging from 2 to 40 μg/ml) at 37 °C for 2 h, followed by cooling to room temperature over 20 min, and measuring the absorbance of the samples at 595 nm. The equipment (TECAN fluorimeter) was calibrated with CP standard solutions (Appendix I). The concentration of PSA was measured by UV absorption at 262 nm after

compensating for the contribution of the PC using equation (3-4) and (3-1). Loading efficiency and the number of PSA molecules loaded in each PC were calculated using equations (3-8) and (3-9), respectively.

3.3.3.3 Other characterization techniques

PSA- and PAA-loaded PC were purified by sucrose gradient centrifugation. Fractions containing the PC were pooled together, washed by ultrafiltration with 3 to 4 fold their volumes of buffer A and concentrated to less than 1 ml. Morphology of the particles were observed under the TEM using the method described in section 2.3.3.4. Conformational structures were analyzed by circular dichroism (CD) spectroscopy using the same protocols described in section 2.3.3.3. For the determination of size and zeta potential, the samples were diluted to ~0.1 mg / ml with distilled water and analyzed in a particle sizer as described in chapter 2.3.3.5. For the native agarose gel electrophoresis experiments, the samples were diluted with loading buffer (60% sucrose solution) to about 1 mg/ml and analyzed using the conditions described in section 2.3.3.2.

3.4 Results and discussion

3.4.1 PC loaded with guest molecules

PC loaded with PSA were screened at 262 nm, which corresponded to the λ_{max} of PSA. When subjected to sucrose-gradient centrifugation, free PSA molecules at all mw used were concentrated in fractions collected from the top of the gradient. For the PC

loaded with PSA of 1.4 kDa (PC-1.4PSA), the $OD_{262\ nm}$ values for fractions collected from the top of the sucrose gradient were above baseline levels (Figure 3-3 a), suggesting that the PSA in the sample was predominantly in the free form. For the PC-4.3PSA, the $OD_{262\ nm}$ value was found to decline gradually from the top fraction. The trailing $OD_{262\ nm}$ suggests a poor retention of the loaded PSA, which was probably released and deposited into the various fractions during the centrifugation process. In contrast, the $OD_{262\ nm}$ profiles of PC-PSA loaded with PSA ≥ 13 kDa typically showed a maximum value for fractions near the middle of the gradient, usually centred on fraction 12, which corresponded to fractions that would contain the PC (Figure 3-3 b). Low $OD_{262\ nm}$ values were observed for fractions located at the top of the sucrose gradient. In addition, fractions with high $OD_{262\ nm}$ values also had $OD_{262\ nm}/OD_{280\ nm}$ ratio greater than 1.0, indicating a high PSA to CP content. Based on these results, it is evident that the larger PSA molecules were more successfully loaded in the HCRSV-derived PC than the smaller PSA molecules, a phenomenon that might be attributed to the poor retention of the smaller PSA molecules within the PC. On the basis of their morphology and size, the PC were expected to be similar structurally to the native HCRSV in having nanoscale cavities in the viral shell [Doan et al., 2003; Douglas & Young, 1998]. A cargo of small molecules, like the 1.4 kDa PSA, might be efficiently loaded into the PC, but these would diffuse readily across the cavities and be poorly retained within the PC upon dilution. Conversely, PSA molecules of 13 kDa or greater that were too large to pass through the cavities were effectively retained within the PC even after sucrose density gradient centrifugation. The partial retention of the 4.3 kDa PSA in the PC following sucrose-

density gradient centrifugation suggests that the mw of these PSA molecules was close to the passage limit of the cavities.

One PAA sample of mw 450 kDa was loaded into the PC. Compared with PSA, which contained strong sulfonic acid groups (pKa < 1), PAA contained weaker carboxylic acid groups (pKa ~ 4.5) that would become partially ionized at pH 5. The PC-PAA had a sucrose gradient separation profile similar to those observed for the PC-PSA samples, in that the $OD_{280\ nm}$ value measured for fractions located at the top of the sucrose gradient was minimal, but it increased to a maximum value in the fraction near the middle of the gradient, centering on fraction 11 (Figure 3-3, c). This suggests that different types of polyacids could be loaded into the PC. In addition, for both the PC-PSA (≥ 13 kDa) and PC-PAA samples, the fraction with maximum absorbance corresponded to the fraction with maximum native HCRSV (Figure 2-3), suggesting that these cargo-loaded PC were comparable in size and density to the native virus.

In contrast, all samples in which the neutral FD (4–150 kDa) was mixed with the CP for reassembly into PC-FD showed strong fluorescence only in those fractions located at the top of the sucrose gradient, at positions corresponding to the respective controls of free FD (Figure 3-3, d). Negligible fluorescence was detected in the middle fractions collected from the sucrose gradient, suggesting that the FD was not loaded into the PC. This failure to load might be attributed to the FD not being encapsulated when the CP reassembled into PC, or to the entrapped FD being poorly retained within the PC after being subjected to sucrose gradient centrifugation. The former hypothesis appears more likely because two of the FD samples (75 and 150 kDa) were of higher mw than the successfully loaded 13-kDa PSA molecules. If they were successfully encapsulated

within the PC, they would have been effectively retained upon dilution because their large size would limit loss through the cavities in the PC. Since FD did not contain ionizable groups and was neutral at the loading pH, the failure to encapsulate FD suggests that electrostatic interaction may be necessary for cargo encapsulation during CP reassembly. This is in agreement with previous findings that the amino acid groups in the interior of a plant virus capsid play an important role in material loading [Douglas and Young, 1998; Douglas and Young, 1999]. In the case of HCRSV, the positively charged Arg and Lys moieties located at the N terminus of the CP would render the inner cavity of the PC attractive for the binding of negatively charged compounds. This has been aptly demonstrated by the successful loading of polyacids during CP reassembly.

Two lines of evidence affirmed that the polyacids were encapsulated within the cavity of the PC rather than adsorbed or conjugated onto the PC surface. The first evidence was the negligible encapsulation of polyacids with low mw. Had the polyacids been bound onto the surface of the PC, the reaction would proceed even with smaller sized polyacids. The other evidence was the failure to load the guest molecules in control experiments in which the reassembled PC were incubated with either PSA (13 to 990 kDa) or PAA (450 kDa) (data presented in Appendix II). If the polyacid molecules were bound to the surface of the PC, loading should be facilitated with preformed PC. However, for the polyacids to be encapsulated within the cavity of the preformed PC, the molecules must enter the PC through the surface cavities and be effectively retained upon dilution. This would be difficult to achieve, for small molecules that could permeate the cavities during loading would not be efficiently retained upon dilution, while larger polyacids that might be efficiently retained would not be able to enter the cavities for successful loading in the

first place. On the basis of these evidences, it may be concluded that both PSA and PAA were loaded into the PC during CP reassembly.

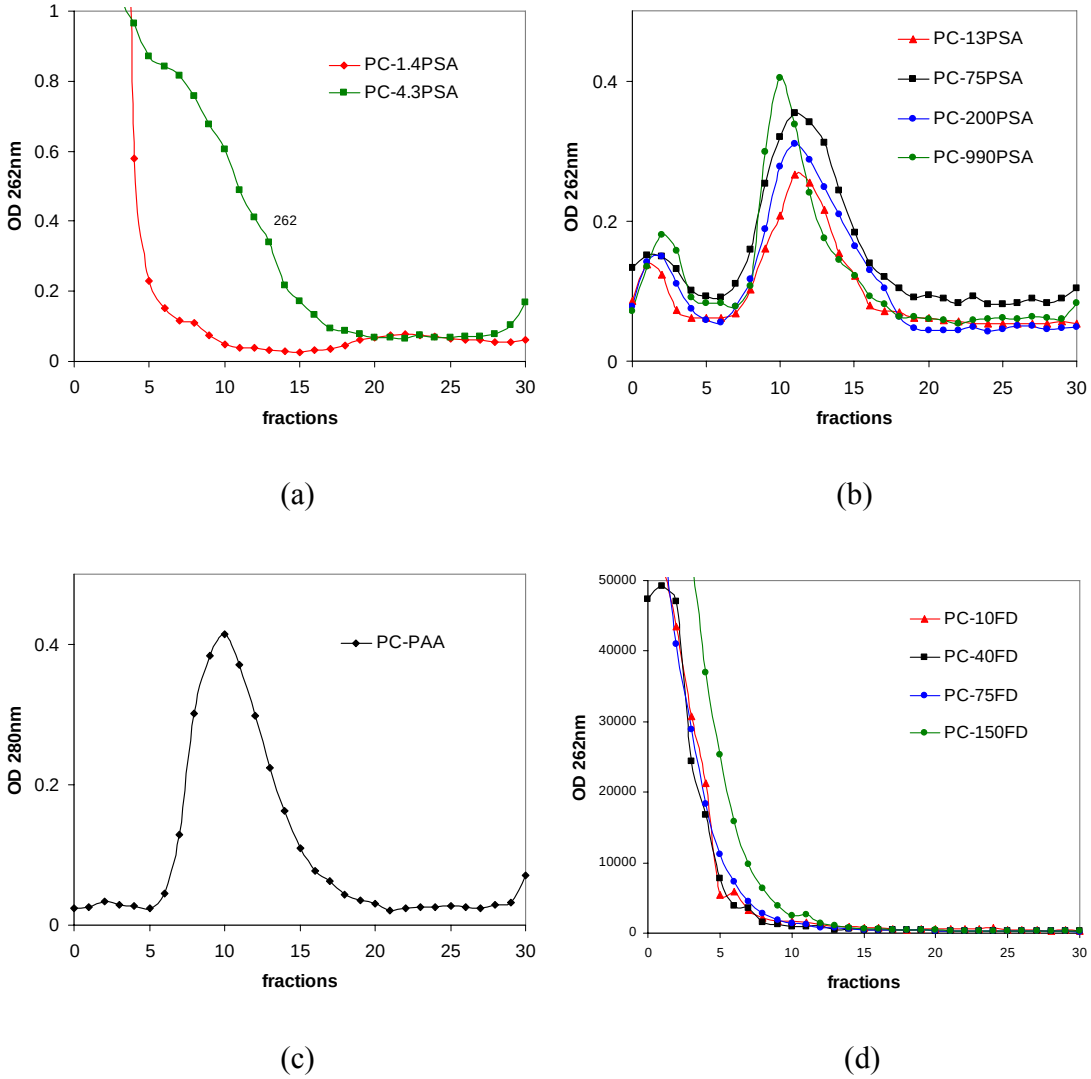

Figure 3-3. Analysis by sucrose gradient centrifugation of the efficiency of loading guest compounds into the HCRSV-derived PC. (a) PC loaded with PSA of mw 1.4 and 4.3 kDa (b) PC loaded with PSA of mw 13, 75, 200 and 990 kDa, (c) PC loaded with PAA of mw 450 kDa, (d) PC loaded with FD of mw 4, 10, 75 and 150 kDa.

3.4.2 fPC loaded with guest molecules

Folic acid was conjugated onto the CP of native HCRSV by the 2-step carbodiimide method. Successful conjugation was confirmed by UV absorption profile. Unlike the CP isolated from the native HCRSV, the CP purified from folic acid-conjugated HCRSV exhibited significant absorbance at wavelengths longer than 300 nm (Figure 3-4). A comparison with the UV spectrum of folic acid suggests that this difference in UV absorbance profile could be attributed to the conjugated folic acid. Folic acid conjugation efficiency (Weight $_{\text{folic acid}}$ / Weight $_{\text{CP}}$) was 1.9 ± 0.1% (n = 3), which translated to about 2 folic acid molecules conjugated to each CP. Since the icosahedral HCRSV capsid is made up of 180 CP units [Doan et al., 2003], the implication is that each fPC particle would have 360 conjugated folic acid molecules.

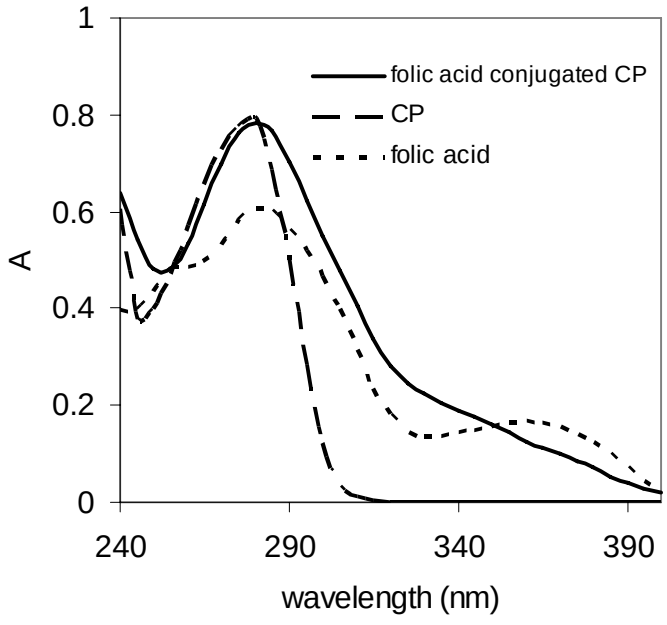

Figure 3-4. UV spectra of folic acid, CP and folic acid-conjugated CP.

The 2-step carbodiimide method selectively coupled carboxyl groups to primary amines. For this reason, the Lys amino acids located on the surface of the PC were hypothesized to be the target sites for folic acid conjugation. The amino acid sequence of HCRSV CP is well established [Doan et al., 2003], and a conformational modeling of the HCRSV CP was performed using the software, SwissModel [Schwede et al., 2003]. The SwissModel contained amino acid sequences of known structure in its template library and, based on the structures of sequences with >25% identity with the HCRSV, an optimized structure for the HCRSV CP was generated (Figure 3-5). This structure was similar to that generated from another study [Doan et al., 2003] in showing the P domain connecting to the S domain through a thin hinge. Based on the generated conformation, three Lys groups in the P domain, indicated by yellow boxes in Figure 3-5, were identified as the possible sites for folic acid conjugation due to their accessibility. Lys groups were also present in the S and N domains of the HCRSV CP, but these would be more difficult to access when the conjugation reaction was performed on intact HCRSV capsids. The number of protruding Lys groups in the conformation also agreed well with the conjugation efficiency of 2 folic acid molecules per CP. Assuming the purified HCRSV-derived CP retained the same conformation upon reassembly in vitro, the Lys conjugation sites on the P domain could be advantageous as the protruded folic acid were more likely to retain their receptor recognition capability. This was confirmed by the data generated in chapter 5.

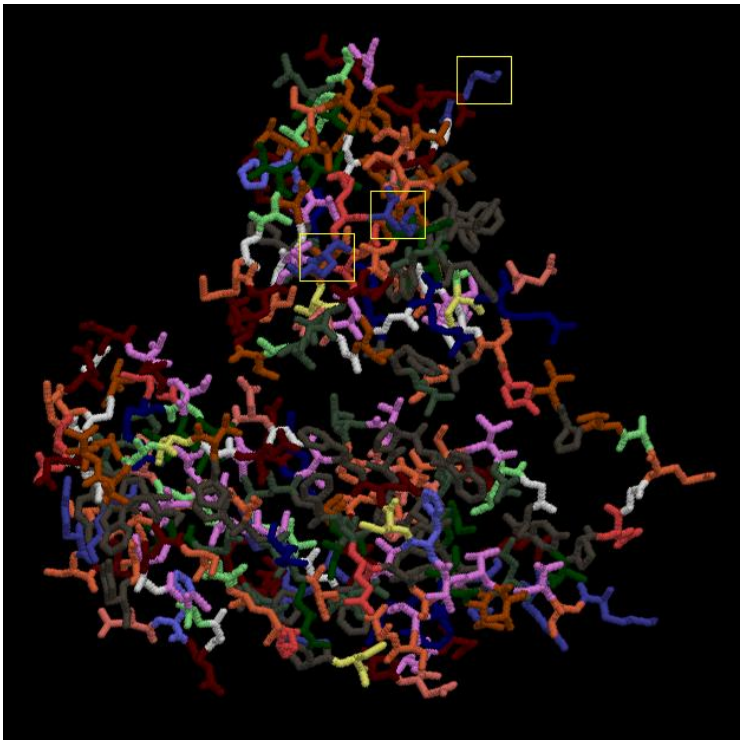

Figure 3-5. A conformation model of the HCRSV CP as generated by the SwissModel. The three Lys amino acid groups (marked by yellow boxes) in the protruding (P) domain are postulated to be the sites for folic acid conjugation.

The capacity of the resultant fPC to load guest molecules was studied using PSA (mw ≥ 13 kDa) and PAA as model compounds. As was observed of the corresponding unconjugated PC samples, the fPC-PSA and fPC-PAA samples showed maximum UV absorption at 260 nm in fraction 12 after sucrose gradient centrifugation (Figure 3-6). The conjugated folic acid therefore did not adversely affect the reassembly of the CP into PC, nor did it hinder the encapsulation of guest compounds into the PC. Thus the fPC could also be considered to be a potential carrier for drug delivery.

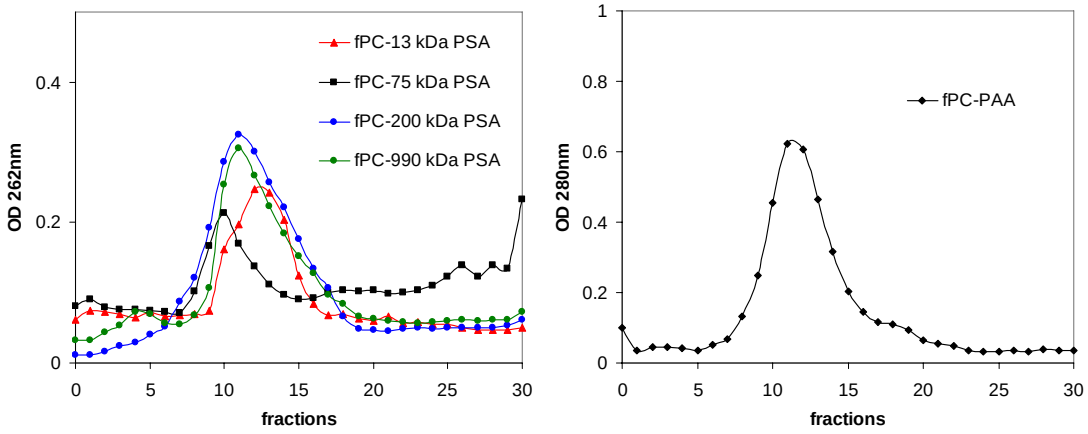

(a) (b)

Figure 3-6. Analysis by sucrose gradient centrifugation of the efficiency of loading guest compounds into the folic acid-conjugated HCRSV-derived PC (fPC) (a) fPC loaded with PSA of mw 13, 75, 200 and 990 kDa (b) fPC loaded with PAA of mw 450 kDa.

3.4.3 Characterization of polyacid-loaded PC and fPC

Further characterization was performed on PC and fPC successfully loaded with PSA (mw ≥ 13 kDa) and PAA. Folic acid conjugation was observed not to change the CD spectrum of the HCRSV-derived PC. Neither did the loading of PSA and PAA. The CD spectra for all the polyacid-loaded PC and fPC samples showed a minimum wavelength around 215 nm, indicating that the encapsulated PSA and PAA did not affect the β-sheet in the CP structure (Figure 3-7).

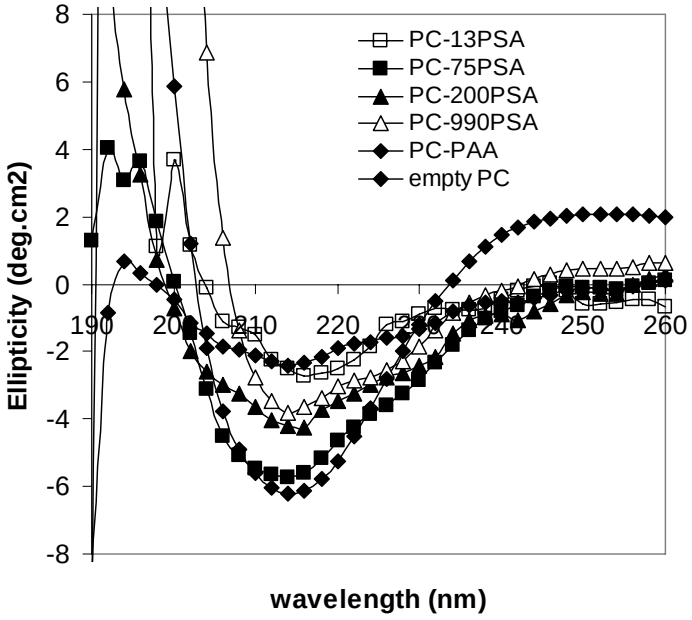

(a)

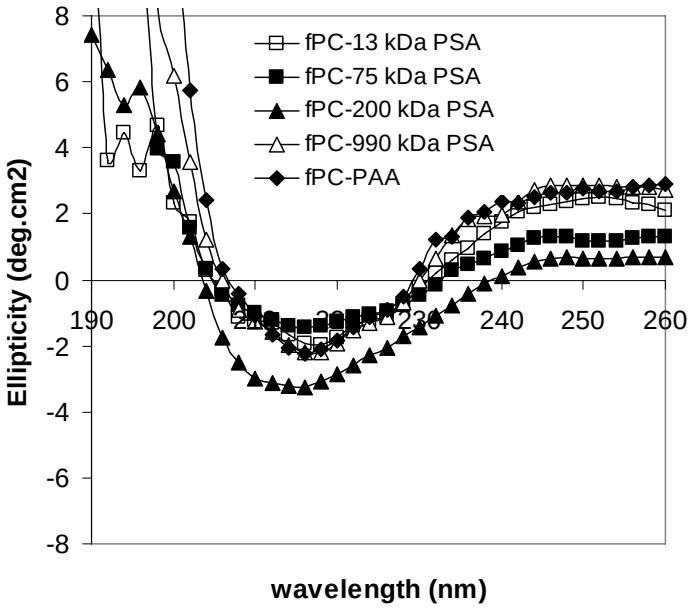

(b)

Figure 3-7. CD spectra of (a) PC-PSA and PC-PAA, and (b) fPC-PSA and fPC-PAA samples. All samples showed a characteristic β-sheet structure with a valley between 210 to 220 nm.

Observed under the TEM, the polyacid-loaded PC and fPC samples appeared as monodispersed, discrete spherical particles with diameter of approximately 30 nm (Figure 3-8). This morphology was observed regardless of the mw and nature of polyacid loaded, and it was comparable to the morphologies of native HCRSV and empty PC shown in Figure 2-7.

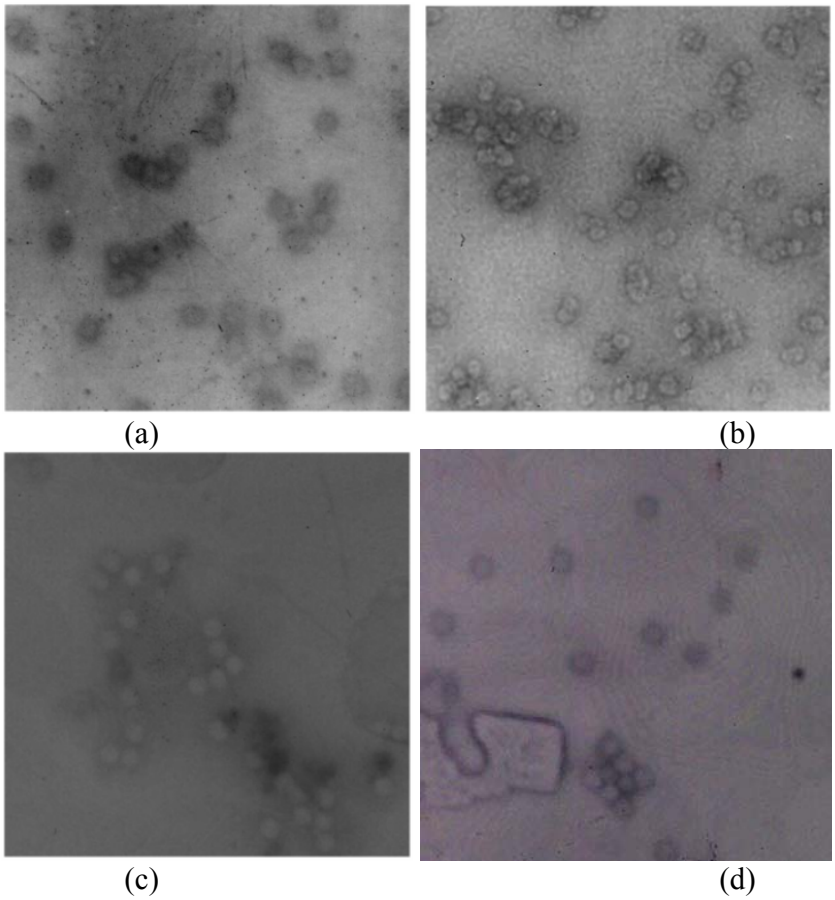

(a) (b)

(c) (d)

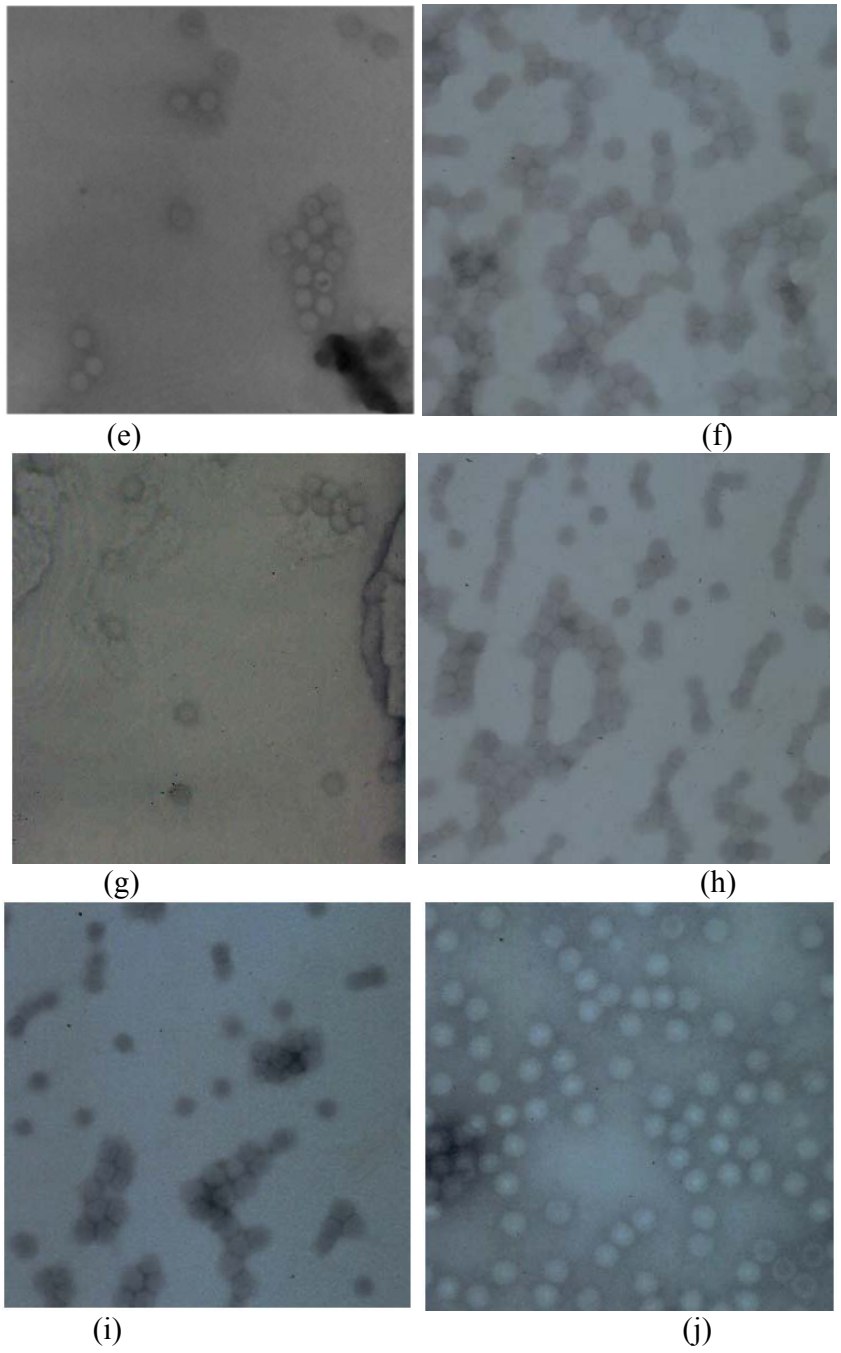

Figure 3-8. TEM of HCRSV-derived PC loaded with guest molecules. (a) PC-13PSA, (b) PC-75PSA, (c) PC-200PSA, (d) PC-990PSA, (e) PC-PAA, (f) fPC-13PSA, (g) fPC-75PSA, (h) fPC-200PSA, (i) fPC-990PSA, (j) fPC-PAA.

Mean size of the polyacid-loaded PC and fPC, as measured by the particle size analyzer, was within the narrow range of 46 (fPC-75 kDa PSA) to 55 nm (PC-13 kDa PSA) (Table 3-1). As with the native HCRSV, these values were larger than the particle diameter observed under the TEM as they represented the hydrodynamic volume of the particles. However, the mean sizes of the cargo-loaded PC and fPC were comparable to that of the native HCRSV (44 nm). The polyacid-loaded PC and fPC samples had zeta potential of between -2.3 to -2.9 mV (Table 3-1). These values were again comparable with the zeta potential of native HCRSV (-2.4 mV), suggesting that the polyacid-loaded PC had similar negative surface charges as the native virus. Given the differences in mw and acid type among PSA, PAA and the native viral RNA, it would appear that the total charge conferred was independent of the type and mw of the polyacids contained within the viral structure. It was also not influenced by differences in the degree of ionization of the three polyacids at pH 5. This phenomenon may be attributed to the existence of a buffering system in the PC, possibly the basic amino acids in the CP could neutralize the anionic charges on the polyacid cargo.

Native gel electrophoresis was performed to provide further information on the size and surface charge of the polyacid-loaded PC and fPC samples**.** As shown in Figure 3-9 (a), the native HCRSV moved towards the anode due to the presence of the negatively charged viral RNA. The absence of RNA in the CP and PC resulted in these samples remaining at the loading sites. Once the PC was loaded with a polyacid, however, the sample once again migrated towards the anode. Despite the differences in mw and acid type of the cargo, all the PC-PSA and PC-PAA samples were observed to migrate to comparable distances upon electrophoresis, and this position was comparable to that of

the native HCRSV. These data are in agreement with the particle size, zeta potential and TEM data in suggesting that the polyacid-loaded PC had comparable size and charge to the native HCRSV. Folic acid conjugation did not affect this phenomenon, the polyacid-loaded fPC showing similar electrophoresis rates as the native HCRSV and polyacid-loaded PC samples, while the empty fPC had comparable electrophoresis rate as the empty PC (Figure 3-9, b and c).

Sample	Zeta size (nm)	Zeta potential (mV)
HCRSV	44 ± 2	-2.4 ± 0.2
PC-13PSA	55 ± 2	-2.4 ± 0
PC-75PSA	52 ± 1	-2.4 ± 0.2
PC-200PSA	53 ± 3	-2.9 ± 0.5
PC-990PSA	50 ± 1	-2.4 ± 0.1
PC-450PAA	50 ± 3	-2.3 ± 0.2
fPC-13PSA	49 ± 4	-2.5 ± 0.3
fPC-75PSA	46 ± 7	-2.3 ± 0.3
fPC-200PSA	47 ± 3	-2.4 ± 0.4
fPC-990PSA	52 ± 2	-2.4 ± 0.5
fPC-450PAA	48 ± 2	-2.3 ± 0.1

Table 3-1. Zeta potential and zeta size of native HCRSV, and polyacid-loaded PC and fPC. Data represent mean ± SD, n = 3.

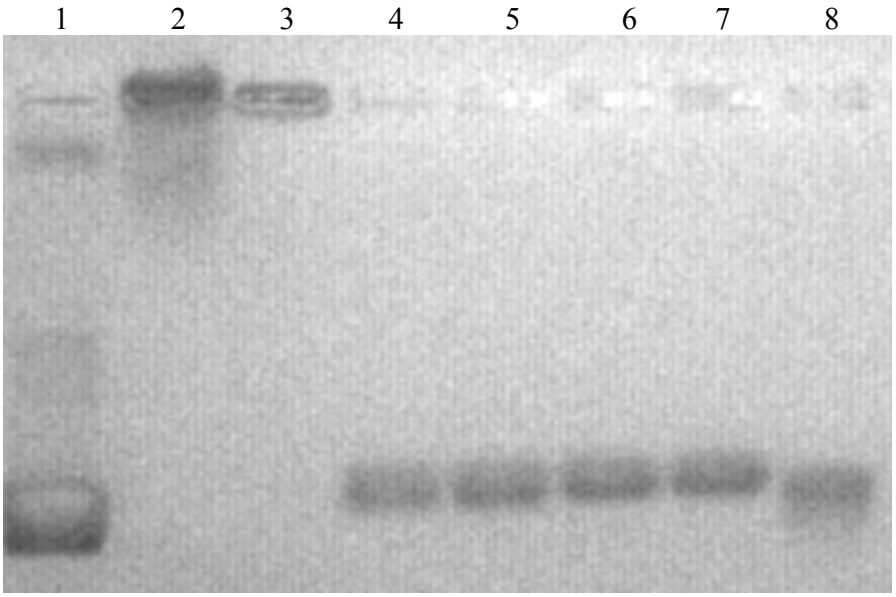

(a)

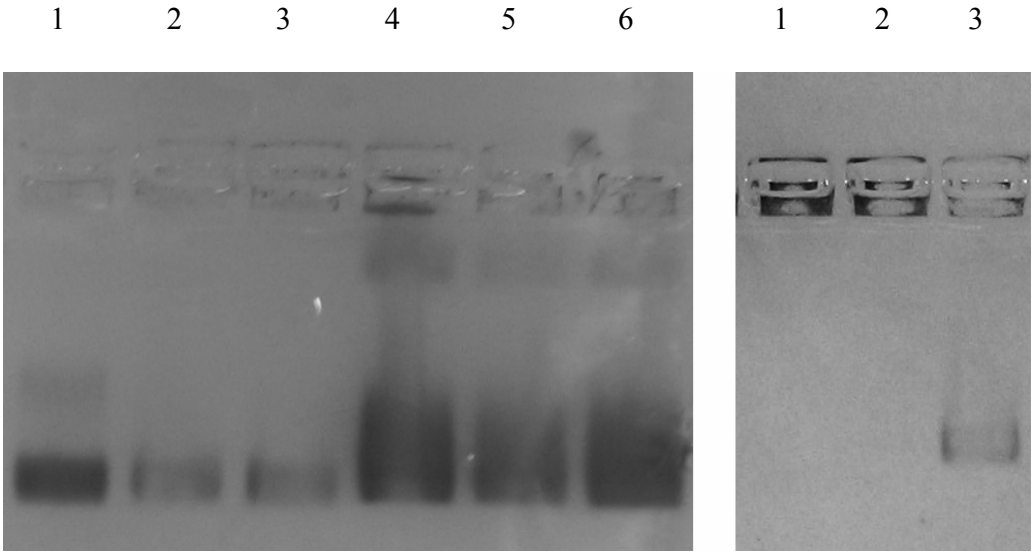

(b) (c)

Figure 3-9.Native gel electrophoresis of native HCRSV and poly-acid loaded PC and fPC samples. (a) Lines 1 to 8 are HCRSV, purified CP, empty PC, PC-13PSA, PC-75PSA, PC-200PSA, PC-990PSA, PC-PAA, (b) Lines 1 to 6 are HCRSV, fPC-13PSA, fPC-75PSA, fPC-200PSA, fPC-990PSA, fPC-PAA, (c) Lines 1 to 3 are folic acid-conjugated CP, empty fPC and native HCRSV.

3.4.4 Loading efficiency of PC-PSA samples

The dual wavelength and BCA-UV methods were used to quantify the amount of PSA loaded in the PC. The loading efficiency was calculated on the basis of the weight of loaded PSA to weight of CP in the system. As seen in Table 3-2, the data obtained from both assay methods correlated well with each other.

Despite a 75-fold difference in mw, PSA of 13 to 990 kDa were encapsulated with comparable efficiency into the PC. The PSA loading efficiency of 15 to 20% also correlated closely with the value of 19% calculated for the genomic RNA (3911 bytes, 1,260 kDa) in the native HCRSV. This suggests that the PC of HCRSV was capable of encapsulating exogenous materials to an amount equivalent to the mass of its native genomic material.

The number of PSA molecules encapsulated per PC was approximated based on the PSA loading data and the corresponding PSA mw (Table 2). For the largest PSA molecule, whose mw (990 kDa) approached that of the genomic RNA, only 1 molecule was accommodated in each PC. This restriction in cargo loading size is not surprising, and is in fact an acknowledged limitation in viral-based gene delivery systems [Dong et al., 1996]. A linear relationship ($n = 1/mw \times 10^6$, $R^2 = 0.9969$) was observed to describe the relationship between the number of PSA molecules loaded into each PC (n) and the mw of the PSA. The protein cage of the PC therefore showed considerable ability for loading exogenous materials.

Mw of cargoes		13 kDa	75 kDa	200 kDa	990 kDa
BCA-UV method	Loading efficiency (%)	19.6 ± 1.7	17.1 ± 1.7	20.0 ± 1.0	15.8 ± 2.1
	Number of PSA per PC (n)	101	15	7	1
Dual wavelength method	Loading efficiency (%)	20.9 ± 2.6	16.7 ± 4.8	20.3 ± 1	14.9 ± 2.6
	Number of PSA per PC (n)	107	14	6	1

Table 3-2. Efficiency of loading PSA of different mw into the HCRSV-derived PC.

3.5 Conclusion

Our study indicated that empty PC derived from the HCRSV had the capacity to accommodate exogenous materials in its cavity. The loading of guest molecules was influenced by the electrostatic interactions between the cargo and the amino acids presenting in the cavity of the PC. The positively charged Arg and Lys moieties located at the N-terminal of the CP appeared to make the inner cavity of the PC attractive for the binding of negatively charged compounds, as demonstrated by the successful loading of PSA and PAA. In contrast, as neutral molecules without ionizable groups, all of the FDs were not encapsulated within the PC, suggesting that electrostatic interaction was the mechanism for cargo encapsulation in the HCRSV-derived PC. Aside from the negative charge, the size of the cargo molecule was another prerequisite for successful encapsulation, as only polyacids with mw no less than 13 kDa were encapsulated into the

PC. In addition, the loading of guest molecules into the HCRSV-derived PC had to be carried out simultaneously with the reassembly of CP into PC, and not with preformed PC.

Folic acid could be conjugated to the CP prior to its reassembly into PC without affecting the conformational structure of the PC. About 360 folic acid molecules could be successfully conjugated onto each PC, and the presence of the folic acid did not appear to affect the capability of the PC to encapsulate guest molecules.

The PSA (≥13 kDa)- and PAA-loaded PC and fPC, despite differences in the mw and acid type of their cargoes, were comparable in size, morphology and protein conformation to each other and to the native HCRSV with its RNA load. The loading efficiency of PSA was also independent of its mw, but the number of PSA molecules that could be accommodated per PC particle was inversely proportional to the mw of the PSA. This suggests that the number of guest molecules that could be accommodated was limited by the volume of the PC cavity. Reassembly of the CP into PC was not affected by the size of the guest molecules, but continued to occur by a precise mechanism that yielded particles of uniform size and morphology. This is an advantage over the drug-loaded liposome and polymer nanoparticle systems, which tended to present in a range of sizes even within a batch. The collective data therefore suggest that the HCRSV-derived PC had attractive features as a platform for drug delivery applications.

Chapter 4

Preparation and characterization of doxorubicin-loaded PC

4.1 Introduction

Literature reports on plant viruses to be employed as potential carriers have shown cargo loading to be achieved through covalent reaction between the guest molecules and specific amino acids presenting on the interior surface of the viral protein coat [Hooker et al., 2004; Schlick et al., 2005]. Experiments conducted with the HCRSV-derived PC had indicated, however, that it was possible to encapsulate guest molecules during the reassembly of CP into PC without involving a chemical reaction (Chapter 2). Two prerequisites have been identified for the successful loading and retention of guest molecules in the HCRSV-derived PC. Firstly, the guest molecule should possess a net negative charge as the entrapment was achieved via non-covalent electrostatic attractions between the guest molecule and the amino acids of the PC. This reversible binding also appeared to initiate the reassembly of the icosahedral PC structure. Secondly, the guest molecule should have an adequately high mw to avoid excessive leaching of encapsulated material via the surface cavities of the PC upon dilution. Successful loading of polyacids with mw above 13 kDa had been demonstrated with the HCRSV-derived PC. However, there is to date no report on the loading of small chemotherapeutic drugs into plant viral PC by non-covalent encapsulation, although this method has proven effective for the loading of crystals [Douglas and Young, 1998; Douglas et al., 2002], polymers [Douglas and Young, 1998] and gold nanoparticles [Chen et al., 2006; Loo et al., 2006]. For the HCRSV-derived PC to be applied as a targeting anticancer drug delivery platform, it must possess the capacity to hold the anticancer drug securely until the drug is due for release at the target tissue. The objective of the experiments in this chapter was to

evaluate the feasibility of loading a model anticancer drug, doxorubicin, into the HCRSV-derived PC.

Doxorubicin is widely used in cancer chemotherapy. It is indicated for the treatment of ovarian cancer [Rose, 2005], breast cancer [Kaklamani and Gradishar, 2005], lung cancer [Koukourakis et al., 2002], non-Hodgkin's lymphoma [Schriber, 2002], and Hodgkin's sarcoma [Connors, 2005]. Doxorubicin has manifold mechanisms of action. It can bind to cellular DNA by intercalating between the base pairs of the DNA helix [Capranico et al., 1986], cause DNA fragmentation by inhibiting topoisomerase II [Jarvinen et al., 2000], or form complexes with iron to produce free radicals that cleave DNA and cell membranes [Xu et al., 2005]. Unfortunately, doxorubicin therapy, although highly effective, is also associated with many side effects, including nausea, vomiting, low blood cell counts, mouth ulcers and hair loss. These side effects have been attributed to the non-selectivity of action and low therapeutic index of doxorubicin. Consequently, it is believed that doxorubicin therapy can be optimized by confining drug release only to the tumor tissues [Rivera, 2003]. A successful example of such a delivery system is Doxil®, a liposomal doxorubicin formulation where the drug is encapsulated within the aqueous core of the liposomes via a salt gradient [Lasic et al., 1992]. Following intravenous administration, doxorubicin is accumulated in the cancer tissues via the enhanced permeability and retention phenomenon [Greish et al., 2004]. The liposomes are PEGylated (Figure 4-1) to reduce uptake by the RES, thus further improving the clinical outcome of doxorubicin therapy [Gabizon et al., 1993].

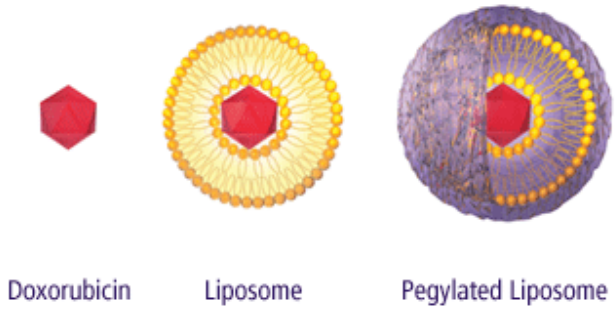

Figure 4-1. Schematic diagram showing the principles underlying the formulation of Doxil® - doxorubicin is encapsulated within a liposome whose surface is covered by a layer of methoxypolyethylene glycol [http://www.doxil.com].

Liposomes, as well as many polymeric nanoparticles, are products of the top-down approach in nanotechnology. Liposomes are prepared by the spontaneous assembly of lipid and/or PEGylated lipid molecules, while polymer nanoparticles are prepared by the condensation of soluble polymer macromolecules through solvent evaporation or the addition of a poor solvent or counterion. These methods of synthesis often result in particles that vary considerably in size and shape, even within a batch [Mozafari, 2005]. For example, liposomes classified as multilamellar vesicles (MLV) or large unilamellar vesicles (LUV) are inherently polydisperse, exhibiting sizes that may vary within hundreds of nanometers or even several microns [Szoka and Papahadjopoulos, 1978; Mozafari, 2005]. Small unilamellar vesicles (SUV) can be more homogeneously sized, but they have a tendency to undergo rapid aggregation and fusion, which in turn increases the effective particle size and size range [Wilschut et al., 1985]. Such within-batch variability is undesirable because size and shape are important parameters that can

influence the biodistribution profile of nanoparticles. Larger particles are less efficiently taken up by cells, and are more readily detected and removed by the RES [Panyam and Labhasetwar, 2003]. Tomii [Tomii 2002] has estimated that particles had to be 50 nm or smaller to evade the RES. Such particles could also more readily localize at tumor and inflammatory sites that present with high vascular permeability [Tomii, 2002; Seki et al., 1994]. Particle shape also influences nanoparticle-cell interactions, for the uptake of spherical gold nanoparticles by Hela cells was reported to be at least 3-fold higher than that of similarly sized rod-shape gold particles [Chithrani et al 2006].

These reasons provide the impetus to produce a nanoscale drug delivery system of doxorubicin with uniform size and morphology. Nanoscale platforms with precise structure and function, such as ferritin, carbon nanotube and viral capsid, have shown promise as drug carriers. Of these, the icosahedral plant viruses are the most extensively researched. Proof of concept was first demonstrated with the PC of CCMV, which could host foreign ions as well as polyacids [Douglas and Young, 1998]. Through gene mutation, the inner surface of the CCMV PC could be modulated to host positive or negative ions [Douglas et al., 2002]. More recently, gold nanoparticles of 16 nm were also encapsulated within the *brome mosaic virus*- (BMV) derived PC [Chen et al., 2006].

However, doxorubicin, like many other anticancer drugs, is a small molecule (mw = 545 Da), and it is positively charged (pK_a = 8.4) in physiological fluids as well as under the conditions employed for the reassembly of the HCRSV-derived PC [Gallois et al., 1998]. These properties made it difficult to load and retain doxorubicin within the PC by simple encapsulation during the reassembly process. To impart the requisite size and charge to the anticancer agent, we employed the aid of a polyacid. This method, which

we termed “polyacid association”, involved the simultaneous loading of doxorubicin with polystyrenesulfonic acid (PSA) of mw 200 kDa into the PC of the HCRSV. The 3:1 (PSA:drug) w/w ratio of mixing ensured the attraction of doxorubicin molecules to the polyacid by electrostatic forces, and a net negative charge for the resultant complex. The complex thus provided the nucleus for binding with, and initiation of the final reassembly of CP into the PC (Figure 4-2). This chapter discusses the preparation and characterization of the doxorubicin-loaded HCRSV-derived PC. It also examines the effect of folic acid conjugation on the efficiency of loading doxorubicin into the PC.

4.2 Materials

Doxorubicin hydrochloride injection (50 mg in 25 ml, USP) was purchased from Pharmacia (Bentley, WA, Australia). Tripolyphosphate acid (TPP) was from Sigma Chemical Co. and the the BCA Protein Assay Reagent Kit was from Pierce Chemical Company. The following buffers were used: buffer A (50 mM NaOAc, 50 mM NaCl, 2 mM EDTA, 20 mM $CaCl_2$, pH 5.0), buffer B (Tris buffer made up with 50 mM of Tris, 2 mM of DTT, 0.2 mM of PMSF, and 5 mM of EDTA, pH 8.0) and buffer D (50 mM Tris/base, 5 mM EDTA, 2 mM DTT, 0.2 mM PMSF, 1 M NaCl, pH 7.0). All other materials and buffers were the same as those listed in sections 2.2 and 3.2.

4.3 Methods

4.3.1 Preparation of PC-Dox and fPC-Dox

The following operations were performed at 4 ºC unless otherwise stated. HCRSV-derived CP were purified by the dialysis method as described in section 3.3.1. In brief, 0.1 ml of HCRSV (10 mg/ml) in re-suspension buffer was dialyzed overnight against 1000 ml of buffer B. It was then incubated with $CaCl_2$ (0.5 M) for 30 min and centrifuged at 25 000 g for 30 min to pellet the viral RNA. The supernatant was further dialyzed against 1000 ml of buffer D for 4 h to obtain the purified CP.

Several methods were explored for the preparation of doxorubicin-loaded PC (PC-Dox). In method A, 1 ml of purified CP (1 mg/ml) in buffer D was incubated with doxorubicin (10% w/w based on the weight of CP used) for 8 h. The solution was adjusted to pH 5 with a concentrated NaOAc buffer (1 M NaOAC, pH 5.0), and $CaCl_2$ was added to a final concentration of 5 mM to reassemble the PC. The solution was incubated for 15 h at ambient temperature to reassemble the PC. Similar processing steps were used for methods B and C. However, in method B, 30% (w/w) of TPP was added to the mixture of CP and doxorubicin to evaluate whether the negatively charged TPP could aid in initiating CP reassembly and in binding the doxorubicin to the PC cavity. Method C employed polystyrenesulfonic acid (PSA) (Figure 4-2) in place of TPP. In this case, the CP (1 ml, 1 mg/ml) was incubated with 0.5 ml of solution containing 0.2 mg/ml of doxorubicin and 0.6 mg/ml of PSA (mw 200 kDa) in buffer D.

Control experiments were designed to evaluate whether it was possible to load doxorubicin through the induced opening of cavities on the surface of preformed PC To do this, PC loaded with PSA of mw 200 kDa (PC-200PSA) was prepared as described in section 3.3.1. The preformed PC-200PSA in buffer A (1 mg/ml, 0.1 ml) was dialyzed against 500 ml of buffer A (pH 5.0), NaOAc buffer (50 mM NaAc, 50 mM NaCl, 2 mM

EDTA, 5 mM $CaCl_2$, pH 6.0) or Tris buffer (50 mM Tris, 50 mM NaCl, 2 mM EDTA, 2 mM of DTT, 0.2 mM PMSF, 5 mM $CaCl_2$, pH 7.0) for 4 h to induce the opening of surface cavities, then incubated overnight with 0.1 mg/ml of doxorubicin. The resultant solutions were adjusted to pH 5 with NaOAc buffer (1 M NaOAc, pH 5.0) to complete the drug loading process.

All samples following drug loading were subjected to 10-40% sucrose gradient centrifugation at 100 000 *g* for 3 h (as described in section 4.3.2.1) to identify the existence of doxorubicin-loaded PC. Samples which showed successful drug loading were centrifuged at 100 000 *g* for 1 h at 4 ºC on a 15% sucrose gradient cushion. The supernatant and sucrose solution were discarded and the pellet containing PC-Dox was resuspended in a small volume (~ 0.1 ml) of buffer A. Samples were stored at 4 °C until use.

To prepare folic acid-conjugated CP, the native HCRSV was conjugated with folic acid by the 2-step carbodiimide method as outlined in section 3.3.2. These folic acid-conjugated HCRSV was processed as described for the native HCRSV to obtain the folic acid-conjugated CP. Reassembly of the purified folic-acid conjugated CP into fPC, with simultaneous loading of doxorubicin and PSA, was conducted using method C. Doxorubicin was also incubated with preformed fPC at pH 7. The resultant samples were analyzed, and drug-loaded samples (fPC-Dox) were purified by sucrose gradient centrifugation as described for PC-Dox.

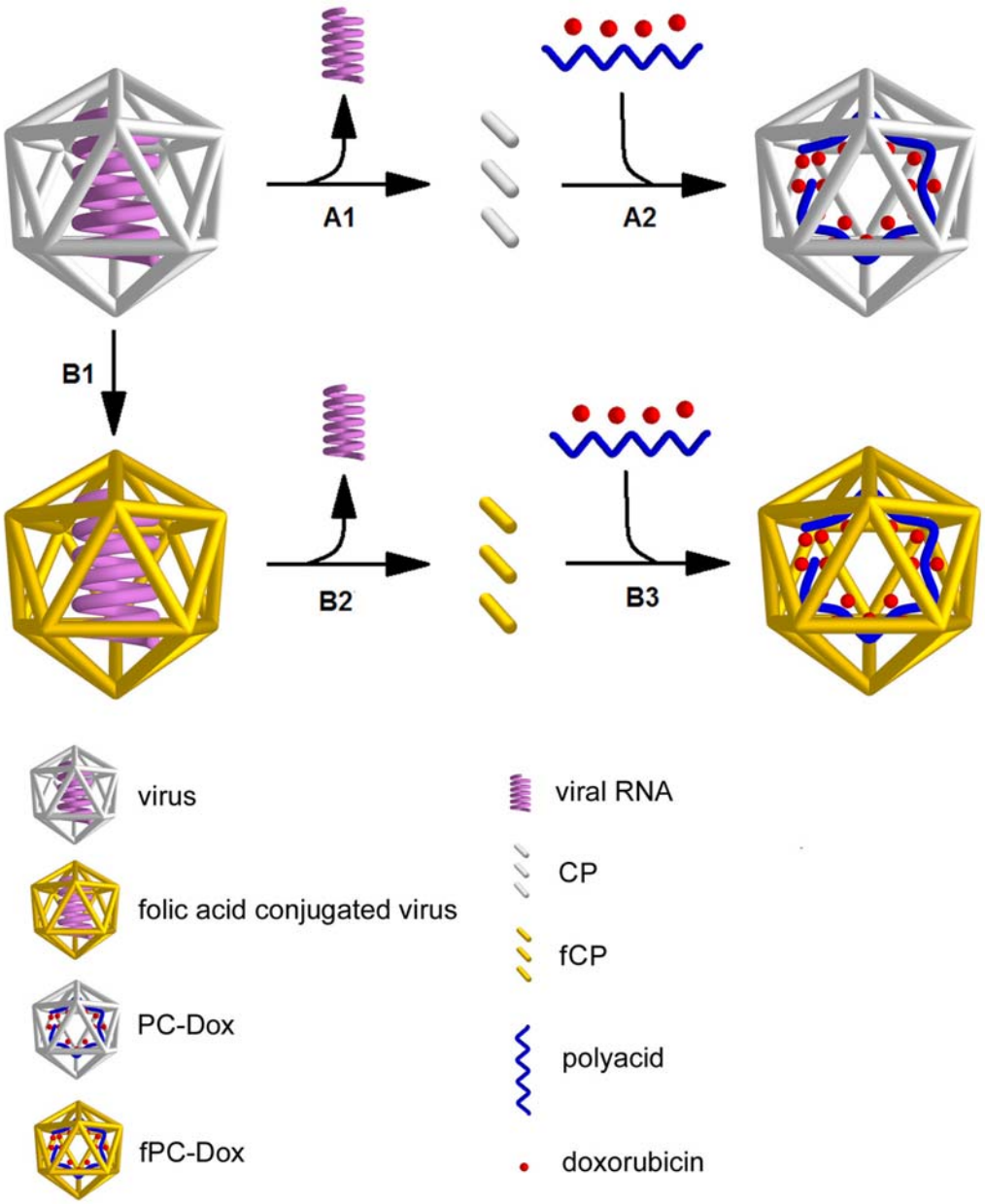

Figure 4-2. Schematic illustration of the preparation of doxorubicin-loaded PC (PC-Dox) and folic acid-conjugated doxorubicin-loaded PC (fPC-Dox). Steps A1 and B2 are indicative of the removal of viral RNA from the plant virus and purification of CP, respectively. Steps A2 and B3 involve the encapsulation of polyacid and doxorubicin during the reassembly of PC. Step B1 refers to the conjugation of folic acid onto the protein coat of the native HCRSV.

4.3.2 Characterization

Sucrose gradient centrifugation was performed to confirm the existence of PC-Dox and fPC-Dox. About 0.5 ml of control or sample solutions were ultracentrifuged on 10-40% sucrose gradient at 100 000 x *g* for 3 h. Controls included solutions of free doxorubicin, doxorubicin and PSA complex (Dox-PSA), empty PC and native HCRSV. Samples analyzed were those of doxorubicin incubated with CP under the reassembly condition (Method A), doxorubicin incubated with TPP and CP under the reassembly condition (Method B), doxorubicin incubated with PSA and CP (or fCP) under the reassembly condition (Method C), and doxorubicin incubated with preformed PC-200PSA (or fPC-200PSA) at pH 5, 6, and 7. Samples containing HCRSV and empty PC were analyzed at 260 nm and 280 nm, respectively, while samples containing doxorubicin were measured at 485 nm.

Native gel electrophoresis was performed on free doxorubicin, Dox-PSA, HCRSV, PC-Dox, fPC-Dox, doxorubicin incubated with preformed PC-200PSA at pH 7, and doxorubicin incubated with preformed fPC-200PSA at pH 7, using the method described in section 3.3.3.3. Bands of CP were visualized by Coomassie blue staining, while the doxorubicin bands were visualized under ultraviolet light (Bio-Rad Molecular Imager ChemiDoc XRS System, CA, USA). Morphology of PC-Dox and fPC-Dox were observed under the TEM using the method described in section 2.3.3.4. Zeta size and zeta potential of PC-Dox and fPC-Dox were analyzed by the zeta sizer using the protocols described in section 2.3.3.5.

4.3.3 Loading efficiency (LE), encapsulation efficiency (EE) and reassembly efficiency (RE)

The loading efficiency (LE), encapsulation efficiency (EE), and reassembly efficiency (RE) were calculated using equations 4-1 to 4-3, respectively. In addition, the number of doxorubicin molecules encapsulated within each PC (N) and the doxorubicin concentration within each PC ($C_{\text{loaded Dox}}$) were calculated using equations 4-4 and 4-5, respectively. Doxorubicin was assayed by fluorimetric spectroscopy. The amount of doxorubicin in the samples was calculated by comparing its $OD_{485\ nm}$ with those of standard solutions, both of which were diluted with buffer A (pH 5) prior to measurement. The amount of CP in each sample was quantified by the BCA assay for protein after the encapsulated doxorubicin was removed via 6-day dialysis against PBS (pH 7.4).

$$\text{LE (\%)} = \text{Weight}_{\text{loaded doxorubicin}} / \text{Weight}_{\text{PC}} \times 100\% \quad (4\text{-}1)$$

$$\text{EE} = \text{Weight}_{\text{loaded doxorubicin}} / \text{Weight}_{\text{total doxorubicin used}} \times 100\% \quad (4\text{-}2)$$

$$\text{RE} = \text{Weight}_{\text{PC}} / \text{Weight}_{\text{total CP used}} \times 100\% \quad (4\text{-}3)$$

$$N = \text{LE} / \text{mw}_{\text{doxorubicin}} \times (\text{mw}_{\text{CP}} \times 180) \quad (4\text{-}4)$$

$$C_{\text{loaded doxorubicin}}\,(\text{mM}) = \text{mw}_{\text{CP}} \times 180 \times \text{LE} / (\text{mw}_{\text{doxorubicin}} \times V \times 6.02 \times 10^{23}) \quad (4\text{-}5)$$

$\text{mw}_{\text{doxorubicin}}$ and mw_{CP} values were 545 and 37 000, respectively. V refers to the inner cavity volume of PC, which was calculated based on a radius of 11 nm [Doan et al., 2003].

4.3.4 Drug Release Profile

Drug release experiments were performed by the dialysis method [Liu et al., 2005]. Fifty μl of free doxorubicin solution, PC-Dox and fPC-Dox dispersions, each equivalent to doxorubicin concentration of 1000 μg/ml, were placed in separate dialysis tubes (mw cut-off 12 400, Sigma-Aldrich) and dialyzed against 25 ml of PBS (pH 7.4) at 37 °C. At specified time points, 0.2 ml of the dialysis buffer was sampled for fluorescence measurements (Ex $_{480\ nm}$, Em $_{535\ nm}$) (TECAN SpectraFluor, MA, USA) to quantify the released doxorubicin. Doxorubicin diluted with PBS to 0.2 to 4 μg/ml was used as standard solutions for calibrating the spectrophotometer.

4.4 Results and discussion

4.4.1 Preparation of PC-Dox and fPC-Dox

Three different methods were used to load doxorubicin, a small molecule (mw = 545 Da) with a positive charge (pKa = 8.4), into the HCRSV-derived PC during the reassembly process. Method A, where doxorubicin alone was incubated with the CP under the reassembly conditions, had been successfully applied to the loading of negatively charged macromolecules, PSA and PAA (Chapter 3). This method was, however, ineffective at loading the doxorubicin molecules. Analysis of the sample by sucrose gradient centrifugation (Figure 4-4b) showed fraction 2 to have the highest doxorubicin concentration, and fractions 9 to 15 to have negligible doxorubicin content.

Method B was an adaptation of the "pH gradient method", which was reported to be highly efficient for the loading of doxorubicin into liposomes [Fritze et al., 2006]. In this method, the liposomes were first loaded with a high concentration of acid, such as citric acid, before incubation with doxorubicin. As the weakly basic drug became attracted to the encapsulated acid, an influx of doxorubicin ensued, resulting in high drug loading. Applying the same principle, TPP, a polyvalent acid, was incubated with doxorubicin and the CP under the reassembly conditions. TPP was chosen because it had similar chemical structure to the phosphate groups present in viral RNA, and was therefore unlikely to destabilize the HCRSV CP. The addition of TPP, however, failed to facilitate the loading of doxorubicin into the HCRSV-derived PC. Sucrose gradient centrifugation again showed the drug to be concentrated in the initial fractions, not in the middle fractions which contained the reassembled PC (Figure 4-4 b). This failure to load was probably due to the mw of the cargos. As both TPP and doxorubicin were small molecules, the TPP-doxorubicin complex might not meet the threshold size essential for effective retention within the PC cavity. Even if the TPP or TPP-doxorubicin complex had a high affinity for the inner space of the PC, they would still leach out through the surface cavities of the PC upon dilution. For the same reasons, no attempt was made at preloading the HCRSV-derived PC with TPP before the addition of doxorubicin.

Method C was inspired by the viral RNA structure, which had the organic bases of purine and pyrimidine covalently attached to the phosphoric acid-sugar chain (Figure 4-3, a), thus providing a mechanism for retaining the bases within the PC. We hypothesized that basic drugs of low mw, like doxorubicin, could also be retained within the viral PC by binding with a negatively charged macromolecule that was encapsulated within the PC.

This principle was utilized in method C, where the CP was incubated with doxorubicin and PSA of 200 kDa at the weight ratio of 1:3. The employment of a higher PSA content was to ensure adequate binding sites for the doxorubicin molecules, and to allow the resultant doxorubicin-PSA complex to possess the net negative charge essential for interaction with the viral CP. Unlike the covalent bonds that exist between the organic bases and the phosphoric acid-sugar chain in the viral RNA, reversible electrostatic attraction was employed to attach the doxorubicin molecules to the PSA backbone. The reversibility of interaction was important, for it allowed for subsequent drug release from the viral PC upon appropriate stimulation. This novel method of loading doxorubicin with the aid of a high-mw polyacid was termed "polyacid association".

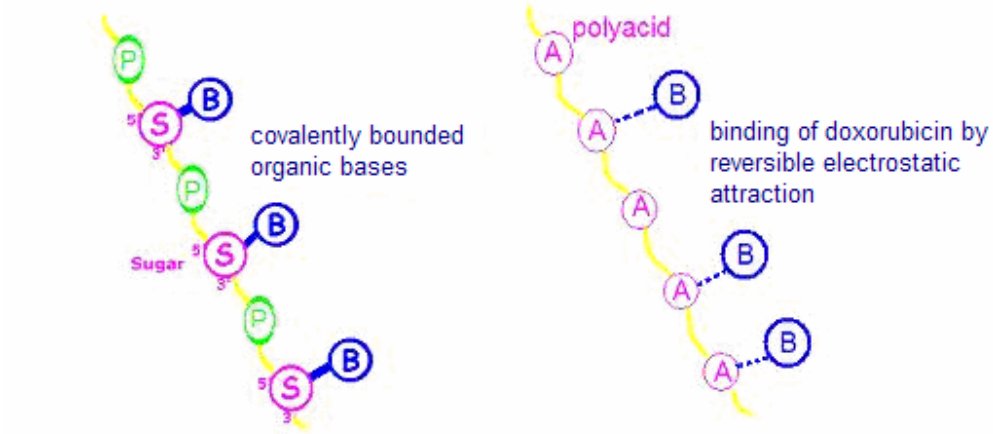

(a) (b)

Figure 4-3 Illustration of the structure of (a) viral RNA, in which bases are covalently conjugated with phosphoric acid-sugar chain, and (b) doxorubicin-PSA complex, in which the weakly basic drug was attached to the polyvalent acid by reversible electrostatic interactions.

Samples prepared by the polyacid association method were subjected to sucrose gradient centrifugation, and the red color typical of doxorubicin was reflected in fraction 12 (Figure 4-4 c). As this fraction was coincident with that containing the reassembled PC-200PSA, it implicated a successful doxorubicin loading into the PC. The product is denoted as PC-Dox. Parallel experiments performed with the folic acid-conjugated CP (fCP) produced comparable results (Figure 4-4, c), indicating that folic acid conjugation did not hinder doxorubicin loading into the PC by the polyacid association method. Both PC-Dox and fPC-Dox after centrifugation were at similar positions on the sucrose gradient as the native HCRSV particles, suggesting that all three particles had comparable densities.

Douglas and Young (1998) had reported yet another method for loading guest molecules into plant virus-derived PC. In their method, the empty virus PC was caused to swell so that cavities on the surface of the PC were sufficiently widened to allow the transfer of guest molecules into the interior of the PC. We adapted this method by loading doxorubicin into preformed PC-200PSA. Again, PC loaded with PSA was used rather than the blank PC to take advantage of the binding sites offered by PSA for retaining the doxorubicin molecules within the PC. Preformed PC-200PSA was incubated in buffers of pH 5, 6 or 7 to induce the opening of surface cavities through protein conformational change. The swollen PC-200PSA was then incubated with doxorubicin before the samples were analyzed by sucrose gradient centrifugation. As seen in Figure 4-4 b, all 3 samples showed high doxorubicin concentration in fractions 1-3, and negligible doxorubicin content in fraction 12, suggesting that doxorubicin was not successfully

loaded into the preformed PC-200PSA. By extension, it may be concluded that doxorubicin loading occurred simultaneously with PC reassembly in method C, and that the loaded doxorubicin was contained predominantly within the PC cavity, not on the PC surface. The data also support the proposition that doxorubicin loading was dependent upon its interaction with the polyacid, PSA. In the preformed PC-200PSA, drug loading could not take place because the PSA was less accessible for interaction following its encapsulation within the PC.

4.4.2 Characteristics of PC-Dox and fPC-Dox

Native agarose gel electrophoresis was applied to analyze the size and charge properties of the samples. Bands containing doxorubicin were observed with the naked eye (red spot) or under UV illumination (strong fluorescence), while bands containing proteins were visualized after coomassie blue staining.

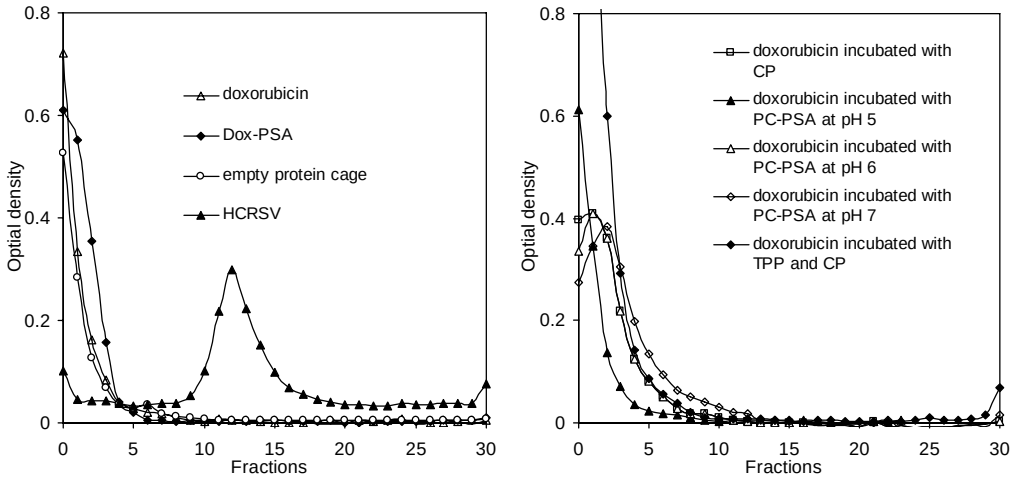

(a) (b)

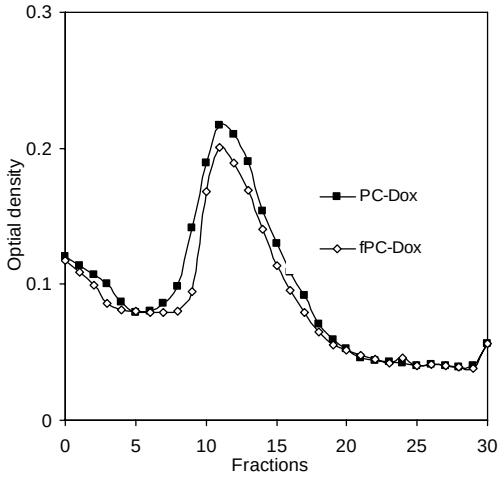

(c)

Figure 4-4 Sucrose gradient centrifugation analysis of samples following different methods of doxorubicin loading. Samples without doxorubicin were analyzed at 260 nm and 280 nm, to detect HCRSV and reassembled PC, respectively, while samples containing doxorubicin were measured at 485 nm. (a) Control samples of HCRSV, empty PC, free doxorubicin and doxorubicin-200PSA complex; (b) Samples obtained by incubating doxorubicin with CP, with and without the addition of TPP; and samples obtained by incubating doxorubicin with preformed PC-200PSA at pH 5, 6 and 7. (c) Samples obtained by incubating doxorubicin with CP (or fCP) in the presence of PSA (200 kDa). These samples are denoted as PC-Dox and fPC-Dox, respectively.

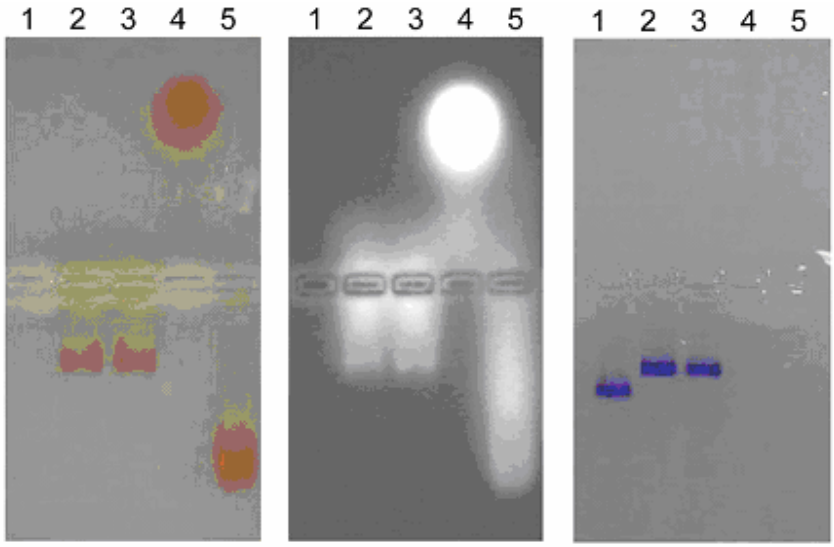

(a)

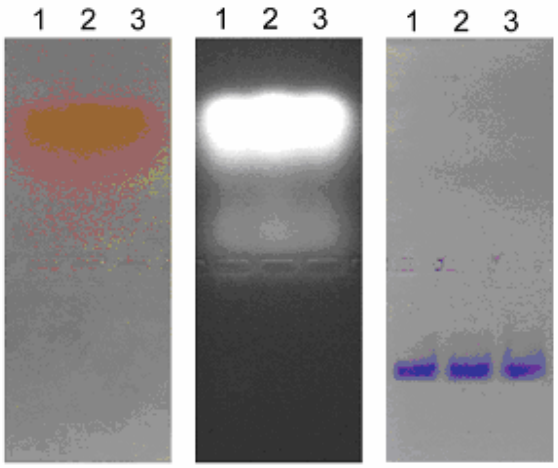

(b)

Figure 4-5 Native agarose gel electrophoresis of (a) HCRSV, fPC-Dox, PC-Dox, doxorubicin, and doxorubicin-PSA complex (Lanes 1 to 5, respectively); (b) samples obtained by incubating doxorubicin with native HCRSV, pre-formed PC-200PSA and fPC-200PSA (Lane 1 to 3, respectively). The three columns represent images obtained using a digital camera (left), under ultraviolet light illumination (middle) and after staining with coomassie blue (right).

As shown in Figure 4-5 a, gel electrophoresis caused the free doxorubicin to migrate to the cathode, while PC-Dox, fPC-Dox, and the doxorubicin-PSA complex moved in the opposite direction towards the anode. The relative positions of the bands indicated the opposing polarity of the samples, and confirmed that the PSA-doxorubicin complex possessed a net negative charge. A comparison of the gels following coomassie blue staining showed that the doxorubicin band co-localized with the protein bands in the PC-Dox and fPC-Dox samples, once more underscoring the successful encapsulation of the drug in the viral PC. Compared with the native HCRSV, the PC-Dox and fPC-Dox possessed a slightly lower charge density. In previous experiments, HCRSV-derived PC loaded with PSA alone was determined to have the same negative charge density as the native HCRSV (section 3.4.3). Therefore the lower charge density of PC-Dox and fPC-Dox might be attributed to the loaded doxorubicin. The result obtained for fPC-Dox was comparable to that for PC-Dox, again indicating that the conjugation of folic acid did not affect the size or charge of the CP and PC.

Samples in which doxorubicin was incubated with the pre-formed PC-200PSA showed an absence of drug-loaded PC (Figure 4-5, b). This negative control, together with the results obtained from the sucrose gradient analysis, further confirmed the necessity of encapsulating doxorubicin during the process of PC reassembly.

A trail of doxorubicin was observed in the gel samples for PC-Dox and fPC-Dox (Figure 4-5, a and b), suggesting that the drug was released during the electrophoresis process. A similar phenomenon was observed for the doxorubicin-PSA complex. These

results affirmed the reversible interaction between doxorubicin and PSA, and suggested that drug release from the PC readily occurred upon dilution.

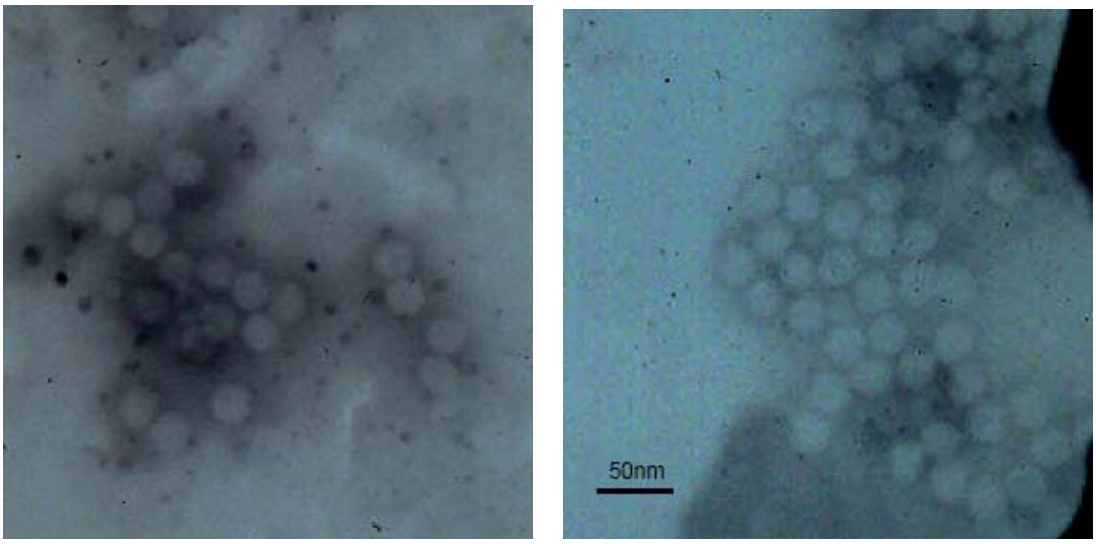

(a) (b)

Figure 4-6 TEM micrographs of (a) PC-Dox, and (b) fPC-Dox. The doxorubicin-loaded viral like particles were comparable in size and morphology to the native HCRSV (Figure 2-7).

Under the TEM, PC-Dox and fPC-Dox appeared as spherical particles with diameter of about 30 nm, which was comparable with the native HCRSV (Figure 4-6). The morphology of the HCRSV-derived PC was therefore unaffected by the simultaneous loading of polyacid and doxorubicin, together with surface folic acid conjugation. It may thus be considered to be a robust nanosize drug delivery platform.

Like the polyacid-loaded PC (section 3.4.3) and native HCRSV (section 2.4.9), the PC-Dox and fPC-Dox appeared larger when measured by the zeta sizer (Table 4-1) than when observed under the TEM. The mean diameters were, however, no different from

corresponding sizes for the HCRSV and PC-200PSA. Zeta potentials for PC-Dox and fPC-Dox were -1.6 mV and -1.4 mV, respectively (Table 4-1), lower than the value of -2.4 mV measured for the native HCRSV. This difference in surface charge, which was in agreement with the agarose gel electrophoresis results, could only be attributed to the positively charged doxorubicin. It has previously been shown in section 3.4.3 that the zeta potential of PSA-loaded PC and fPC (Table 3-1) were comparable with that of native HCRSV, and were independent of the mw and nature of polyacids encapsulated within the PC. The lower zeta potentials of PC-Dox and fPC-Dox might be due to the presence of adsorbed doxorubicin molecules. These molecules were, however, unlikely to be present in significant amounts as the PC-Dox and fPC-Dox retained a net negative charge. Moreover, negligible doxorubicin content was registered when the drug was incubated with preformed PC-200PSA and fPC-200PSA (Figure 4-4), although surface adsorption of doxorubicin, if it occurred, would be favored under such circumstances.

	PC-Dox	fPC-Dox	PC-200PSA	HCRSV
Zeta size (nm)	48 ± 4	49 ± 2	53 ± 3	44 ± 2
Zeta potential	-1.6 ± 0.1	-1.4 ± 0.1	-2.9 ± 0.5	-2.4 ± 0.2

Table 4-1. Zeta size and potential of PC-Dox and fPC-Dox (mean ± SD, n = 3).

4.4.3. Loading efficiency (LE), encapsulation efficiency (EE) and reassembly efficiency (RE)

Various parameters were determined to evaluate the efficiency of method C in loading doxorubicin into the HCRSV-derived PC and fPC. The EE of doxorubicin was

expressed as the percent weight of doxorubicin loaded in a sample relative to the total weight of doxorubicin used for the preparation. EE for PC-Dox and fPC-Dox amounted to 59% and 49%, respectively (Table 4-2). Considering the small size and positive charge of doxorubicin, these EE values were deemed to be satisfactory, and were possibly achieved through the formation of a stable doxorubicin-PSA complex during encapsulation**.**

RE, which was the ratio of reassembled PC to the total CP used in the sample preparation, was another parameter measured. A high RE was important as the drug could only be encapsulated within the reassembled PC. RE for PC-Dox and fPC-Dox were relatively low, at 75% and 64%, respectively (Table 4-2). Loss of CP and reassembled PC during processing and transfers would account for the low values obtained.

LE was calculated as the weight of loaded doxorubicin relative to the weight of PC in a sample. The number of doxorubicin molecules encapsulated within each PC (N_{Dox}) was then determined based on the LE value, the mw of doxorubicin (mw = 544) and the mw of CP (mw = 37000). In addition, the concentration of loaded doxorubicin ($C_{loaded\ Dox}$) was estimated (equation 4-5) based on the LE value and the inner volume of the PC. LE values of 7.8% and 7.5% were obtained for PC-Dox and fPC-Dox, respectively (Table 4-2), comparable with other nano-sized systems, such as chitosan micelles and alginate nanoparticles [Xiangyang et al., 2007; Chavanpatil et al., 2007]. These values would translate to about 900 doxorubicin molecules encapsulated in each PC for both samples. The encapsulated doxorubicin concentration was about 300 mM, based on an inner diameter of 110 Å for the HCRSV-derived PC [Doan et al., 2003].

Samples	Loading efficiency (%)	Encapsulation efficiency (%)	Reassembly efficiency (%)	N_{Dox}
PC-Dox	7.8 ± 0.5	59.3 ± 13.7	74.7 ± 12.1	953
fPC-Dox	7.5 ± 0.3	48.7 ± 4.7	63.8 ± 5.1	916

Table 4-2. Loading efficiency, encapsulation efficiency, reassembly efficiency and N_{Dox} calculated for PC-Dox and fPC-Dox (mean ± SD, n = 3).

4.4.4 Drug release profile

The release of doxorubicin from PC-Dox and fPC-Dox following dilution was evident during sucrose gradient centrifugation and agarose gel electrophoresis. Spectrophotometric measurements following sucrose gradient centrifugation showed increasing doxorubicin concentration from fractions 0 to 10. Since the PC was retained in fraction 12, this suggested that doxorubicin was released from the PC as they sediment along the centrifugation path. The agarose gel also showed a strong trail of doxorubicin associated with the bands for PC-Dox and fPC-Dox (Figure 4-5, a). As the protein bands of PC-Dox and fPC-Dox (Figure 4-5, a) did not exhibit degradation trails, the PC were probably stable under the experimental conditions. The orange color trails and fluorescence trails might therefore be attributed to the doxorubicin which had been leached from the PC.

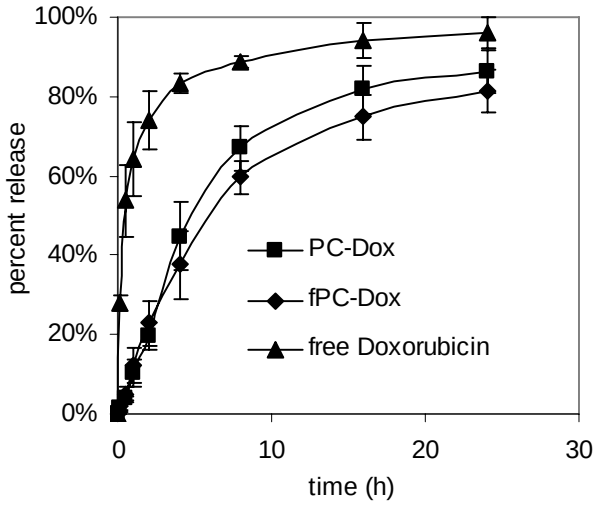

Figure 4-7. *In vitro* doxorubicin release profiles of PC-Dox and fPC-Dox under simulated physiological conditions (n = 3). Free doxorubicin served as control.

To obtain the drug release profile, *in vitro* drug release experiments were conducted under simulated physiological conditions (pH 7.4, 37 °C) [Liu et al., 2005]. Sustained release was evident when the drug release profiles of PC-Dox and fPC-Dox were compared with that of free doxorubicin (Figure 4-7). More than 80% of the drug load was released from the free doxorubicin into the receptor chamber after 5 h, whereas the drug-loaded PC yielded the same amount of doxorubicin only after 24 h. Drug release from the PC-Dox and fPC-Dox did not, however, occur at a constant rate. There was a fairly rapid release of doxorubicin in the initial phase, where 40% of the drug load was released in 4 h, followed by a slower pace of release of the remaining drug load from the PC. The mechanisms that effect drug release upon dilution were probably similar to those that allowed doxorubicin to be loaded into the viral PC in the first place, i.e. reversible electrostatic attraction with the polyacid and physical entrapment by the viral PC. The

sustained-release profile, coupled with the almost complete release of the entire drug load, rendered the HCRSV PC as an attractive platform for controlled release drug delivery. However, to reduce drug release during storage, the samples should be stored in small volumes of resuspension buffer at low temperature (4°C).

4.5 Conclusion

Doxorubicin, being a positively charged small molecule, could not be loaded into the HCRSV-derived PC without the addition of a negatively-charged adjuvant. The size of the adjuvant was important, as a small molecule like TPP was inefficient at retaining the doxorubicin within the PC cavity. A novel method, named "polyacid association", which involved the simultaneous encapsulation of doxorubicin with a polyacid, was successfully employed to load doxorubicin into the HCRSV-derived PC. This method was equally efficient at loading doxorubicin into the folic acid-conjugated PC. The resultant samples, denoted as PC-Dox and fPC-Dox, were homogenously sized and shaped, and they retained similar morphology and size to the native HCRSV. Drug encapsulation efficiency for both samples was within the acceptable range of 49 – 59%, with each PC particle containing about 900 entrapped doxorubicin molecules. The encapsulated drug was readily released from the PC-Dox and fPC-Dox upon dilution, with both samples exhibiting a sustained drug release profile at simulated physiological conditions. On the basis of these results, it may be concluded that the PC-Dox and fPC-Dox could be efficiently produced and they have potential as a drug delivery platform for anticancer agents.

Chapter 5

In vitro evaluation of the efficacy of doxorubicin-loaded PC

5.1 Introduction

In chapter 4, the anticancer agent, doxorubicin, was shown to be successfully loaded into the cavity of the HCRSV-derived PC by a "polyacid association" method to give PC-Dox and fPC-Dox. To investigate the potential of applying PC-Dox and fPC-Dox as cancer chemotherapeutic agents, *in vitro* studies were performed to determine their uptake and cytotoxicity in cancer and normal cells.

The *in vitro* experiments were conducted on cell cultures. Cell culture is a convenient, cheap and standardized technique for the evaluation of biomedical materials. Unlike *in vivo* animal models, cell cultures can provide ideal models with a high degree of consistency and reproducibility. Cell cultures have been applied to determine the effects of compounds on the physiology and biochemistry of specific cell types [Mosmann, 1983; Lim and Lim, 2006] and to provide mechanistic data under standardized conditions [Reddy et al., 2001]. In addition, techniques such as fluorimetry [Ren and Wei, 2004] and laser confocal microscopy [Xiong, et al., 2005] have been developed to monitor the effects of exogenous materials on intracellular biological processes in cell cultures. Other techniques, such as the MTT assay [Mosmann, 1983; Grailer et al., 1988], have been established to quantify cell viability as well as the *in vitro* efficacy of anticancer agents.

Three cell lines were used in our study. The CCL-186 cells [Nichols et al., 1977] were derived from human lung fibroblasts and were chosen to represent normal cells. The OVCAR-3 cell line was derived from a human ovarian adenocarcinoma [Hamilton et al., 1983], and it was chosen because ovarian cancer is responsive to doxorubicin [Markman, 2006] and the FR has been reported to be over-expressed in ovarian cancer

cells [Ross et al., 1994], including the OVCAR-3 [van Steenis et al., 2003]. A human nasopharyngeal carcinoma cell line, CNE-1, was also used as a cancer cell model because nasopharyngeal cancer is prevalent in South-East Asia [Li et al., 2004; Wu et al., 2006].

Four doxorubicin formulations, denoted as I, II, III and IV (Table 5-1), were evaluated. Free doxorubicin (I) served as a control. Formulations II and III consisted of PC-Dox and fPC-Dox, respectively, and were used to compare the effectiveness of the HCRSV-derived PC as a delivery platform and the conjugated folic acid as a cancer targeting ligand. The vehicle for these formulations was folic acid-deficient RPMI-1640 medium. Formulation IV comprised of fPC-Dox dispersed in the RPMI-1640 medium supplemented with 1 mM folic acid, and this formulation was applied to determine the role of the FR in the cellular uptake of fPC-Dox.

Formulation	Description
I	Free doxorubicin
II	PC-Dox
III	fPC-Dox
IV	fPC-Dox with 1 mM folic acid

Table 5-1. Doxorubicin formulations used in the *in vitro* evaluation of the efficacy of PC-Dox and fPC-Dox. I, II and III were dispersed or dissolved in folic acid-deficient RPMI-1640 medium while IV was dispersed in the same medium supplemented with 1 mM of folic acid

Several techniques were applied to evaluate the biological activity of the formulations. Cell-associated doxorubicin following uptake experiments was quantified by fluorescence spectroscopy, while the viewing of the cells under a confocal scanning laser microscope aided in the localization of intracellular doxorubicin. Flow cytometry was also applied to measure the intracellular doxorubicin at single-cell level, while the efficacy of the formulations was evaluated via the MTT assay. Results from these experiments were consolidated to provide a profile of the targeting capability, uptake efficiency and cytotoxicity of PC-Dox and fPC-Dox in cancer cells.

5.2 Materials

Except for acetonitrile (CH_3CN), which was from the Sigma Chemical Co., all materials and cell lines were the same as those listed in sections 2.2, 3.2 and 4.2. The cells were cultured using the same conditions as those described in section 2.2.

5.3 Methods

5.3.1 Folic acid uptake

Folic acid uptake experiments were performed to confirm the over-expression of the folic acid receptor in the OVCAR-3 and CNE-1 cells cultured in folic acid-deficient RPMI-1640 medium. CCL-186, OVCAR-3 and CNE-1 cells cultured in 75 cm^2 flasks to 80% confluence were trypsinized after washing thrice with 10 ml of PBS. During culture, the OVCAR-3 and CNE-1 cells were incubated in folic acid-deficient RPMI-1640

medium while the CCL-186 cells were cultured in normal RPMI-1640 medium. To prepare for the folic acid uptake experiments, all 3 cell lines after detachment were pre-incubated with 10 ml of folic acid-deficient RPMI-1640 medium for 4 h at 37 ºC in the CO_2 incubator. The medium was discarded, and the cells were subjected to 3 cycles of washing with 10 ml of PBS followed by centrifugation at 2 000 rpm for 2 min. The cells were then incubated at 37 ºC at a density of 1000 000 cells/ml with fresh RPMI 1640 medium supplemented with 1 mg/L of folic acid. At specified periods of 30, 60 and 120 min, 1 ml-aliquots were sampled, and the uptake process was immediately quenched on ice. The cell aliquots were washed thrice, each time with 1 ml of ice-cold PBS, and vortexed with 0.5 ml of lysis buffer (50 mM Tris, 0.8% Triton X-100, 0.2% SDS, pH 7.4). One volume of CH_3CN was added with vigorous mixing to precipitate the proteins. After centrifugation at 25 000 *g* for 15 min, the supernatants were collected for folic acid assay by HPLC.

HPLC analysis was conducted at ambient temperature in a reverse phase C_{18} column (4.6 × 250 mm, Waters Corporation, Milford, MA, USA) using a mobile phase of NaOAc buffer (50 mM NaOAc, pH 5.5) and CH_3CN in a volume ratio of 93:7. Flow rate was set at 1.0 ml/min and the eluent was detected at 290 nm. Folic acid dissolved at 30 to 200 ng/ml in the cell lysate solutions of the corresponding unexposed cell cultures were used to calibrate the HPLC. Cellular protein in each sample was quantified by the BCA method as described in section 3.3.3.2, and the cell-associated folic acid was expressed as ng folic acid/mg protein.

5.3.2 Doxorubicin uptake

The strong fluorescence emitted by doxorubicin (Ex $_{480nm}$ and Em $_{540nm}$) made it possible to quantify cellular doxorubicin uptake by fluorescence spectroscopy and cell cytometry. It also rendered it possible to use the confocal scanning laser microscope to visualize the intracellular location of the doxorubicin following its cellular uptake.

5.3.2.1 Fluorescence spectroscopy

Fluorescence spectroscopy provides a simple and accurate method for quantifying the cellular uptake of the formulations under investigation. The cells could be washed with an appropriate buffer after an uptake experiment to remove unassociated doxorubicin, and the residual cell-associated doxorubicin was quantified by measuring the fluorescence of the cell lysate [Xiong, et al., 2005].

To perform the cellular uptake experiments, formulations I, II, III and IV were prepared at 5 μg/ml equivalent doxorubicin concentration. The 3 cell types were separately seeded onto 6-well plates (Nunc™, Nalge Nunc International, Denmark) at a density of 100 000 cells/well and incubated for 24 h at 37 ^{o}C in the CO_2 incubator. After the cells were rinsed thrice with PBS, they were incubated for 2 h with 1 ml of specified formulation. The cells were subsequently washed thrice with ice-cold PBS and lyzed with 0.5 ml of lysis buffer [Veldman et al., 2005]. Cell-associated doxorubicin was determined by measuring the fluorescence of the lysate using a microplate reader (TECAN fluorometer) while the protein content in the cell lysate was measured using the BCA protein assay kit (section 3.3.3.2). The microplate reader was calibrated with

solutions of doxorubicin dissolved at 1 to 10 μg/ml in the corresponding cell lysate solutions. Drug uptake was expressed as the weight of cell-associated doxorubicin (ng) per unit weight (μg) of cellular protein.

5.3.2.2 Confocal scanning laser microscopy

Confocal scanning laser microscopy (CSLM), otherwise known as laser scanning confocal microscopy (LSCM), is a well established method to obtain high-resolution images or 3-D reconstructions of biological specimens [Hale and Matsumoto, 1993]. Compared with the conventional fluorescence microscope, the confocal microscope has several advantages. CLSM can be used to detect more than one fluorescent material in cellular milieu simply by varying the excitation and emission wavelengths used for viewing a sample [Mo and Lim, 2005]. Unlike the photomicrographs of conventional fluorescence microscopy, which tended to be blurred and to give poor contrast due to the fluorescent light scattered around the image, especially fluorescence originating from planes other than the plane of focus, the confocal microscope can exclude most of this unfocused light to provide sharp images. The confocal microscope also enables the observation of selected thin layers from a thick specimen, further improving resolution and contrast [Cullander, 1998; Robinson, 2001].

To prepare cells for CSLM, formulations I, II, III and IV were prepared at 5 μg/ml equivalent doxorubicin concentration. Cells grown in 75 cm^2 flasks were trypsinized after reaching 80% confluence and resuspended in 10 ml of cell culture medium. About 0.4 ml of cell suspension was placed in the well of a Lab-Tek chambered cover glass system (Nalge Nunc International, Naperville, IL, USA) and incubated at 37 ^{o}C in 95%

air/5% CO_2 environment for 24 h. The cells were rinsed thrice with PBS, and incubated with 0.4 ml of a specified formulation for 1 h at 37 ºC in 95% air/5% CO_2 environment. Uptake was terminated by aspirating the formulation and washing the cells thrice with PBS. Residual doxorubicin in the cell samples was visualized under a confocal microscope at Ex_{480nm} and Em_{540nm} (CSLM, Zeiss Axiovert 200M, Oberkochen, Germany) [Xiong et al., 2005].

5.3.2.3 Flow cytometry

Flow cytometry provides a means to measure certain physical and chemical characteristics of cells as they travel in suspension through a sensing point one by one [Xiong et al., 2005]. Both living and fixed cells can be analyzed as long as they present as single cells. At the sensing point, cells are detected based on fluorescence measurements. Although the flow cytometer makes measurement on one cell at a time, it can process thousands of cells in a few seconds, and is therefore a powerful tool for counting cells with different optical characteristics and structural features [Jorgensen, 2005]. In this project, successful doxorubicin uptake by a cell was reflected by higher fluorescence measurement in flow cytometry, and the fluorescence distribution profiles of cell populations were used to compare the uptake efficiency of the 4 formulations.

Cells cultured in 75 cm^2 flasks were trypsinized after washing thrice with 5 ml of PBS. Formulations I, II, III and IV were prepared at 20 µg/ml equivalent doxorubicin concentration. The trypsinized cells (100 000 cells**)** were incubated with 1 ml of specified formulation for 1 h at 37 ºC in 95% air/5% CO_2 environment. Doxorubicin uptake was

then quenched on ice and the cell suspensions were washed thrice with ice cold PBS. The cells were pelleted by centrifugation at 2 000 rpm for 2 min and resuspended in PBS at a density of 1000 000 cells/ml. The cell suspensions were subjected to flow cytometry analysis at Ex $_{480nm}$ and Em $_{540nm}$ (Altra ^{TM}, Beck-Coulter Inc., Germany). Data for each sample was based on the analysis of 20 000 cells.

5.3.3 Cytotoxicity assay

The *in vitro* efficacy of formulations I to IV was evaluated using the MTT assay. The experimental protocols were adapted from methods reported for folic acid-targeting systems [Lee and Low, 1995; Saul et al., 2003; Pan et al., 2002; Yang et al., 2004]. The CCL-186 and CNE-1 cells were cultured in 96 well-plates at a seeding density of 5 000 cells/well while the OVCAR-3 cells were similarly cultured at a seeding density of 20 000 cells/well. OVCAR-3 and CNE-1 cells were cultured in folic acid-deficient RPMI 1640 medium, and CCL-186 cells were cultured in normal RPMI 1640 medium. After 24 h incubation at 37^{o} C in a 5% CO_2/95% air atmosphere, the culture medium was aspirated, and the cells were washed thrice with PBS. The four formulations (Table 5-1) were prepared to give equivalent doxorubicin concentrations in the range of 0.005 to 30 μg/ml. After 2 h incubation with 0.1 ml of a specified formulation, the cells were washed thrice in PBS followed by incubation with 0.2 ml of fresh cell culture medium for 3 days. Cell viability was then determined by the MTT assay as described in section 2.3.4, and the IC_{50} values were calculated by the nonlinear regression sigmoidal dose-response equation (GraphPad Prism Version 3.00, CA, USA) .

5.4 Results and discussion

5.4.1 Folic acid uptake

The two cancer cell models were cultured in folic acid-deficient media to induce the expression of the FR [Reddy et al., 2001]. Cellular folic acid uptake experiments were subsequently performed to determine the level of expression of the receptor in each cell line. The cell-associated folic acid was determined by HPLC assay. This method was convenient for the quantification of cellular folic acid uptake, provided the intracellular enzymes did not degrade the internalized folic acid too rapidly.

Under the experimental conditions employed, folic acid was observed to elute from the HPLC chromatogram as a well-resolved peak at 9 min. Figure 5-1 shows typical HPLC chromatographs of the cell lysate solutions obtained from CCL-186, OVCAR-3 and CNE-1 cells following the folic acid uptake experiments. A similar folic acid peak was clearly discernible in the chromatographs of the OVCAR-3 and CNE-1 samples, indicating that the folic acid uptake rates in these cells were sufficiently large to overwhelm any intracellular metabolic pathways. Conversely, the absence of an apparent folic acid peak in the chromatographs of the CCL-186 cells was suggestive of a poor folic acid uptake rate by these cells.

Figure 5-2 shows the cell-associated folic acid content as a function of exposure time for the 3 cell models. Folic acid uptake by the OVCAR-3 cells was rapid, with saturation evident at 30 min of incubation. CNE-1 cells showed time-dependent folic acid uptake,

the cell-associated folic acid content following 30 min incubation being about 65% of that obtained after 1 h. However, folic acid uptake by the CNE-1 cells appeared to also peak after 1 h, the cells exhibiting a comparable cell-associated folic acid content as the OVCAR-3 cells. By comparison, the CCL-186 cells registered negligible folic acid uptake even after 2 h of incubation. Taken together, the results suggested that the OVCAR-3 and CNE-1 cells over-expressed the FR to comparable extents, while the CCL-186 cells appeared to lack the FR. Therefore, the OVCAR-3 and CNE-1 cells were appropriately applied as cancer cell models for the FR-targeting fPC-Dox formulation, while the CCL-186 cells were a suitable model of FR-deficient normal cells.

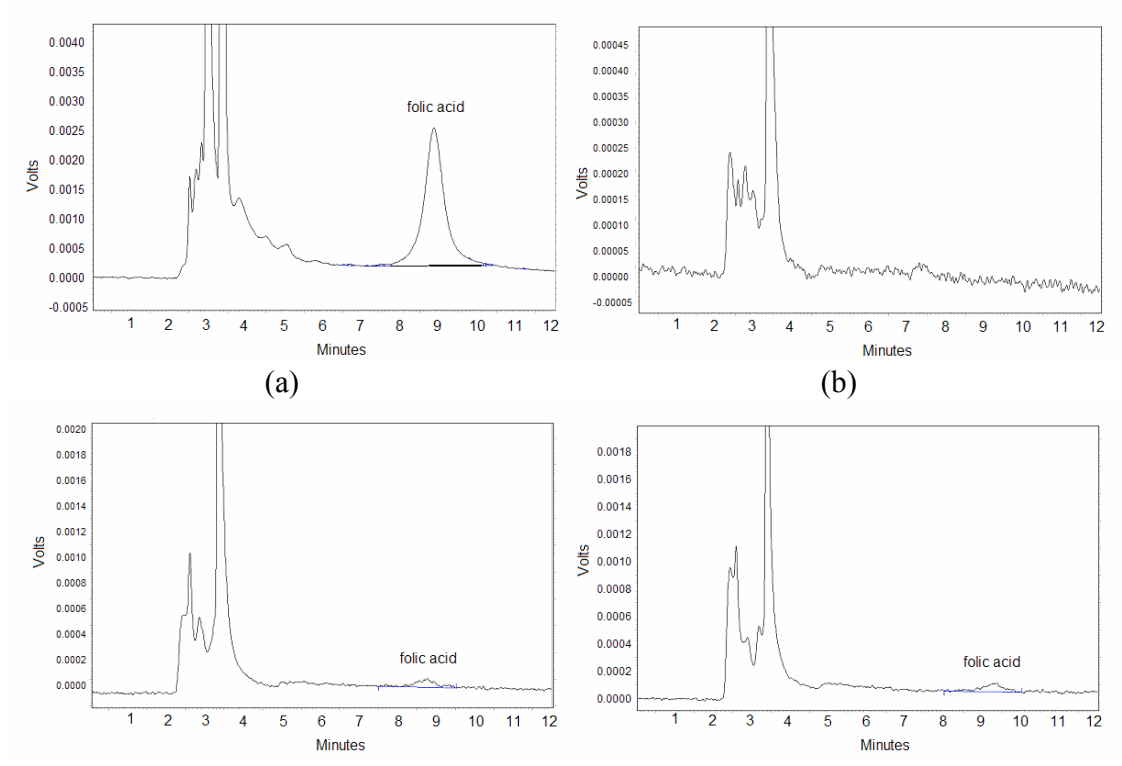

Figure 5-1. HPLC chromatographs of (a) folic acid (Retention time, R_t = 9 min); and (b) CCL-186 cells, (c) OVCAR-3 cells and (d) CNE-1 cells after 2 h of incubation with 1 mg/L of folic acid at 37°C.

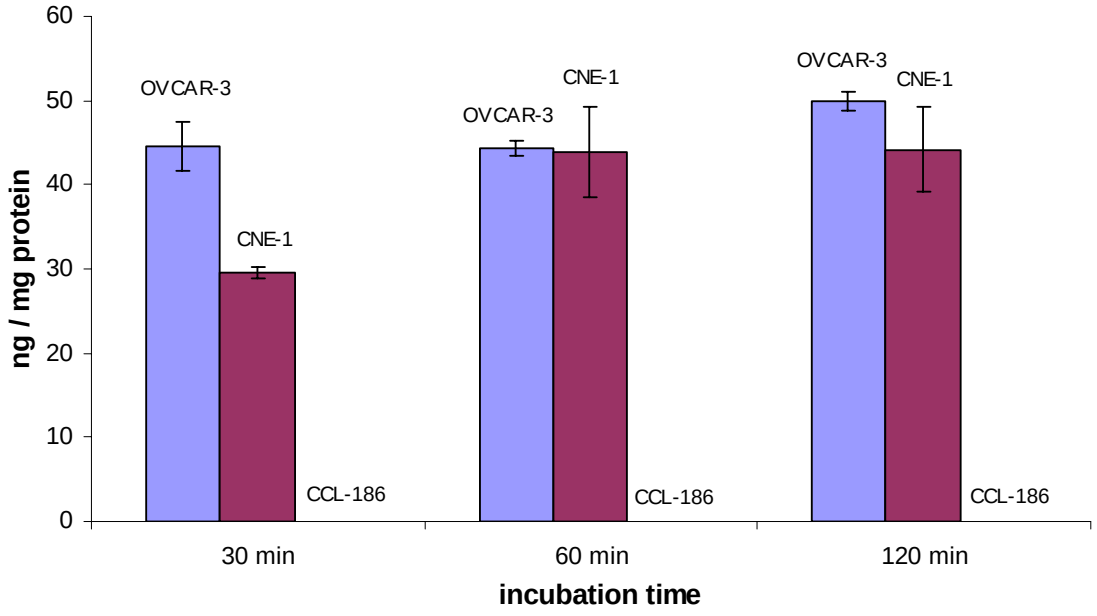

Figure 5-2 Effects of incubation time on folic acid uptake (ng/mg cellular protein) in the OVCAR-3, CNE-1 and CCL-186 cell models (Mean ± SD, n = 3). At 0 min, all 3 cell lines did not contain detectable levels of cell-associated folic acid.

5.4.2 Doxorubicin uptake

Cellular doxorubicin uptake was visualized by confocal microscopy and quantified by fluorimetry. Quantitative data showed a 2-fold higher cellular uptake of doxorubicin from fPC-Dox than from PC-Dox by the OVCAR-3 cells (Figure 5-3). A similar phenomenon was observed for the CNE-1 cells, which showed a 3-fold higher uptake of doxorubicin when incubated with fPC-Dox than with PC-Dox. Uptake of doxorubicin from PC-Dox was, however, no different from that from free doxorubicin for both cell lines, suggesting that doxorubicin encapsulation within the HCRSV-derived PC could not by itself aid in the intracellular accumulation of the drug in the OVCAR-3 and CNE-

1 cells. The fPC-Dox formulation did not result in an enhanced uptake of doxorubicin for the CCL-186 cells, which showed comparable drug uptake (2 ng/μg protein after 2 h incubation) from the free doxorubicin, PC-Dox and fPC-Dox samples (Figure 5-3).

The higher uptake rate of fPC-Dox in the cancer cells relative to normal cells might be explained by the up-regulation of FR in the former. To confirm a folic acid-mediated mechanism, the uptake experiments for fPC-Dox were conducted in the presence of excess free folic acid (formulation IV). The folic acid served as a competitive inhibitor, and if it were added at sufficiently high concentration, would block cellular fPC-Dox internalization via the FR-mediated endocytosis pathway. This was indeed observed, as the co-incubation of fPC-Dox with folic acid was found to negate the higher cellular doxorubicin uptake associated with the fPC-Dox sample for both the OVCAR-3 and CNE-1 cells. That a FR-mediated uptake mechanism was operative in the cellular uptake of fPC-Dox would affirm the participation of the conjugated folic acid in ligand-receptor binding at the cell surface. Thus, it may be concluded that the conjugation of folic acid to the HCRSV-derived PC did not hinder its targeting capability.

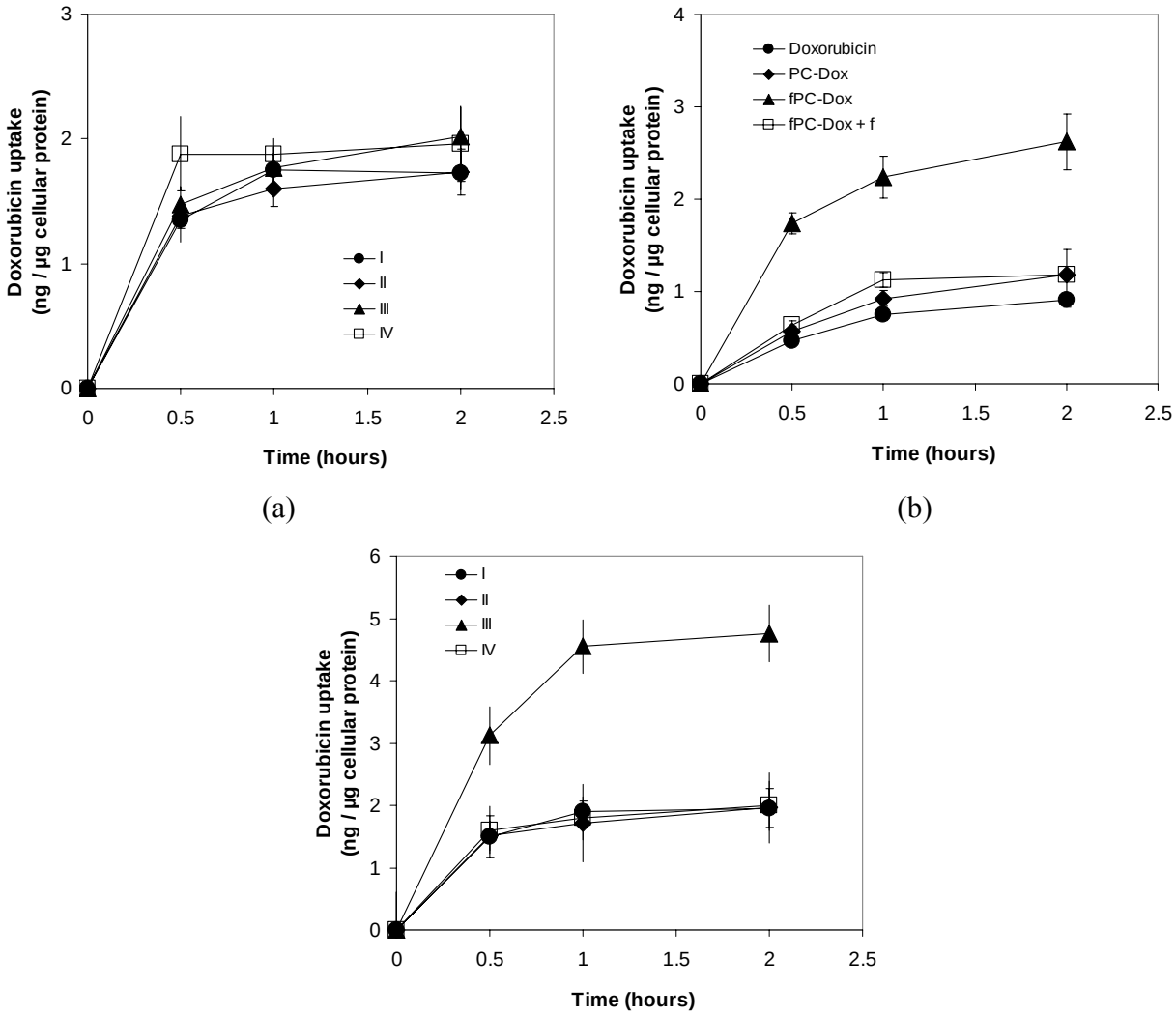

Figure 5-3. Cellular uptake of doxorubicin by (a) CCL-186, (b) OVCAR-3 and (c) CNE-1 cells incubated with free doxorubicin (I), PC-Dox (II) and fPC-Dox (III). Uptake of fPC-Dox was also undertaken in the presence of folic acid (IV). Data represent mean ± SD (n = 3).

Confocal micrographs provided supporting evidence for the folic acid-mediated preferential uptake of fPC-Dox by the OVCAR-3 and CNE-1 cells (Figure 5-4). OVCAR-3 and CNE-1 cells incubated with fPC-Dox showed more intense fluorescence compared to corresponding cells incubated with free doxorubicin or PC-Dox. Upon the addition of folic acid to the fPC-Dox sample, however, the fluorescence exhibited by the cells was reduced to a level similar to those observed in cells incubated with PC-Dox or free doxorubicin. For the CCL-186 cells, slightly stronger fluorescence was observed in cells incubated with free doxorubicin than in cells incubated with PC-Dox or fPC-Dox. The implication is that the loading of doxorubicin into the HCRSV-derived PC might actually decrease its uptake by the FR-deficient cells. These observations are therefore in good agreement with the quantitative uptake data.

The confocal micrographs provided another interesting observation. Doxorubicin typically accumulates in the nuclei of cells [Goren et al., 2000], and this was observed when formulation I (free doxorubicin) was administered to the 3 cell lines (Figure 5-4). However, the bright fluorescence spots attributed to the fPC-Dox were observed to be scattered in the cell cytoplasm rather than concentrated in the nuclei of the cells. This phenomenon was particularly evident in the case of the OVCAR-3 cells (Figure 5-4, b). The distribution of fPC-Dox in the cell cytoplasm would be consistent with a FR-mediated uptake mechanism, as the drug-loaded PC following endocytosis would be directed to the endosomes [Chatterjee et al., 2001].

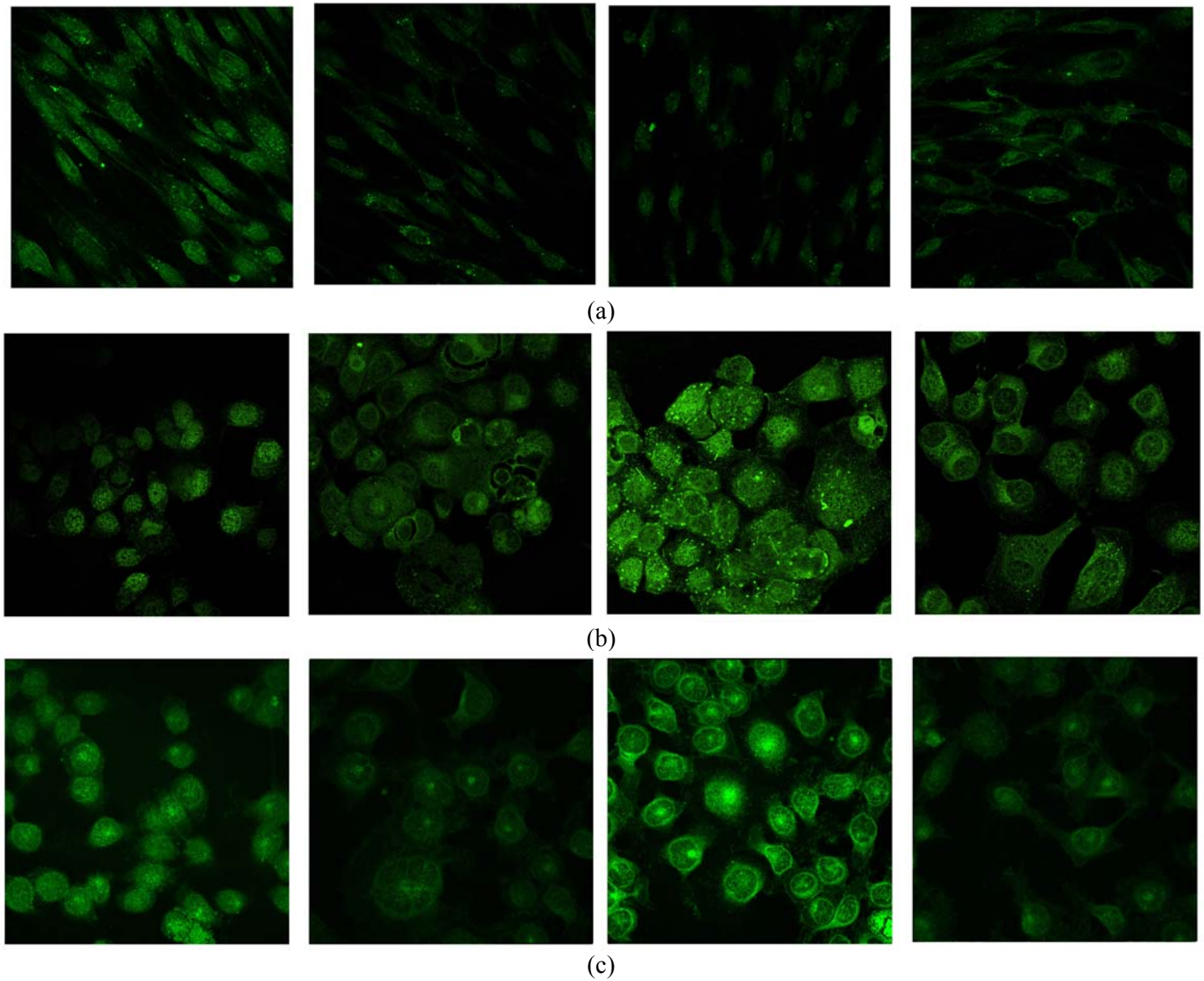

Figure 5-4. Confocal micrographs of (a) CCL-186 cells, (b) OVCAR-3 cells, and (c) CNE-1 cells following incubation for 1 h with formulations I, II, III and IV (from left to right). Green fluorescence is indicative of the presence of doxorubicin.

Flow cytometry provided yet further supporting evidence for the differential uptake of doxorubicin formulations by the cancer and normal cells. Analysis of the CCL-186 cells following uptake experiments showed a shift in the fluorescence peak, with cells incubated with doxorubicin formulations exhibiting stronger fluorescence, consistent with doxorubicin internalization, than untreated blank cells. There were, however, no significant shifts in the flow cytometry data for the CCL-186 cells exposed to the different doxorubicin formulations, indicating that doxorubicin uptake in these cells was not enhanced by the HCRSV-derived PC delivery platform (Figure 5-5, a). In contrast, the flow cytometry profiles of the cancer cell lines, OVCAR-3 and CNE-1, showed a significant shift to higher fluorescence when these cells were incubated with fPC-Dox than with free doxorubicin or PC-Dox. When uptake of fPC-Dox was conducted in the presence of excess folic acid, the resultant flow cytometry profile was similar to that of PC-Dox, again confirming a FR-mediated uptake mechanism.

A comparison of the flow cytometry profiles across different cell lines indicated a more homogeneous distribution of fluorescence in the OVCAR-3 cells than in the CNE-1 cells, which in turn exhibited a more homogenous fluorescence profile than the CCL-186 cells. These differences might be attributed to variation in the cell morphology. While the CNE-1 and OVCAR-3 cells were spherical in shape, the CCL-186 cells were elongated, and this elongation might have contributed to the less than homogeneous fluorescence profile of this cell population.

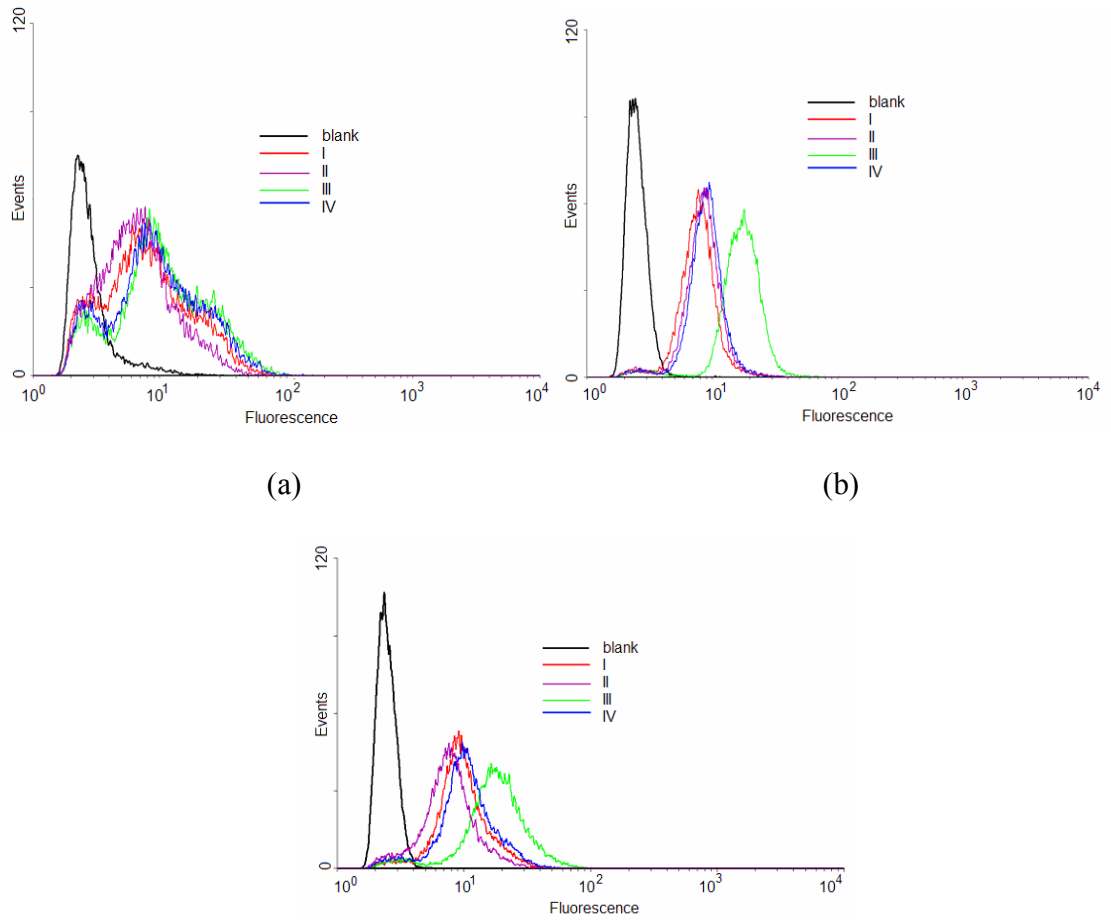

(a) (b)

(c)

Figure 5-5. Distribution of cellular fluorescence as evaluated by flow cytometry of (a) CCL-186 cells; (b) OVCAR-3 cells; and (c) CNE-1 cells following the incubation of the cells for 1 h at 37°C with free doxorubicin (I), PC-Dox (II), fPC-Dox (III) and fPC-Dox with 1 mM folic acid (IV). Untreated cells served as blank. Flow cytometry profile was generated from the analysis of 20 000 cells.

5.4.5 Cytotoxicity assay

Cytotoxicity of the various doxorubicin formulations against the OVCAR-3, CNE-1 and CCL-186 cells was assessed via the MTT assay after 2 h of exposure (Table 2). The $IC50_{doxorubicin}$ values, which represented the concentration of doxorubicin required for reducing the cell viability to 50%, was determined from the sigmoidal dose-response equation (Equation 5-1).

$$Y = min + (max - min) / (1 + 10 \times \log^{IC50-X}) \quad (5\text{-}1)$$

where Y was the cell viability measured by the MTT assay, X was the drug concentration expressed in logarithmic form (log C), and "min" and "max" were the cell viabilities obtained at the highest and lowest doses of 30 and 0.005 μg/ml, respectively [Curran-Everett, 2005]. $IC50_{doxorubicin}$ values were calculated from the equation using the GraphPad Prism 3.0 software.

In previous experiments, the native HCRSV had not been shown to exhibit overt toxicity towards the CCL-186, OVCAR-3 and CNE-1 cells at concentrations of up to 1 mg/ml (section 2.4.3). This concentration was higher than the concentrations of HCRSV-derived PC present in the PC-Dox and fPC-Dox formulations (protein concentration < 500 μg/ml) that were administered to the cells. In addition, a separate MTT assay for PSA (200 kDa), which had been incorporated into the PC-Dox and fPC-Dox formulations, had shown all three cell lines to have a viability of no less than 95% in the presence of 100 μg/ml PSA (Appendix III). On the basis of these preliminary data, any cytotoxicity associated with PC-Dox and fPC-Dox exposure might be attributed to the doxorubicin present in these formulations.

The sigmoidal-dose response curves and resultant $IC50_{doxorubicin}$ values for the various formulations are shown in Figure 5-6 and Table 5-1, respectively. Compared with the free doxorubicin and PC-Dox formulations, the fPC-Dox significantly shifted the dose-response curve to the left for the OVCAR-3 cells (Figure 5-6, b). This resulted in a decrease in the $IC50_{doxorubicin}$ value by 4-fold. In contrast, the PC-Dox formulation produced comparable $IC50_{doxorubicin}$ values to the free doxorubicin formulation, further affirming that drug encapsulation in the HCRSV-derived PC would not by itself confer additional benefits to its delivery to cancer cells. The enhancement of kill associated with fPC-Dox was again mediated by the conjugated folic acid, for the addition of excess free folic acid effectively abolished the added effect.

Similar results were observed for the CNE-1 cells, although these cells were more sensitive to doxorubicin than the OVCAR-3 cells, as evident from the dose-response curves (Figure 5-6, c) and $IC50_{doxorubicin}$ values obtained (Table 5-1). Like the OVCAR-3 cells, the CNE-1 cells were about 4-fold more sensitive to the fPC-Dox formulation than to the free doxorubicin formulation.

A comparison of the $IC50_{doxorubicin}$ across cell types indicated that the CCL-186 cells were the most resistant to doxorubicin cytotoxicity, about 4-fold more than the OVCAR-3 cells, and 20-fold more than the CNE-1 cells. Interestingly, the encapsulation of doxorubicin in either the PC-Dox or fPC-Dox led to a 1.6 to 1.7-fold increase in mean $IC50_{doxorubicin}$ value against the CCL-186 cells, alluding to a conferred protection of the cells against the drug. The differences in values were, however, not statistically significant.

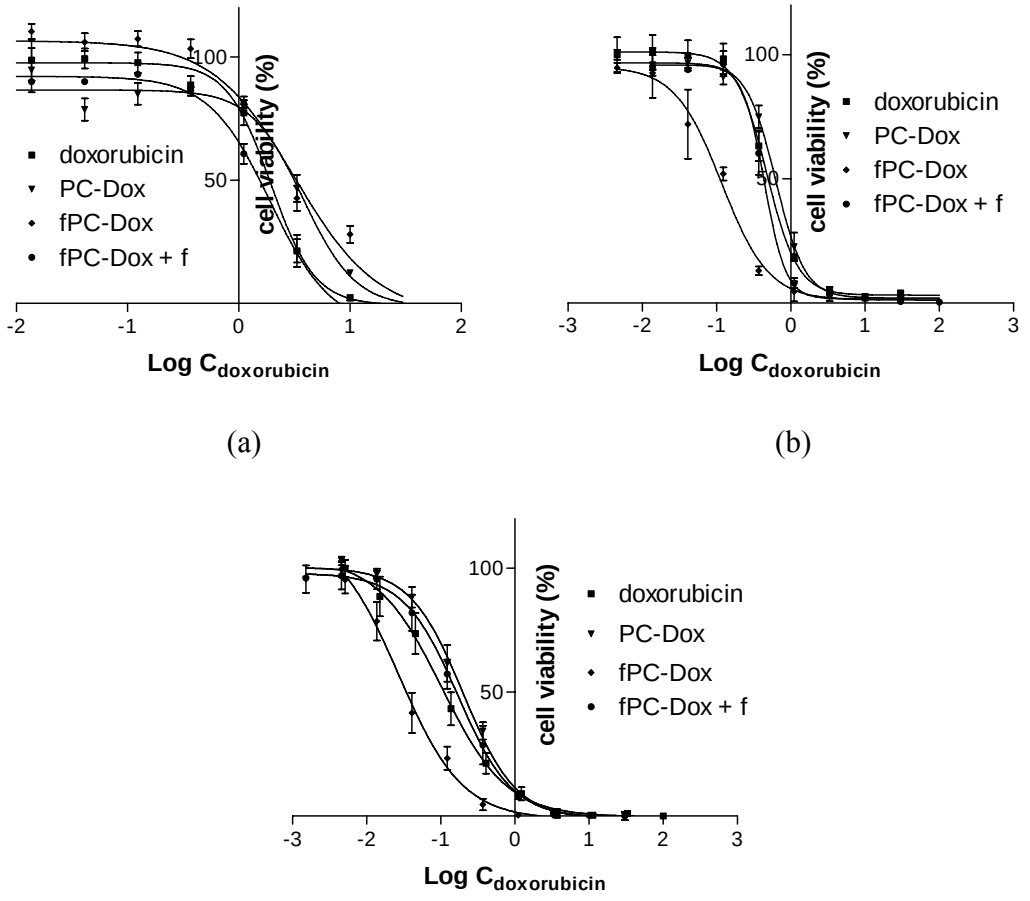

Figure 5-6. Dose-response curves of doxorubicin formulations for (a) CCL-186, (b) OVCAR-3 and (c) CNE-1 cells. Cell viability was determined by the MTT assay. Formulations evaluated comprised of free doxorubicin (I), PC-Dox (II), fPC-Dox (III) and fPC-Dox with 1 mM of folic acid (IV). Data represent mean ± SD, n = 3.

Formulation	IC50 (μg / ml, mean ± SD)		
	CCL-186	OVCAR-3	CNE-1
I	1.95 ± 0.15	0.48 ± 0.02	0.10 ± 0.05
II	3.41 ± 0.15	0.64 ± 0.10	0.20 ± 0.02
III	3.19 ± 0.39	0.11 ± 0.01*	0.027 ± 0.003*
IV	2.27 ± 0.27	0.49 ± 0.02	0.17 ± 0.02

Table 5-2. $IC50_{doxorubicin}$ values for CCL-186, OVCAR-3 and CNE-1 cell lines exposed to free doxorubicin (I), PC-Dox (II), fPC-Dox (III) and fPC-Dox with 1 mM folic acid (IV). Analysis by one-way ANOVA indicated that the $IC50_{doxorubicin}$ produced by fPC-Dox was significantly lower than those of the other formulations for the OVCAR-3 and CNE-1 cells. PC-Dox and fPC-Dox did not decrease the $IC50_{doxorubicin}$ compared with free doxorubicin in the CCL-186 cells (* $P < 0.05$ compared with other formulations, $n = 3$).

5.5 Conclusion

Folic acid uptake experiments confirmed that the cancer cell models comprising of OVCAR-3 and CNE-1 cell lines could over-express the FR when cultured in folic acid-deficient RPMI 1640 medium. The CCL-186 cells, which were derived from a human diploid fibroblast, did not over-express the FR when cultured under normal RPMI 1640 medium. It could therefore be applied as a control cell for the evaluation of FR-targeting systems.

Data obtained from fluorescence spectroscopy, confocal microscopy and flow cytometry indicated that the folic acid-conjugated fPC-Dox formulation could effectively

enhance doxorubicin uptake and cytotoxicity in the OVCAR-3 and CNE-1 cell cultures. On the other hand, the corresponding formulation without folic acid conjugation, the PC-Dox, was not an efficient delivery system for cancer chemotherapy. This is reasonable considering the current lack of evidence to support the cytoinvasive and cytotoxicity properties of plant viruses, including the HCRSV, in animal cells. PC-Dox could, however, be useful in clinical applications where sustained drug release and/or protection against cytotoxic drugs are desired.

The enhanced uptake of fPC-Dox in the cancer cells was inhibited by the co-administration of excess folic acid, indicating with the involvement of the FR-mediated endocytosis pathway. This would account for the failure of fPC-Dox to enhance the uptake and cytotoxicity of doxorubicin in the FR-deficient CCL-186 cells. The selectivity of action of the fPC-Dox in cancer cells warrant further evaluation of this system as a targeting platform for anticancer drug delivery.

The circulating endogenous folate concentration in human is around 10 ng/ml [Mito, Takimoto et. al., 2007]. This concentration was similar to that found in the folic acid-deficient RPMI 1640 medium supplemented with 10% of FBS [Lee and Low, 1995]. As the cellular drug uptake and cytotoxicity experiments were performed with doxorubicin formulations diluted in this medium, the in vitro results may well reflect the effects of endogenous folic acid on the efficiency of the HCRSV-based drug delivery systems. Further in vivo experiments will be helpful to substantiate the findings.

Chapter 6

Final conclusion

The hypothesis for this project was that protein cages (PC) derived from the plant virus, *Hibiscus chlorotic ringspot virus* (HCRSV), could serve as a platform for the development of a targeting anticancer drug delivery system. Compared with other nanoscale drug delivery platforms, the PC reassembled from the identical coat proteins (CP) of plant viruses have the advantages of being uniform in size and precise in structure. To obtain the CP, however, the native virus must be made to undergo capsid disassembly so that the viral RNA could be isolated and removed. The purified CP would require reassembly *in vitro* to give PC of consistent properties, preferably one that would be comparable in size and shape to the stable native viral capsid. In addition, the PC must be capable of holding a drug cargo during storage and to release it selectively into the target cancer tissue. The purpose of this project was to perform experimentation to test the hypothesis.

The raw material for the development of the drug delivery system was the HCRSV-derived CP. To ensure project continuity and reproducibility of data, it was vital to secure a reliable source of purified CP. This started with the cultivation of the HCRSV. The HCRSV was successfully cultured in kenaf leaves under controlled environment and efficiently purified by serial centrifugation on sucrose gradients to give reproducible yields of 4 to 5 mg of purified HCRSV per 100 g of leaves. These yields, although low, were adequate to meet the needs of the project.

The HCRSV capsids could be disassembled by incubation with 8 M of urea or by dialysis against a Tris buffer of pH 8 in the absence of Ca^{2+}. Successful RNA removal was confirmed by the lower $OD_{260\ nm}/OD_{280\ nm}$ values obtained for CP isolated from the disassembled mixture (~ 0.6) than for the native HCRSV (~1.5). The purified CP could

also be readily reassembled into empty PC by dialysis against a sodium acetate buffer of pH 5 in the presence of Ca^{2+}. Particle size measurement, together with transmission electron microscopy (TEM), provided proof that the reassembled PC, in particular those produced by the dialysis method, were comparable in size and morphology to the native HCRSV.

These methods were deemed to be effective and sufficiently mild, as circular dichroism analysis did not register major conformational changes in the protein structure following capsid disassembly and subsequent PC reassembly. They were therefore considered to be satisfactory in providing a stable supply of HCRSV-derived CP and PC for subsequent experimentation in this project. The scale of production was, however, small. On a commercial scale, it is probably not viable to obtain the purified PC from cultivated HCRSV. HCRSV cultivation in plants was influenced by environmental variables that might be difficult to control, and the subsequent processing that was necessary to produce the purified CP could be difficult to reproduce on a large scale. Moreover, the PC yield relative to the amount of resources invested into the process was low. Alternative methods could therefore be explored. One technique is to produce the HCRSV-CP by DNA recombinant technology, as the amino acid sequence of the CP is known. However, the CP produced must be able to fold and reassemble into PC that possesses the uniformity of size and precision of structure of the native HCRSV capsid.

Experiments involving the loading of PSA, PAA and FD into the HCRSV-derived PC indicated that the PC had the capacity to load exogenous materials that were negatively charged and had mw above a threshold value. These two prerequisites were congruent with the structure of the native HCRSV, which comprised of a negatively charged viral

RNA (3911bytes, 1,260 kDa) encapsulated within the protein capsid. Loading of PSA (13 to 990 kDa) and PAA (450 kDa) must be initiated concurrently with the assembly of the PC, for it was not possible to load any of these polyacids into preformed PC. A hypothesis was that surface cavities present on the preformed PC would limit cargo loading post-assembly. Molecules too large to traverse the cavities could not be loaded, while molecules capable of entering the cavities would, as readily, leached out through the cavities during subsequent processing. Conversely, when cargo loading was initiated together with PC reassembly, the cargo molecules participated in electrostatic interactions with the appropriate amino acids of the CP, and this could initiate PC reassembly [Douglas and Young, 1998]. The molecules were then enveloped within the PC during the reassembly process and, if they were too large to penetrate the cavities, would be effectively retained even upon subsequent processing. The partial retention of the 4.3 kDa-PSA in the PC suggested that the size of this molecule was close to the passage size limit of the cavities. The requirement for electrostatic interactions also explained why it was not possible to load the neutral FD molecules into the HCRSV-derived PC, despite some of the FD molecules meeting with the threshold mw.

Native gel electrophoresis data were in agreement with the particle size, zeta potential and TEM data in suggesting that the polyacid-loaded PC had comparable size and charge to the native HCRSV. Moreover, despite the 75-fold difference in mw, PSA of 13 to 990 kDa were encapsulated with comparable efficiency into the PC. The PSA loading efficiency of 15 to 20% also correlated closely with the value of 19% calculated for the genomic RNA in the native HCRSV. This suggests that the PC of HCRSV was capable of encapsulating exogenous materials to an amount equivalent to the mass of its native

genomic material. While the loading efficiency of PSA was independent on its mw, the number of PSA molecules that could be accommodated per PC particle (n) was inversely proportional to the mw of the PSA according to the relationship, $n = 1/mw \times 10^6$ (R^2 = 0.9969). For the largest PSA molecule, whose mw (990 kDa) approached that of the genomic RNA, only 1 molecule was accommodated in each PC. This restriction in cargo loading size based on the capacity of the virus cavity is not surprising, and is in fact an acknowledged limitation in viral-based gene delivery systems [Dong et al., 1996]. Collectively, these data indicated that the reassembly of HCRSV-derived CP into PC, even in the presence of guest molecules, had occurred by a precise mechanism to yield particles of uniform size and morphology. The robustness of structure is an advantage over polymer nanoparticles prepared by condensation for drug delivery, many of which had sizes that would vary with the nature and concentration of drug loaded [Mozafari, 2005; Szoka and Papahadjopoulos, 1978].

To impart a capability to target cancer tissues that over-express the folic acid receptor, the native HCRSV was conjugated with folic acid by a 2-step carbodiimide method. The conjugated folic acid did not affect the disassembly of the HCRSV, nor did it hinder the subsequent reassembly of the CP into fPC. Folic acid conjugation efficiency was 1.9%, which translated to about 360 folic acid molecules per fPC. The conjugation sites had not been determined with certainty in this project but, based on computer simulated modeling, the folic acid molecules were likely to be conjugated at the two exposed Lys sites of the protruding domain of the CP. The folic acid was conjugated at a high number, but it did not affect the capacity of the fPC to encapsulate PSA and PAA at similar loading efficiencies as the unconjugated PC. In addition, the PSA- and PAA-loaded fPC were

comparable in size, morphology and conformational structure to the corresponding polyacid-loaded PC without folic acid conjugation. The results further underscored the robustness of the PC structure.

Doxorubicin, the model anticancer drug used for the project, did not satisfy the twin requisites of possessing a negative charge and a mw above the specified threshold for loading into the PC. To overcome these barriers, a novel method named “polyacid association” was developed. This method involved the simultaneous encapsulation of doxorubicin with PSA (200 kDa), the PSA aiding in the retention of doxorubicin within the PC and fPC through the formation of a semi-stable complex by electrostatic interactions. The resultant systems, denoted as PC-Dox and fPC-Dox, were homogenously sized and shaped, and were similar in morphology and size to the native HCRSV. Drug encapsulation efficiency for both samples was within the acceptable range of 49 – 59%, with each PC containing about 900 entrapped doxorubicin molecules. The drug load in the PC-Dox and fPC-Dox was equivalent to 7 - 8% w/w, comparable with the load of other nano-sized systems of doxorubicin, such as chitosan micelles [Xiangyang et al., 2007] and alginate nanoparticles [Chavanpatil et al., 2007].

The encapsulated drug in PC-Dox and fPC-Dox was readily released upon dilution, with both samples exhibiting a sustained drug release profile at simulated physiological conditions. About 40% of the drug load was released within the initial 4 h, followed by a slower release of the remaining drug load from the PC over the next 20 h. The rapid drug release rate would be advantageous if it could be designed to occur only at the targeted site, since a premature drug release would negate the benefits conferred by the PC formulation. To achieve such a precise and controlled drug release mechanism would

necessitate further optimization of the PC-Dox and fPC-Dox formulations. A suitable dosage form (e.g. using a capsule to hold the PC formulation) or administration method (e.g. direct tumor injection or inhalation of lyophilized PC) may be helpful towards keeping the drug within the PC until it is to be released into the targeted sites.

Proof of concept of the delivery systems was obtained by evaluating the efficacy of the PC-Dox and fPC-Dox formulations in representative cell culture models. The cancer cell models were OVCAR-3 (human ovarian epithelial adenocarcinoma) and CNE-1 (human nasopharyngeal carcinoma), while the CCL-186 (human diploid fibroblast) cell line was used as a normal cell model. To ensure the cell models were appropriate for the evaluation of a folic acid-conjugated delivery system, folic acid uptake experiments were conducted. The data confirmed the over-expression of the folic acid receptor in the OVCAR-3 and CNE-1 cells cultured in folic acid-deficient RPMI-1640 medium, while the CCL-186 cells did not over-express the folic acid receptor when cultured in normal RPMI-1640 medium. Data obtained from fluorescence spectroscopy, confocal microscopy and flow cytometry supported the enhanced efficacy of fPC-Dox relative to PC-Dox and doxorubicin in solution. The fPC-Dox formulation was found to enhance doxorubicin uptake in the OVCAR-3 and CNE-1 cells by 2 to 3-fold. Although this enhancement in cellular uptake might be regarded as modest compared with other folic acid-based targeting systems, which typically increased cellular uptake by 7 [Saul et al., 2003] to 40 [Lee and Low, 1995] folds, it was nevertheless accompanied by significantly higher cytotoxicity as evaluated by the MTT assay. The cytotoxicity of fPC-Dox could not be attributed to the CP or PSA because the HCRSV and PSA at concentrations

equivalent to those applied in the PC-Dox and fPC-Dox formulations had been shown by the MTT assay to be non-cytotoxic towards the 3 cell lines.

Cellular uptake and cytotoxicity of PC-Dox were comparable to doxorubicin in solution, suggesting that doxorubicin encapsulation within the HCRSV-derived PC could not by itself increase drug efficacy in the cancer cell models. This is because drug uptake from the PC-Dox probably occurred by a mechanism similar to that of the free drug, i.e. by passive diffusion [Mulder et al., 1995]. Unlike the fPC-Dox, PC-Dox did not present with a ligand that could stimulate cellular uptake by a receptor-mediated endocytic pathway, and there is currently no evidence to support the cytoinvasive and cytotoxicity properties of plant viruses, including the HCRSV, in animal cells. Moreover, the *in vitro* drug release data had shown a fair amount of the encapsulated drug to be released from the PC-Dox upon dilution, and the released drug would enter the cells in a manner similar to that of the free doxorubicin formulation. This in turn would drive more encapsulated drug to be dissociated from the PSA backbone and be released into the cellular milieu to be taken up by the cells by passive diffusion. However, it might also be argued that the PC-Dox could be internalized by the cells by a non-receptor mediated endocytic pathway, as the size of the PC was comparable to the optimized size of nanoparticles shown to be transported via this pathway [Chithrani et al., 2006]. Certainly the TEM micrographs supported the PC presence in the cell cytoplasm, which was consistent with the trafficking pathway of endocytosed particles.

While the PC-Dox was unable to increase the efficacy of doxorubicin, this formulation could be adapted to applications where sustained drug release is desired. For this to be realized, however, the PC-Dox may have to be further optimized. An example

would be to deliver the PC-Dox in a enteric-coated capsule that is able to deliver the formulation to the intestinal epithelium for drug release and subsequent absorption. Otherwise, the dilution of the formulation during its passage to the site of absorption could lead to premature drug release.

Co-administration of an excessive amount of folic acid was shown to negate the enhanced cellular uptake of fPC-Dox by the OVCAR-3 and CNE-1 cells, thus lending support to the role of the folic acid receptor in mediating the cellular uptake of this formulation. Supporting evidence was provided by the TEM micrographs, which showed the intracellular doxorubicin to be distributed in the cell cytoplasm, consistent with the trafficking pathway of vesicles involved in folic acid-mediated endocytosis. On the basis of these data, it might be surmised that the conjugated folic acid on the fPC-Dox was still capable of binding with the membrane folic acid receptor to initiate endocytic uptake, and that the fPC-Dox was not too large to be endocytosed by this pathway. This mechanism of uptake of the fPC-Dox provided for its selectivity of action, for it failed to show an enhanced uptake in the folic acid receptor-deficient CCL-186 cells. Consequently, the fPC-Dox can be considered to have the potential to be applied as a targeting platform for anticancer drug delivery, and its formulation should be further optimized to realize this potential.

Chapter 7

Future directions

Results from this project have shown that the HCRSV-derived PC can serve as a carrier for drug delivery, and that the PC can be functionalized with folic acid for enhanced drug delivery into cancer cells that over-express the folic acid receptor. Much work remains to be done, however, before this delivery platform can be approved for clinical applications. The following studies will aid in moving the HCRSV-derived PC towards this direction.

Production of the purified CP from plant-cultivated HCRSV has been identified as a possible hindrance towards achieving a scaled up production of the PC for drug delivery. The cultivation of HCRSV-infected kenaf was time-consuming, with each batch of purified HCRSV taking months to produce. Moreover, the yield of HCRSV was low, and its contamination by opportunistic virus remained a constant threat despite the use of an isolated environment for cultivation. For the HCRSV-derived PC to move into animal and clinical studies, a more efficient method has to be developed to produce the purified CP on a larger scale. Protein expression by *E. coli* or yeasts using DNA recombinant technology can be a more cost-effective method for producing a large quantity of purified CP within a few days. However, the recombinant CP must be capable of reassembling into PC that possesses the beneficial characteristics of the native HCRSV capsids.

Biodistribution and pharmacokinetic studies should be conducted on the blank HCRSV-derived PC, fPC-Dox and PC-Dox. In particular, it will be interesting to evaluate whether the PC is capable of trafficking across absorptive epithelia. This is because the CPMV, a plant virus similar to the HCRSV, has been found distributed in a wide variety of tissues following oral administration in mice [Rae et al., 2005]. As the mechanism of absorption is not presently known, this could be determined using the

appropriate cell model, e.g. the Caco-2 cell monolayers cultured on Transwells inserts to represent intestinal epithelium. To apply the HCRSV-derived PC as a carrier for oral drug delivery, experiments must also be conducted to verify its stability in the GI milieu. Therefore, studies on the degradation of the PC under different physiological environment, and in the presence of proteases or the cytochrome P450 family of enzymes, should be undertaken. Studies to determine the predominant mode of clearance of the PC *in vivo*, as well as its propensity to mount an immune response in animal models, will generate further supporting data to assess its potential for clinical application.

The fPC-Dox formulation has been shown to enhance doxorubicin uptake in cancer cell models that over-express the folic acid receptor. Additional studies will have to be performed to confirm its targeting capability and efficacy *in vivo*. In particular, it will be necessary to establish whether the fPC-Dox can target cancer tissues when injected intravenously. The formulation can also be further improved, as the increase in cellular doxorubicin uptake associated with fPC-Dox was modest compared to other folic acid-based targeting systems. For example, a folic acid-targeting liposomal system of aclacinomycin A has been shown to enhance drug uptake by 200-fold in the a human nasopharyngeal cancer line (KB), and to enhance the corresponding drug cytotoxicity by 90 fold [Shiokawa et al., 2005]. In the liposomal system, the folic acid was conjugated to the liposome via a long chain PEG linker (mw 5000) with a view to increase the accessibility of folic acid for interaction with the FR. A similar conjugation strategy can be considered for the HCRSV-based PC system to improve its uptake and cytotoxicity against cancer cells.

Other than doxorubicin, the HCRSV-derived PC can be considered for the delivery of other drugs. The present study has shown that it is possible to use the PC to load negatively charged macromolecules. On this basis, the PC can be evaluated as a gene vector, although surface functionalization is probably required to allow the PC to deliver therapeutic levels of DNA into animal cells. The PC can also be used to load small molecules based on the “polyacid association” concept. This method of loading, however, causes the system to release a bolus dose of the encapsulated drug upon dilution. The formulation will therefore have to be modified to ensure the encapsulated drug is released only at the target site. Studies can be conducted, for example, to test whether it is feasible to place the formulation into enteric-coated capsules or tablets for delivery to the intestinal epithelium.

To summarize, the application of plant virus-derived PC for drug delivery is in its infancy, but the potential appears to be highly promising. As more is understood of how these platforms can be harnessed for drug delivery, it is reasonable to predict that safe and effective drug delivery systems based on plant virus-PC will become available in the not too distant future.

Chapter 8

References

Allen TM, Cheng WW, Hare JI, Laginha KM. Pharmacokinetics and pharmacodynamics of lipidic nano-particles in cancer. Anticancer Agents Med Chem. 2006; 6:513-23

Allen TM, Hansen CB, Guo LS. Subcutaneous Administration of Liposomes: A Comparison with the Intravenous and Intraperitoneal Routes of Injection, Biochim Biophys Acta. 1993; 1150:9–16.

Arimilli, S., M. A. Alexander-Miller, and G. D. Parks. A simian virus 5 (SV5) P/V mutant is less cytopathic than wild-type SV5 in human dendritic cells and is a more effective activator of dendritic cell maturation and function. J. Virol. 2006; 80:3416-27

Bagalkot V, Farokhzad OC, Langer R, Jon S. An Aptamer-Doxorubicin Physical Conjugate as a Novel Targeted Drug-Delivery Platform. Angew Chem Int Ed Engl. 2006; 45:8149-52

Bajetta E, Celio L, Buzzoni R, Ferrari L, Marchiano A, Martinetti A, Longarini R, Becerra C, Ilardi C, John W. Phase II study of pemetrexed disodium (Alimta) administered with oral folic acid in patients with advanced gastric cancer. Ann Oncol. 2003; 14:1543-8

Bancroft JB, Hiebert E. Formation of an infectious nucleoprotein from protein and nucleic acid isolated from a small spherical virus. Virology. 1967; 32:354-6

Bancroft JB, Wagner GW, Bracker CE. The self-assembly of a nucleic-acid free pseudo-top component for a small spherical virus. Virology. 1968; 36:146-9

Baselga J, Albanell J, Molina MA, Arribas J. Mechanism of action of trastuzumab and scientific update, Semin. Oncol. 2001; 28:4–11.

Beachy RN, Heinlein M. Role of P30 in replication and spread of TMV. Traffic. 2000; 1:540-4

Berthome R, Kusiak C, Renou JP, Albouy J, Freire MA, Dinant S. Relationship of the pelargonium flower break carmovirus (PFBV) coat protein gene with that of other carmoviruses. Arch Virol. 1998; 143:1823-9

Bertin PA, Smith D, Nguyen ST. High-density doxorubicin-conjugated polymeric nanoparticles via ring-opening metathesis polymerization. Chem Commun (Camb). 2005; 30:3793-5

Bharali DJ, Lucey DW, Jayakumar H, Pudavar HE, Prasad PN. Folate-receptor-mediated delivery of InP quantum dots for bioimaging using confocal and two-photon microscopy. *J. Am. Chem. Soc.* 2005; *127,* 11364-71

Blum AS, Soto CM, Wilson CD, Brower TL, Pollack SK, Schull TL, Chatterji A, Lin T, Johnson JE, Amsinck C, Franzon P, Shashidhar R, Ratna BR. An engineered virus as a scaffold for three-dimensional self-assembly on the nanoscale. Small. 2005; 1:702-6

Bonetti A, Zaninelli M, Durante E, Fraccon AP, Franceschi T, Pasini F, Zustovich F, Brienza S. Multiple-target chemotherapy (LV-modulated 5-FU bolus and continuous infusion, oxaliplatin, CPT- 11) in advanced 5-FU-refractory colorectal cancer: MTD definition and efficacy evaluation. A phase I-II study. Tumori. 2006; 92:389-95

Bougnoux P, Giraudeau B, Couet C. Diet, cancer, and the lipidome. Cancer Epidemiol Biomarkers Prev. 2006; 15:416-21.

Burden DA, Osheroff N. Mechanism of action of eukaryotic topoisomerase II andd rugs targeted to the enzyme. Biochim Biophys Acta 1998; 1400:139–54

Burish TG, Tope DM. Psychological techniques for controlling the adverse side effects of cancer chemotherapy: findings from a decade of research. J Pain Symptom Manage. 1992; 7:287-301

Capranico G, Dasdia T, Zunino F. Comparison of doxorubicin-induced DNA damage in doxorubicin-sensitive and -resistant P388 murine leukemia cells. Int J Cancer. 1986; 37:227-31

Carrington JC, Heaton LA, Zuidema D, Hillman BI, Morris TJ. The genome structure of turnip crinkle virus. Virology. 1989; 170:219-26

Chajes V, Bougnoux P. N-6/N-3 polyunsaturated fatty acid ratio and cancer. World Rev Nutr Diet 2003; 92:133 – 51.

Chan SH, Aetiology of nasopharyngeal carcinoma. Ann Acad Med Singapore. 1990; 19:201-207.

Chang JC, Mohsin S, Weiss H, Hilsenbeck SG, Guttierez C, Lucci A. Induction of apoptosis without change in cell proliferation in primary breast cancers with neoadjuvant trastuzumab, Breast Cancer Res. Treat. 82 (2003) 24.

Chatterjee S, Smith ER, Hanada K, Stevens VL. Mayor S. GPI anchoring leads to sphingolipid-dependent retention of endocytosed proteins in the recycling endosomal compartment. *EMBO J. 2001; 20,* 1583-92

Chatterji A, Burns LL, Taylor SS, Lomonossoff GP, Johnson JE, Lin T, Porta C. Cowpea mosaic virus: from the presentation of antigenic peptides to the display of active biomaterials. Intervirology. 2002; 45:362-370

Chatterji A, Ochoa W, Shamieh L, Salakian SP, Wong SM, Clinton G, Ghosh P, Lin T, Johnson JE. Chemical conjugation of heterologous proteins on the surface of Cowpea mosaic virus. Bioconjug Chem. 2004; 15: 807-13.

Chavanpatil MD, Khdair A, Panyam J. Surfactant-polymer Nanoparticles: A Novel Platform for Sustained and Enhanced Cellular Delivery of Water-soluble Molecules. Pharm Res. 2007; 24:803-10

Chen C, Daniel MC, Quinkert ZT, De M, Stein B, Bowman VD, Chipman PR, Rotello VM, Kao CC, Dragnea B. Nanoparticle-templated assembly of viral protein cages. Nano Lett. 2006; 6:611-5

Chen Q, Tong S, Dewhirst MW, Yuan F. Targeting tumor microvessels using doxorubicin encapsulated in a novel thermosensitive liposome. Mol Cancer Ther. 2004; 3:1311-7

Chithrani BD, Ghazani AA, Chan WC. Determining the size and shape dependence of gold nanoparticle uptake into mammalian cells. Nano Lett. 2006; 6:662-8

Choi YG, Rao AL. Packaging of tobacco mosaic virus subgenomic RNAs by Brome mosaic virus coat protein exhibits RNA controlled polymorphism. Virology. 2000; 275:249-57

Chu TC, Marks JW 3rd, Lavery LA, Faulkner S, Rosenblum MG, Ellington AD, Levy M. Aptamer:toxin conjugates that specifically target prostate tumor cells. Cancer Res. 2006; 66:5989-92

Citovsky V. Tobacco mosaic virus: a pioneer of cell-to-cell movement. Philos Trans R Soc Lond B Biol Sci. 1999; 354:637-43

Ciuffreda P, Rubino L, Russo M. Molecular cloning and complete nucleotide sequence of galinsoga mosaic virus genomic RNA. Arch Virol. 1998; 143:173-80

Ciuffreda P, Rubino L, Russo M. Molecular cloning and complete nucleotide sequence of galinsoga mosaic virus genomic RNA. Arch Virol. 1998; 143:173-80

Colomer R, Menendez JA. Mediterranean diet, olive oil and cancer. Clin Transl Oncol. 2006; 8:15-21

Connors JM. State-of-the-art therapeutics: Hodgkin's lymphoma. J Clin Oncol. 2005; 23:6400-08

Cooley S, Burns LJ, Repka T, Miller JS, Natural killer cell cytotoxicity of breast cancer targets is enhanced by two distinct mechanisms of antibody-dependent cellular cytotoxicity against LFA-3 and HER2/neu, Exp. Hematol. 1999; 27:1533–41.

Craparo EF, Cavallaro G, Bondi ML, Mandracchia D, Giammona G. PEGylated Nanoparticles based on a polyaspartamide. preparation, physico-chemical characterization, and intracellular uptake. Biomacromolecules. 2006; 7:3083-92.

Crescenzi A, Comes S, Napoli C, Fanigliulo A, Pacella R, Accotto GP.Severe outbreaks of tomato yellow leaf curl Sardinia virus in Calabria, Southern Italy. Commun Agric Appl Biol Sci. 2004; 69:575-80.

Crick FH, Watson JD, Structure of small viruses. Nature. 1956; 177:473-5

Crystal RG, McElvaney NG, Rosenfeld MA, Chu CS, Mastrangeli A, Hay JG., Brody SL, Jaffe HA., Eissa NT. Danel C. Administration of an adenovirus containing the human CFTR cDNA to the respiratory tract of individuals with cystic fibrosis. *Nat. Genet*. 1994; **8**: 42-51

Cullander C. Light microscopy of living tissue: the state and future of the art. J Investig Dermatol Symp Proc. 1998; 3:166-71

Cunningham MJ, Brooks JS, Noumoff JS. Treatment of primary ovarian angiosarcoma with ifosfamide and doxorubicin. Gynecol Oncol. 1994; 53:265-68.

Curran-Everett D. Estimation of dose-response curves and identification of peaks in hormone pulsations: classic marriages of statistics to science. Am J Physiol Endocrinol Metab. 2005; 289:E363-E365

da Costa M, Rothenberg SP. Purification and characterization of folate binding proteins from rat placenta, Biochim Biophys Acta. 1996; 1292:23-30

da Poian AT, Oliveira AC, Silva JL. Cold denaturation of an icosahedral virus. The role of entropy in virus assembly. Biochemistry. 1995; 34:2672-7

de Jonge J, Holtrop M, Wilschut J, Huckriede A. Reconstituted influenza virus envelopes as an efficient carrier system for cellular delivery of small-interfering RNAs. Gene Ther. 2006; 13:400-11.

De Mey M, Lequeux G, Maertens J, De Maeseneire S, Soetaert W, Vandamme E. Comparison of DNA and RNA quantification methods suitable for parameter estimation in metabolic modeling of microorganisms. Anal Biochem. 2006; 353:198-203

Deutz A, Fuchs K, Schuller W, Nowotny N, Auer H, Aspock H, Stunzner D, Kerbl U, Klement C, Kofer J: Seroepidemiological studies of zoonotic infections in hunters in southeastern Austria—Prevalences, risk factors, and preventive methods. Berl Munch Tierarztl Wochenschr 2003; 116: 306–311

Di Filippo F, Garinei R, Anza M, Cavaliere F, Giannarelli D, Cagol PP, Rossi CR, Santinami M, Deraco M, Botti C, Perri P, Di Filippo S, Piarulli L, Bruno P. Doxorubicin in isolation limb perfusion in the treatment of advanced limb soft tissue sarcoma. J Exp Clin Cancer Res. 2003; 22:S81-7

Doan DN, Lee KC, Laurinmaki P, Butcher S, Wong SM, Dokland T. Three-dimensional reconstruction of hibiscus chlorotic ringspot virus. J Struct Biol. 2003; 144:253-61

Doll R, Hill AB. Mortality in relation to smoking. 10 years observations of British doctors. BR Med J. 1964; 5396:1460-1467

Dong JY, Fan PD, Frizzell RA. Quantitative analysis of the packaging capacity of recombinant adeno-associated virus. Hum Gene Ther. 1996; 7:2101-2112

Douglas T, Young M. Host-guest encapsulation of materials by assembled virus protein cages. Nature, 1998; 393:152-5

Douglas T, Young M. Protein Engineering of a Viral Cage for Constrained Nanomaterials Synthesis. Adv Mater. 2002; 14:415-8

Douglas, T., Young, M. Viruses: Making Friends with Old Foes. *Science 2006; 312,* 873-5.

Drabick JJ, Bhattacharjee AK, Hoover DL, Siber GE, Morales VE, Young LD, Brown SL, Cross AS. Covalent polymyxin B conjugate with human immunoglobulin G as an antiendotoxin reagent. Antimicrob Agents Chemother. 1998; 42:583-8.

Drabick, J. J., Bhattacharjee, A. K., Hoover, D. L., Siber, G. E., Morales, V. E., Young, L. D., Brown, S. L. and Cross, A. S. Covalent polymyxin B conjugate with human

immunoglobulin G as an antiendotoxin reagent. Antimicrob. Agents Chemother. 1998; 42:583-8.

Drummond DC, Hong K, Park JW, Benz CC, Kirpotin DB, Liposome targeting to tumors using vitamin and growth factor receptors, Vitam. Horm. 2000; 60:285–332.

Dube D, Francis M, Leroux JC Winnik FM. Preparation and tumor cell uptake of poly(N-isopropylacrylamide) folate conjugates. *Bioconjug. Chem.* 2002; *13:*685-92.

Dvorak HF, Nagy JA, Dvorak JT, Dvorak AM. Identification and characterization of the blood vessels of solid tumors that are leaky to circulating macromolecules. Am J Pathol. 1988; 133:95-109.

Dzianott AM, Bujarski JJ. The nucleotide sequence and genome organization of the RNA-1 segment in two bromoviruses: broad bean mottle virus and cowpea chlorotic mottle virus. Virology. 1991; 185:553-62

Falo LD Jr, Kovacsovics-Bankowski M, Thompson K, Rock KL. Targeting antigen into the phagocytic pathway in vivo induces protective tumour immunity. Nat Med. 1995; 1:649-53

Fazzi R, Caracciolo F, Galimberti S, Petrini M. Early reappearance of primary solid cancer in patients treated with purine analogs. J Chemother. 2003; 15:406-8

Feinstein E, Canaani E, Weiner LM. Dependence of nucleic acid degradation on in situ free-radical production by Adriamycin. Biochemistry 1993; 32:13156-61.

Fisher MS, Kripke ML. Suppressor T lymphocytes control the development of primary skin cancers in ultraviolet-irradiated mice. Science 1982; 216: 1133-4.

Fox JM, Wang G, Speir JA, Olson NH, Johnson JE, Baker TS, Young MJ Comparison of the native CCMV virion with in vitro assembled CCMV virions by cryoelectron microscopy and image reconstruction. Virology. 1998; 244:212-8

Fritze A, Hens F, Kimpfler A, Schubert R, Peschka-Suss R. Remote loading of doxorubicin into liposomes driven by a transmembrane phosphate gradient. Biochim Biophys Acta. 2006;1758:1633-40

Fujimoto-Ouchi K, Sekiguchi F, Yasuno H, Moriya Y, Mori K, Tanaka Y. Antitumor activity of trastuzumab in combination with chemotherapy in human gastric cancer xenograft models. Cancer Chemother Pharmacol. 2007; 59:795-805

Fuller SD, Wilk T, Gowen BE, Krausslich HG, Vogt VM. Cryo-electron microscopy reveals ordered domains in the immature HIV-1 particle. Curr Biol. 1997; 7:729-38

Gabizon AA, Barenholz Y, Bialer M. Prolongation of the circulation time of doxorubicin encapsulated in liposomes containing a polyethylene glycol-derivatized phospholipid: pharmacokinetic studies in rodents and dogs. Pharm Res 1993; 10:703-8

Gallois L, Fiallo M, Garnier-Suillerot A. Comparison of the interaction of doxorubicin, daunorubicin, idarubicin and idarubicinol with large unilamellar vesicles. Circular dichroism study. Biochim. Biophys. Acta 1998; 1370:31-40.

Gamble GR.Variation in surface chemical constituents of cotton (Gossypium hirsutum) fiber as a function of maturity. J Agric Food Chem. 2003; 51:7995-8

Gerlier D, Thomasset N. Use of MTT colorimetric assay to measure cell activation. J Immunol Methods. 1986; 94:57-63

Goll JH, Stock GB. Determination by photon correlation spectroscopy of particle size distributions in lipid vesicle suspensions. Biophys J. 1977; 19:265-73

Goren D, Horowitz AT, Tzemach D, Tarshish M, Zalipsky S, Gabizon A. Nuclear delivery of doxorubicin via folate-targeted liposomes with bypass of multidrug-resistance efflux pump. Clin Cancer Res. 2000; 6:1949-57

Grabarek Z, Gergely J. Zero-length crosslinking procedure with the use of active esters. Anal Biochem. 1990; 185:131-5

Grailer A, Sollinger HW, Burlingham WJ. A rapid assay for measuring both colony size and cytolytic activity of limiting dilution microcultures. J Immunol Methods. 1988; 107:111-7

Greenfield NJ. Methods to estimate the conformation of proteins and polypeptides from circular dichroism data. Anal Biochem. 1996; 235:1-10

Greish K, Sawa T, Fang J, Akaike T, Maeda H. SMA-doxorubicin, a new polymeric micellar drug for effective targeting to solid tumours. J Control Release. 2004; 97:219-30

Guilley H, Carrington JC, Balazs E, Jonard G, Richards K, Morris TJ. Nucleotide sequence and genome organization of carnation mottle virus RNA. Nucleic Acids Res. 1985; 13:6663-77

Hacker DL, Petty IT, Wei N, Morris TJ. Turnip crinkle virus genes required for RNA replication and virus movement. Virology 1992; 186:1–8.

Hale IL, Matsumoto B.Resolution of subcellular detail in thick tissue sections: immunohistochemical preparation and fluorescence confocal microscopy. Methods Cell Biol. 1993; 38:289-324

Hamaguchi T, Matsumura Y, Suzuki M, Shimizu K, Goda R, Nakamura I, Nakatomi I, Yokoyama M, Kataoka K, Kakizoe T. NK105, a paclitaxel-incorporating micellar nanoparticle formulation, can extend in vivo antitumour activity and reduce the neurotoxicity of paclitaxel. Br J Cancer. 2005; 92:1240-6.

Hamilton TC, Young RC, McKoy WM, Grotzinger KR, Green JA, Chu EW, Whang-Peng J, Rogan AM, Green WR, Ozols RF. Characterization of a human ovarian carcinoma cell line (NIH:OVCAR-3) with androgen and estrogen receptors. Cancer Res. 1983; 43):5379-89

Harrison SC. The familiar and the unexpected in structures of icosahedral viruses. Curr Opin Struct Biol. 2001; 11:195-9

Hattori Y, Maitani Y. Folate-linked lipid-based nanoparticle for targeted gene delivery. Curr Drug Deliv. 2005; 2:243-52

Henderson HI, Hope TJ. The temperature arrested intermediate of virus-cell fusion is a functional step in HIV infection. Virol J. 2006; 3:36.

Hermonat PL, Muzyczka N. Use of adeno-associated virus as a mammalian DNA cloning vector: transduction of neomycin resistance into mammalian tissue culture cells. Proc Natl Acad Sci U S A. 1984; 81:6466-70

Hiebert E, Bancroft JB, Bracker CE. The assembly in vitro of some small spherical viruses, hybrid viruses, and other nucleoproteins. Virology. 1968; 34:492-508

Hiebert E, Bancroft JB. Factors affecting the assembly of some spherical viruses. Virology. 1969; 39:296-311

Hooker JM, Kovacs EW, Francis MB. Interior Surface Modification of Bacteriophage MS2. J. Am. Chem. Soc. 2004; 126: 3718-9.

Huang M, Fong CW, Khor E, Lim LY. Transfection efficiency of chitosan vectors: effect of polymer molecular weight and degree of deacetylation. J Control Release. 2005; 106:391-406

Huang M, Khor E, Lim LY. Uptake and cytotoxicity of chitosan molecules and nanoparticles: effects of molecular weight and degree of deacetylation. Pharm Res. 2004; 21:344-53

Huang M, Koh DC, Weng LJ, Chang ML, Yap YK, Zhang L, Wong SM. Complete nucleotide sequence and genome organization of hibiscus chlorotic ringspot virus, a new member of the genus Carmovirus: evidence for the presence and expression of two novel open reading frames. J Virol. 2000; 74:3149-55

Ickenstein LM, Sandstrom MC, Mayer LD, Edwards K. Effects of phospholipid hydrolysis on the aggregate structure in DPPC/DSPE-PEG2000 liposome preparations after gel to liquid crystalline phase transition. Biochim Biophys Acta. 2006; 1758:171-80

Ishida T, Okada Y, Kobayashi T, Kiwada H. Development of pH-sensitive liposomes that efficiently retain encapsulated doxorubicin (DXR) in blood. Int J Pharm. 2006; 309:94-100.

Jain KK. Nanotechnology-based drug delivery for cancer. Technol Cancer Res Treat. 2005; 4:407-16

Jarvinen TA, Tanner M, Rantanen V, Barlund M, Borg A, Grenman S, Isola J. Amplification and deletion of topoisomerase IIalpha associate with ErbB-2 amplification

and affect sensitivity to topoisomerase II inhibitor doxorubicin in breast cancer. Am J Pathol. 2000; 156:839-47

Jiang W, Chang J, Jakana J, Weigele P, King J, Chiu W. Structure of epsilon15 bacteriophage reveals genome organization and DNA packaging/injection apparatus. Nature. 2006; 439:612-16

Johnson JE, Speir JA. Quasi-equivalent viruses: a paradigm for protein assemblies. J Mol Biol. 1997; 269:665-75

Johnson, J. Alternative agriculture: what is kenaf. Rural Enterprise Alternative Dev. Initiative Rep. 2001; 1:1-4.

Jorgensen JL. State of the Art Symposium: flow cytometry in the diagnosis of lymphoproliferative disorders by fine-needle aspiration. Cancer. 2005; 105:443-51

Kafri T, Blomer U, Peterson DA, Gage FH, Verma IM. Sustained expression of genes delivered directly into liver and muscle by lentiviral vectors. Nat Genet. 1997; 17:314-17

Kaklamani VG, Gradishar WJ. Adjuvant therapy of breast cancer. Minerva Ginecol. 2005; 57:521-36.

Kalra AV, Campbell RB. Development of 5-FU and Doxorubicin-Loaded Cationic Liposomes against Human Pancreatic Cancer: Implications for Tumor Vascular Targeting. Pharm Res. 2006; 23:2809-17

Kamen BA, Caston JD. Properties of a folate binding protein (FBP) isolated from porcine kidney. Biochem Pharmacol. 1986; 35:2323-9

Kaper, J.M. Alkaline degradation of turnip yellow mosaic virus. I. The controlled formation of empty protein shells. Biochemistry 1964; 3:486-93.

Ke J, Schmidt T, Chase E, Bozarth RF, Smith TJ. Structure of Cowpea mottle virus: a consensus in the genus Carmovirus. Virology. 2004; 321:349-58

Kearns WG, Afione SA, Fulmer SB, Pang MC, Erikson D, Egan M, Landrum MJ, Flotte TR, Cutting GR. Recombinant adeno-associated virus (AAV-CFTR) vectors do not integrate in a site-specific fashion in an immortalized epithelial cell line. Gene Ther. 1996; 3:748-55

Keldsen N, Havsteen H, Vergote I, Bertelsen K, Jakobsen A. Altretamine (hexamethylmelamine) in the treatment of platinum-resistant ovarian cancer: a phase II study. Gynecol Oncol. 2003; 88:118-22

Khor IW, Lin T, Langedijk JP, Johnson JE, Manchester M. Novel strategy for inhibiting viral entry by use of a cellular receptor-plant virus chimera. J Virol. 2002; 76:4412-19

Kim R, Yokota H, Kim SH. Electrophoresis of proteins and protein-protein complexes in a native agarose gel. Anal Biochem. 2000; 282:147-49

Kim SH, Jeong JH, Chun KW, Park TG. Target-specific cellular uptake of PLGA nanoparticles coated with poly(L-lysine)-poly(ethylene glycol)-folate conjugate. Langmuir. 2005; 21:8852-7.

Kleemann E, Neu M, Jekel N, Fink L, Schmehl T, Gessler T, Seeger W, Kissel T. Nano-carriers for DNA delivery to the lung based upon a TAT-derived peptide covalently coupled to PEG-PEI. J Control Release. 2005; 109:299-316

Klug A, Caspar DLD. The structure of simple viruses. Adv.Virus Res. 1960; 13:1-63.

Koh DC, Liu DX, Wong SM. A six-nucleotide segment within the 3' untranslated region of hibiscus chlorotic ringspot virus plays an essential role in translational enhancement. J Virol. 2002; 76:1144-53.

Kohler N, Sun C, Fichtenholtz A, Gunn J, Fang C, Zhang M. Methotrexate-immobilized poly(ethylene glycol) magnetic nanoparticles for MR imaging and drug delivery. Small. 2006; 2:785-92

Kosobe T, Moriyama E, Tokuoka Y, Kawashima N. Size and surface charge effect of 5-aminolevulinic acid-containing liposomes on photodynamic therapy for cultivated cancer cells. Drug Dev Ind Pharm. 2005; 31:623-9

Koukourakis MI, Romanidis K, Froudarakis M, Kyrgias G, Koukourakis GV, Retalis G, Bahlitzanakis N. Concurrent administration of Docetaxel and Stealth liposomal doxorubicin with radiotherapy in non-small cell lung cancer : excellent tolerance using subcutaneous amifostine for cytoprotection. Br J Cancer. 2002; 87:385-92

Lane HA, Motoyama AB, Beuvink I, Hynes NE. Modulation of p27/Cdk2 complex formation through 4D5-mediated inhibition of HER2 receptor signaling, Ann. Oncol. 2001; 12:21–22.

Langeveld JP, Brennan FR, Martinez-Torrecuadrada JL, Jones TD, Boshuizen RS, Vela C, Casal JI, Kamstrup S, Dalsgaard K, Meloen RH, Bendig MM, Hamilton WD. Inactivated recombinant plant virus protects dogs from a lethal challenge with canine parvovirus. Vaccine. 2001; 19:3661-70

Lasic DD, Frederik PM, Stuart MC, et al. Gelation of liposome interior: a novel method for drug encapsulation. FEBS Lett 1992; 312: 255-8

Lawley PD. Alkylation of DNA and its aftermath. Bioessays. 1995; 17:561-8.

Leamon CP, Low PS, Delivery of macromolecules into living cells: a method that exploits folate receptor endocytosis, Proc. Natl. Acad. Sci. USA 1991; 88:5572–6.

Lee CM, Choi Y, Huh EJ, Lee KY, Song HC, Sun MJ, Jeong HJ, Cho CS, Bom HS. Polyethylene glycol (PEG) modified 99mTc-HMPAO-liposome for improving blood circulation and biodistribution: the effect of the extent of PEGylation. Cancer Biother Radiopharm. 2005; 20:620-8

Lee KC, Lim D, Wong SM, Dokland T. Purification, crystallization and X-ray analysis of Hibiscus chlorotic ringspot virus. Acta Crystallogr D Biol Crystallogr. 2003; 59(Pt 8):1481-3

Lee RJ, Low PS. Folate-mediated tumor cell targeting of liposome-entrapped doxorubicin in vitro. Biochim Biophys Acta. 1995; 1233:134-44

Lee SC, Lee KE, Kim JJ, Lim SH. The effect of cholesterol in the liposome bilayer on the stabilization of incorporated Retinol. J Liposome Res. 2005; 15:157-66

LeimkuÈhler M. Druckinduzierte Decapsidation von Virionen and Dissoziation von Proteincapsiden des Turnip Yellow Mosaic Virus und des Brome Mosaic Virus, PhD Thesis, University of OsnabruÈck, Germany. 1994

Leodevico L. Ilag, Robert McKenna, Madhav P. Yadav, James N. BeMiller, Nino L. Incardona and Michael G. Rossmann. Calcium Ion-induced Structural Changes in Bacteriophage φ X174. J Mo.l Biol. 1994; 244:291-300

Li Z, Ren Y, Wu QC, Lin SX, Liang YJ, Liang HZ. Macrophage migration inhibitory factor enhances neoplastic cell invasion by inducing the expression of matrix

metalloproteinase 9 and interleukin-8 in nasopharyngeal carcinoma cell lines. Chin Med J (Engl). 2004; 117:107-14

Li Z, Zhao R, Wu X, Sun Y, Yao M, Li J, Xu Y, Gu J. Identification and characterization of a novel peptide ligand of epidermal growth factor receptor for targeted delivery of therapeutics. FASEB J. 2005; 19:1978-85.

Li WZ, Qu F, Morris TJ. Cell-to-cell movement of turnip crinkle virus is controlled by two small open reading frames that function in trans. Virology 1998; 244:405–16.

Liang XZ, Lucy AP, Ding SW, Wong SM. The p23 protein of hibiscus chlorotic ringspot virus is indispensable for host-specific replication. J Virol. 2002; 76:12312-9

Lico C, Capuano F, Renzone G, Donini M, Marusic C, Scaloni A, Benvenuto E, Baschieri S. Peptide display on Potato virus X: molecular features of the coat protein-fused peptide affecting cell-to-cell and phloem movement of chimeric virus particles. J Gen Virol. 2006; 87:3103-12

Lim SL, Lim LY. Effects of citrus fruit juices on cytotoxicity and drug transport pathways of Caco-2 cell monolayers. Int J Pharm. 2006; 307:42-50

Liu J, Lee H, Allen C. Formulation of drugs in block copolymer micelles: drug loading and release. Curr Pharm Des. 2006; 12:4685-701.

Liu SQ, Tong YW, Yang YY. Incorporation and in vitro release of doxorubicin in thermally sensitive micelles made from poly(N-isopropylacrylamide-co-N,N-dimethylacrylamide)-â-poly(D,L-lactide-co-glycolide) with varying compositions. Biomaterials 2005; 26, 5064-74.

Loo L, Guenther RH, Basnayake VR, Lommel SA, Franzen S. Controlled encapsidation of gold nanoparticles by a viral protein shell. J Am Chem Soc. 2006; 128:4502-3

Louz D, Bergmans HE, Loos BP, Hoeben RC. Cross-species transfer of viruses: implications for the use of viral vectors in biomedical research, gene therapy and as live-virus vaccines. J Gene Med. 2005; 7:1263-74

Lu Y, Low PS. Folate-mediated delivery of macromolecular anticancer therapeutic agents. Adv Drug Deliv Rev. 2002; 54:675-93

Luo Y, Chen D, Ren L, Zhao X, Qin J. Solid lipid nanoparticles for enhancing vinpocetine's oral bioavailability. J Control Release. 2006; 114(1):53-9

Ma Z, Lim TM, Lim LY. Pharmacological activity of peroral chitosan-insulin nanoparticles in diabetic rats. Int J Pharm. 2005; 293:271-80

Ma Z, Yeoh HH, Lim LY. Formulation pH modulates the interaction of insulin with chitosan nanoparticles. J Pharm Sci. 2002; 91:1396-404

Mach H, Middaugh CR, Lewis RV. Statistical determination of the average values of the extinction coefficients of tryptophan and tyrosine in native proteins, Anal. Biochem. 1992; 200:74-80.

Mah C, Byrne BJ, Flotte TR. Virus-based gene delivery systems. Clin Pharmacokinet. 2002; 41:901-11

Mamot C, Ritschard R, Kung W, Park JW, Herrmann R, Rochlitz CF. EGFR-targeted immunoliposomes derived from the monoclonal antibody EMD72000 mediate specific and efficient drug delivery to a variety of colorectal cancer cells. J Drug Target. 2006; 14:215-23

Markman M. Pegylated liposomal doxorubicin in the treatment of cancers of the breast and ovary. Expert Opin Pharmacother. 2006; 7:1469-74

Martens HJ, Roberts AG, Oparka KJ, Schulz A. Quantification of plasmodesmatal endoplasmic reticulum coupling between sieve elements and companion cells using fluorescence redistribution after photobleaching. Plant Physiol. 2006; 142:471-80

Maruyama K, Itoh Y, Arisaka F. Circular dichroism spectra show abundance of β-sheet structure in connectin, a muscle elastic protein FEBS Letters. 1986; 202: 353-5

Maruyama K, Itoh Y, Arisaka F. Circular dichroism spectra show abundance of beta-sheet structure in connectin, a muscle elastic protein. FEBS Lett. 1986; 202:353-5

McCormick AA, Corbo TA, Wykoff-Clary S, Nguyen LV, Smith ML, Palmer KE, Pogue GP. TMV-peptide fusion vaccines induce cell-mediated immune responses and tumor protection in two murine models. Vaccine. 2006; 24:6414-23

McPherson RM. Incidence of thrips and tomato spotted wilt Tospovirus in fluecured tobacco protected from early season insect pest infestations. J Econ Entomol. 2006; 99:764-70.

Michels B, Leimkuhler M, Lechner MD, Adrian M, Lorber B, Witz J. Polymorphism of turnip yellow mosaic virus empty shells and evidence for conformational changes occurring after release of the viral RNA. A differential scanning calorimetric study. Eur J Biochem. 1999; 264:965-972

Miller M, Kennewell A, Takayama Y, Bruskin A, Bishop JM, Johnson G, Symonds G. Transformation of early erythroid precursor cells (BFU-E) by a recombinant murine retrovirus containing v-erb-B. Oncogene. 1990; 5:1125-31

Mito N, Takimoto H, Umegaki K, Ishiwaki A, Kusama K, Fukuoka H, Ohta S, Abe S, Yamawaki M, Ishida H, Yoshiike N. Folate intakes and folate biomarker profiles of pregnant Japanese women in the first trimester. Eur J Clin Nutr. 2007; 61:83-90

Miyoshi H, Smith KA, Mosier DE, Verma IM, Torbett BE. Transduction of human CD34+ cells that mediate long-term engraftment of NOD/SCID mice by HIV vectors. Science. 1999; 283:682-6

Mo Y, Lim LY. b Paclitaxel-loaded PLGA nanoparticles: potentiation of anticancer activity by surface conjugation with wheat germ agglutinin. J Control Release. 2005; 108:244-62.

Mo Y, Lim LY. Preparation and in vitro anticancer activity of wheat germ agglutinin (WGA)-conjugated PLGA nanoparticles loaded with paclitaxel and isopropyl myristate. J Control Release. 2005; 107:30-42.

Morgunova EYu, Dauter Z, Fry E, Stuart DI, Stel'mashchuk VYa, Mikhailov AM, Wilson KS, Vainshtein BK. The atomic structure of Carnation Mottle Virus capsid protein. FEBS Lett. 1994; 338:267-71

Morris TJ, Carrington JC. The Plant Viruses, 1988; 3:73-112.

Mosmann T. Rapid colorimetric assay for cellular growth and survival: application to proliferation and cytotoxicity assays. J Immunol Methods. 1983; 65:55-63.

Mozafari MR. Liposomes: an overview of manufacturing techniques. Cell Mol Biol Lett. 2005; 10:711-9.

Muggia FM, Green MD. New anthracycline antitumor antibiotics. Crit Rev Oncol Hematol. 1991; 11:43-64

Mulder HS, Dekker H, Pinedo HM, Lankelma J. The P-glycoprotein-mediated relative decrease in cytosolic free drug concentration is similar for several anthracyclines with varying lipophilicity. Biochem Pharmacol. 1995; 50:967-74

Mutombo K, Michels B, Ott H, Cerf R, Witz J. The thermal stability and decapsidation of tymoviruses: a differential calorimetric study. Biochimie 1993; 75:667-74.

Naldini L, Blomer U, Gallay P, Ory D, Mulligan R, Gage FH, Verma IM, Trono D. In vivo gene delivery and stable transduction of nondividing cells by a lentiviral vector. Science. 1996; 272:263-7

Nasongkla N, Bey E, Ren J, Ai H, Khemtong C, Guthi JS, Chin SF, Sherry AD, Boothman DA, Gao J. Multifunctional polymeric micelles as cancer-targeted, MRI-ultrasensitive drug delivery systems. Nano Lett. 2006; 6:2427-30.

Newman M, F.M. Suk, M. Cajimat, P.K. Chua, C. Shih, Stability and morphology comparisons of self-assembled virus-like particles from wild-type and mutant human hepatitis B virus capsid proteins, J. Virol. 2003; 77:12950-60.

Nicholas BL, Brennan FR, Martinez-Torrecuadrada JL, Casal JI, Hamilton WD, Wakelin D. Characterization of the immune response to canine parvovirus induced by vaccination with chimaeric plant viruses. Vaccine 2002; 20:2727-34

Nichols WW , et al. Characterization of a new human diploid cell strain, IMR-90. Science 1977; 196: 60-3

O'Brien ME, Wigler N, Inbar M, Rosso R, Grischke E, Santoro A, Catane R, Kieback DG, Tomczak P, Ackland SP, Orlandi F, Mellars , Alland L, Tendler C; CAELYX Breast Cancer Study Group. Reduced cardiotoxicity and comparable efficacy in a phase III trial

of pegylated liposomal doxorubicin HCl (CAELYX/Doxil) versus conventional doxorubicin for first-line treatment of metastatic breast cancer. Ann Oncol. 2004;15:440-9.

Olson NH, Baker TS, Willingmann P, Incardona NL. The three-dimensional structure of frozen-hydrated bacteriophage phi X174. J Struct Biol. 1992; 108:168-75

Pacha RF, Ahlquist P. Substantial portions of the 5' and intercistronic noncoding regions of cowpea chlorotic mottle virus RNA3 are dispensable for systemic infection but influence viral competitiveness and infection pathology. Virology. 1992; 187:298-307

Pan XQ, Zheng X, Shi G, Wang H, Ratnam M, Lee RJ. Strategy for the treatment of acute myelogenous leukemia based on folate receptor beta-targeted liposomal doxorubicin combined with receptor induction using all-trans retinoic acid. Blood. 2002; 100:594-602

Panyam J, Labhasetwar V. Biodegradable nanoparticles for drug and gene delivery to cells and tissue. Adv drug deliv Rev. 2003; 55:329-47

Papahadjopoulos D, Allen TM, Gabizon A, et al. Sterically lipostabilized liposomes: improvements in pharmacokinetics and antitumor therapeutic efficacy. Proc Natl Acad Sci U S A 1991; 88: 11460-4

Park SH, Oh SG, Mun JY, Han SS. Loading of gold nanoparticles inside the DPPC bilayers of liposome and their effects on membrane fluidities. Colloids Surf B Biointerfaces. 2006; 48:112-8

Patrick TA, Kranz DM, van Dyke TA, Roy EJ. Folate receptors as potential therapeutic targets in choroid plexus tumors of SV40 transgenic mice. J Neurooncol. 1997 32:111-23

Peiris JS, Lai ST, Poon LL, Guan Y, Yam LY, LimW, Nicholls J, Yee WK, YanWW, Cheung MT, Cheng VC, Chan KH, Tsang DN, Yung RW, Ng TK, Yuen KY. Coronavirus as a possible cause of severe acute respiratory syndrome. Lancet 2003; 361:1319–25.

Perez J, Defrenne S, Witz J, Vachette P. Detection and characterization of an intermediate conformation during the divalent ion-dependent swelling of tomato bushy stunt virus. Cell Mol Biol (Noisy-le-grand). 2000; 46:937-48.

Poeschla E, Gilbert J, Li X, Huang S, Ho A, Wong-Staal F. Identification of a human immunodeficiency virus type 2 (HIV-2) encapsidation determinant and transduction of nondividing human cells by HIV-2-based lentivirus vectors. J Virol. 1998; 72:6527-36.

Quintanar-Guerrero D, Allemann E, Doelker E, Fessi H. Preparation and characterization of nanocapsules from preformed polymers by a new process based on emulsification-diffusion technique. Pharm Res. 1998; 15:1056-62

Rae CS, Khor IW, Wang Q, Destito G, Gonzalez MJ, Singh P, Thomas DM., Estrada MN, Powell E, Finn MG, Manchester M. Systemic trafficking of plant virus nanoparticles in mice via the oral route. Virology 2005; 343:224-35.

Raja KS, Wang Q, Gonzalez MJ, Manchester M, Johnson JE, Finn MG. Hybrid virus-polymer materials. 1. Synthesis and properties of PEG-decorated cowpea mosaic virus. Biomacromolecules. 2003; 4:472-6

Reddy JA, Clapp DW, Low PS. Retargeting of viral vectors to the folate receptor endocytic pathway J Control Release. 2001; 74:77-82

Ren Y, Wei D. Quantification intracellular levels of oligodeoxynucleotide-doxorubicin conjugate in human carcinoma cells in situ. J Pharm Biomed Anal. 2004; 36:387-91

Rivera E. Liposomal anthracyclines in metastatic breast cancer: clinical update. Oncologist. 2003; 8 Suppl 2:3-9

Riviere CJ, Rochon DM. Nucleotide sequence and genomic organization of melon necrotic spot virus. J Gen Virol. 1990; 71:1887-96

Robinson JP. Principles of confocal microscopy. Methods Cell Biol. 2001;63:89-106.

Rose PG. Pegylated liposomal doxorubicin: optimizing the dosing schedule in ovarian cancer. Oncologist. 2005; 10:205-14

Ross JF, Chaudhuri PK, Ratnam M, Differential regulation of folate receptor isoforms in normal and malignant tissues in vivo and in established cell lines. Physiologic and clinical implications, Cancer 1994; 73: 2432–43.

Rouse RJ, Seifried W, Mistry SK, Goins WF, Glorioso JC. Herpes simplex virus-enhanced cationic lipid/DNA-mediated transfection. Biotechniques. 2000; 29:810-4

Saul JM, Annapragada A, Natarajan JV, Bellamkonda RV. Co ntrolled targeting of liposomal doxorubicin via the folate receptor in vitro. J Control Release. 2003; 92:49-67

Scharfmann R, Axelrod JH, Verma IM. Long-term in vivo expression of retrovirus-mediated gene transfer in mouse fibroblast implants. Proc Natl Acad Sci U S A. 1991; 88:4626-30.

Schettini DA, Ribeiro RR, Demicheli C, Rocha OG, Melo MN, Michalick MS, Frezard F. Improved targeting of antimony to the bone marrow of dogs using liposomes of reduced size. Int J Pharm. 2006; 315:140-7

Schlick TL, Ding Z, Kovacs EW, Francis MB. Dual-surface modification of the tobacco mosaic virus. J. Am. Chem. Soc. 2005; 127: 3718-3723.

Scholthof HB. Plant virus transport: motions of functional equivalence. Trends Plant Sci. 2005; 10:376-82

Schriber J.Treatment of aggressive non-Hodgkin's lymphoma with chemotherapy in combination with filgrastim. Drugs. 2002; 62 Suppl 1:33-46

Schwartz MD, Peshkin BN, Tercyak KP, Taylor KL, Valdimarsdottir H. Decision making and decision support for hereditary breast-ovarian cancer susceptibility. Health Psychol. 2005; 24:S78-84.

Schwede T, Kopp J, Guex N, and Peitsch MC. SWISS-MODEL: an automated protein homology-modeling server. Nucleic Acids Research 2003; 31:3381-5.

Seki J, Sasaki H, Doi M, Yoshikawa H, Takahashi Y, Yamane S, Fukui H, Sonoke S, Yamamoto H, Hirose M, Ezure Y, Ando T, Ushimaru K, Sugiyama M. Lipid Nano-Sphere(LNS), a protein-free analogue of lipoproteins, as a novel drug carrier for parenteral administration. IV. J. Control. Release. 1994; 28:352-3

Shadwick FS, Doran PM. Propagation of plant viruses in hairy root cultures: A potential method for in vitro production of epitope vaccines and foreign proteins. Biotechnol Bioeng. 2007; 96:570-83

Shen F, Ross JF, Wang X, Ratnam M. Identification of a novel folate receptor, a truncated receptor, and receptor type beta in hematopoietic cells: cDNA cloning, expression, immunoreactivity, and tissue specificity. Biochemistry. 1994;33:1209-15

Shen F, Wu M, Ross JF, Miller D, Ratnam M. Folate receptor type gamma is primarily a secretory protein due to lack of an efficient signal for glycosylphosphatidylinositol modification: protein characterization and cell type specificity. Biochemistry. 1995; 34:5660-5.

Shinoda T, Takagi A, Maeda A, Kagatani S, Konno Y, Hashida M. In vivo fate of folate-BSA in non-tumor- and tumor-bearing mice. J. Pharm. Sci. 1998; 87:1521-6.

Shiokawa T, Hattori Y, Kawano K, Ohguchi Y, Kawakami H, Toma K, Maitani Y. Effect of polyethylene glycol linker chain length of folate-linked microemulsions loading aclacinomycin A on targeting ability and antitumor effect in vitro and in vivo. Clin Cancer Res. 2005;11:2018-25

Shirley BA. Urea and guanidine hydrochloride denaturation curves. Methods Mol Biol. 1995; 40:177-90

Skotnicki ML, Mackenzie AM, Torronen M, Gibbs AJ. The genomic sequence of cardamine chlorotic fleck carmovirus. J Gen Virol. 1993; 74:1933-7

Sloat BR, Cui Z. Strong mucosal and systemic immunities induced by nasal immunization with anthrax protective antigen protein incorporated in liposome-protamine-DNA particles. Pharm Res. 2006; 23:262-9

Smith JA, Ngo H, Martin MC, Wolf JK. An evaluation of cytotoxicity of the taxane and platinum agents combination treatment in a panel of human ovarian carcinoma cell lines. Gynecol Oncol. 2005; 98:141-5

Smith PK, Krohn RI, Hermanson GT, Mallia AK, Gartner FH, Provenzano MD, Fujimoto EK, Goek, NM, Olson BJ, Klenk DC. Measurement of protein using bicinchoninic acid. *Anal. Biochem.* 1985; *150:*76-85.

Sorger PK, Stockley PG, Harrison SC. Structure and assembly of turnip crinkle virus. II. Mechanism of reassembly in vitro. J Mol Biol. 1986; 191:639-58

Soto CM, Blum AS, Wilson CD, Lazorcik J, Kim M, Gnade B, Ratna BR. Separation and recovery of intact gold-virus complex by agarose electrophoresis and electroelution: application to the purification of cowpea mosaic virus and colloidal gold complex. Electrophoresis. 2004; 25:2901-6

Speir JA, Munshi S, Wang G, Baker TS, Johnson JE. Structures of the native and swollen forms of cowpea chlorotic mottle virus determined by X-ray crystallography and cryo-electron microscopy. Structure. 1995; 3:63-78.

St George JA. Gene therapy progress and prospects: adenoviral vectors. Gene Ther. 2003;10:1135-41

Staczek J, Bendahmane M, Gilleland LB, Beachy RN, Gilleland HE Jr. Immunization with a chimeric tobacco mosaic virus containing an epitope of outer membrane protein F of Pseudomonas aeruginosa provides protection against challenge with P. aeruginosa. Vaccine. 2000; 18:2266-74

Stanger O. Physiology of folic acid in health and disease. Curr Drug Metab. 2002; 3:211-23

Staros JV, Wright RW, Swingle DM. Enhancement by N-hydroxysulfosuccinimide of water-soluble carbodiimide-mediated coupling reactions. Anal Biochem. 1986; 156:220-2.

Stella B, Arpicco S, Peracchia MT, Desmaele D, Hoebeke J, Renoir M, D'Angelo J, Cattel L. Couvreur P. Design of folic acid-conjugated nanoparticles for drug targeting. J. Pharm. Sci. 2000; 89:1452-64.

Sun DS, Chen JH, Ling R, Yao Q, Wang L, Ma Z, Li Y. Treatment of hepatoma with liposome-encapsulated adriamycin administered into hepatic artery of rats. World J Gastroenterol. 2006; 12:4741-4

Swift LP, Rephaeli A, Nudelman A, Phillips DR, Cutts SM. Doxorubicin-DNA adducts induce a non-topoisomerase II-mediated form of cell death. Cancer Res. 2006; 66:4863-71

Szabo I, Maguire MH. On-line recognition and quantitation of coeluting hypoxanthine and guanine in reversed-phase high-performance liquid chromatography of placental tissue extracts: photodiode-array detection and spectral analysis of coeluting peaks, Anal. Biochem. 1993; 215:253-60.

Szakonyi G, Klein MG, Hannan JP, Young KA, Ma RZ, Asokan R, Holers VM, Chen XS. Structure of the Epstein-Barr virus major envelope glycoprotein. Nat Struct Mol Biol. 2006; 13:996-1001

Szoka F.Jr. and Papahadjopoulos, D. Procedure for preparation of liposomes with large internal aqueous space and high capture by reverse-phase evaporation. Proc. Natl. Acad. Sci. U.S.A. 1978; 75:4194-8.

Takemoto Y, Kanehira T, Shinohara M, Yamashita S, Hibi T. The nucleotide sequence and genome organization of Japanese iris necrotic ring virus, a new species in the genus Carmovirus. Arch Virol. 2000; 145:651-7

Tama F, Brooks CL III. The mechanism and pathway of pH induced swelling in cowpea chlorotic mottle virus. J Mol Biol 2002; 318:733–47.

Temmink OH, de Bruin M, Turksma AW, Cricca S, Laan AC, Peters GJ. Activity and substrate specificity of pyrimidine phosphorylases and their role in fluoropyrimidine sensitivity in colon cancer cell lines. Int J Biochem Cell Biol. 2007; 39:565-75

Thomasset N. Use of MTT colorimetric assay to measure cell activation. J Immunol Methods. 1986; 94:57-63

Toffoli G, Cernigoi C, Russo A, Gallo A, Bagnoli M, Boiocchi M. Overexpression of folate binding protein in ovarian cancers. Int. J. Cancer 1997; 74:193-8.

Toffoli G, Russo A, Gallo A, Cernigoi C, Miotti S, Sorio R, Tumolo S, Boiocchi M. Expression of folate binding protein as a prognostic factor for response to platinum-containing chemotherapy and survival in human ovarian cancer. Int J Cancer. 1998; 79:121-6

Tomii Y. Lipid formulation as a drug carrier for drug delivery. Curr Pharm Des. 2002; 8:467-74

Torabian SZ, Fazel N, Knuttle R. Necrobiotic xanthogranuloma treated with chlorambucil. Dermatol Online J. 2006; 12:11.

van Steenis JH, van Maarseveen EM, Verbaan FJ, Verrijk R, Crommelin DJ, Storm G, Hennink WE. Preparation and characterization of folate-targeted pEG-coated pDMAEMA-based polyplexes. J Control Release. 2003; 87:167-76.

Veldman RJ, Koning GA, van Hell A, Zerp S, Vink SR, Storm G, Verheij M, van Blitterswijk WJ. Coformulated N-octanoyl-glucosylceramide improves cellular delivery and cytotoxicity of liposomal doxorubicin. J Pharmacol Exp Ther. 2005; 315:704-10

Vergnenegre A, Daniel C, Lena H, Fournel P, Kleisbauer JP, Le Caer H, Letreut J, Paillotin D, Perol M, Bouchaert E, Preux PM, Robinet G; Groupe Francais de Pneumo-Cancerologie. Docetaxel and concurrent radiotherapy after two cycles of induction chemotherapy with cisplatin and vinorelbine in patients with locally advanced non-small-cell lung cancer. A phase II trial conducted by the Groupe Francais de Pneumo-Cancerologie (GFPC). Lung Cancer. 2005; 47:395-404

Villella JA, Cohen S, Smith DH, Hibshoosh H, Hershman D. HER-2/neu overexpression in uterine papillary serous cancers and its possible therapeutic implications. Int J Gynecol Cancer. 2006; 16:1897-902

Vogel CL, Cobleigh MA, Tripathy D, Gutheil JC, Harris LN, Fehrenbacher L, Slamon DJ, Murphy M, Novotny WF, Burchmore M, Shak S, Stewart SJ, Press M. Efficacy and safety of trastuzumab as a single agent in first-line treatment of HER2-overexpressing metastatic breast cancer. J Clin Oncol 2002; 20:719–726

Waelti E, Wegmann N, Schwaninger R, Wetterwald A, Wingenfeld C, Rothen-Rutishauser B, Gimmi CD: Targeting her-2/neu with antirat Neu virosomes for cancer therapy. Cancer Res 2002; 62:437-44.

Walters K. Modelling the probability distribution of the number of DNA double-strand breaks due to sporadic alkylation of nucleotide bases. J Theor Biol. 2007; 245:161-8

Wang Q, Lin T, Tang L, Johnson JE, Finn MG. Icosahedral Virus Particles as Addressable Nanoscale Building Blocks. Angew Chem 2002; 41:459-62

Waterworth HE, Lawson RH, Monroe RL. Purification and properties of hibiscus chlorotic ringspot virus. Phytopathology 1976; 64: 570-75.

Wei H, Zhang XZ, Cheng H, Chen WQ, Cheng SX, Zhuo RX. Self-assembled thermo- and pH responsive micelles of poly(10-undecenoic acid-b-N-isopropylacrylamide) for drug delivery. J Control Release. 2006; 116:266-74

Weitman SD, Weinberg AG, Coney LR, Zurawski VR, Jennings DS, Kamen BA. Cellular localization of the folate receptor: potential role in drug toxicity and folate homeostasis. Cancer Res. 1992; 52:6708-11

Wellink J, van Lent JW, Verver J, Sijen T, Goldbach RW, van Kammen A. The cowpea mosaic virus M RNA-encoded 48-kilodalton protein is responsible for induction of tubular structures in protoplasts. J Virol. 1993;67:3660-64

Weng Z, Xiong Z. Genome organization and gene expression of saguaro cactus carmovirus. J Gen Virol. 1997; 78:525-34

Westerfeld N, Pluschke G, Zurbriggen R. Optimized Malaria-antigens delivered by immunostimulating reconstituted influenza virosomes. Wien Klin Wochenschr. 2006; 118 Supplement 3:50-57

Wilschut J, Duzgunes N, Hoekstra D, Papahadjopoulos D. Modulation of membrane fusion by membrane fluidity: temperature dependence of divalent cation induced fusion of phosphatidylserine vesicles. Biochemistry. 1985; 24:8-14

Wolf S, Deom CM, Beachy RN, Lucas WJ. Movement protein of tobacco mosaic virus modi¢es plasmodesmatal size exclusion limit. Science 1989; 246:377-9

Wong HL, Rauth AM, Bendayan R, Manias JL, Ramaswamy M, Liu Z, Erhan SZ, Wu XY. A new polymer-lipid hybrid nanoparticle system increases cytotoxicity of Doxorubicin against multidrug-resistant human breast cancer cells. Pharm Res. 2006; 23:1574-85

Wong SM, Chng CG. Occurrence of hibiscus chlorotic ringspot virus in Singapore. Phytopathology 1992; 82:722.

Wu J, Xiao X, Zhao P, Xue G, Zhu Y, Zhu X, Zheng L, Zeng Y, Huang W. Minicircle-IFNgamma induces antiproliferative and antitumoral effects in human nasopharyngeal carcinoma. Clin Cancer Res. 2006;12:4702-4713

Wujcik D. Current research in side effects of high-dose chemotherapy. Semin Oncol Nurs. 1992; 8:102-12.

Xiangyang X, Ling L, Jianping Z, Shiyue L, Jie Y, Xiaojin Y, Jinsheng R. Preparation and characterization of N-succinyl-N'-octyl chitosan micelles as doxorubicin carriers for effective anti-tumor activity. Colloids Surf B Biointerfaces. 2007; 55:222-8

Xiong XB, Huang Y, Lu WL, Zhang X, Zhang H, Nagai T, Zhang Q. Enhanced intracellular delivery and improved antitumor efficacy of doxorubicin by sterically

stabilized liposomes modified with a synthetic RGD mimetic. J Control Release. 2005; 107:262-75

Xu P, Van Kirk EA, Li S, Murdoch WJ, Ren J, Hussain MD, Radosz M, Shen Y. Highly stable core-surface-crosslinked nanoparticles as cisplatin carriers for cancer chemotherapy. Colloids Surf B Biointerfaces. 2006; 48:50-7.

Xu X, Persson HL, Richardson DR. Molecular pharmacology of the interaction of anthracyclines with iron. Mol Pharmacol. 2005; 68:261-71

Yang F, Niu Q, Lan Q, Sun D. Effect of dispersion pH on the formation and stability of Pickering emulsions stabilized by layered double hydroxides particles. J Colloid Interface Sci. 2007; 306:285-95

Yang L, Li J, Zhou W, Yuan X, Li S. Targeted delivery of antisense oligodeoxynucleotides to folate receptor-overexpressing tumor cells. J Control Release. 2004; 95:321-31

Zamboni WC. Liposomal, nanoparticle, and conjugated formulations of anticancer agents. Clin Cancer Res. 2005; 11:8230-8234

Zhang HG, Wang YM, Xie JF, Liang X, Hsu HC, Zhang X, Douglas J, Curiel DT, Mountz JD. Recombinant adenovirus expressing adeno-associated virus cap and rep proteins supports production of high-titer recombinant adeno-associated virus. Gene Ther. 2001; 8:704-12

Zhang L, Hou S, Mao S, Wei D, Song X, Lu Y. Uptake of folate-conjugated albumin nanoparticles to the SKOV3 cells. Int J Pharm. 2004; 287:155-62.

Zhang L, Hou S, Mao S, Wei D, Song X, Lu Y. Uptake of folate-conjugated albumin nanoparticles to the SKOV3 cells. *Int. J. Pharm.* 2004; *287:*155-62.

Zhang X, Godbey WT. Viral vectors for gene delivery in tissue engineering. Adv Drug Deliv Rev. 2006; 58:515-34

Zhang YJ, Yang WZ, Liu XF, Tang JH, Chang WK, Yin WB. Radiobiological effects of fast neutron/photon mixed irradiation on nasopharyngeal cancer cell line CNE-1 Zhonghua Zhong Liu Za Zhi. 2005; 27:408-11

Zhao X, Fox JM, Olson NH, Baker TS, Young MJ. In vitro assembly of cowpea chlorotic mottle virus from coat protein expressed in Escherichia coli and in vitro-transcribed viral cDNA. Virology. 1995; 207:486-94

Zhou T, Fan ZF, Li HF, Wong SM. Hibiscus chlorotic ringspot virus p27 and its isoforms affect symptom expression and potentiate virus movement in kenaf (Hibiscus cannabinus L.). Mol Plant Microbe Interact. 2006; 19:948-57.

Zhu P, Liu J, Bess J Jr, Chertova E, Lifson JD, Grise H, Ofek GA, Taylor KA, Roux KH. Distribution and three-dimensional structure of AIDS virus envelope spikes. Nature. 2006; 441:847-52

Chapter 9

Appendices

Appendix I. BCA calibration curve produced using CP.

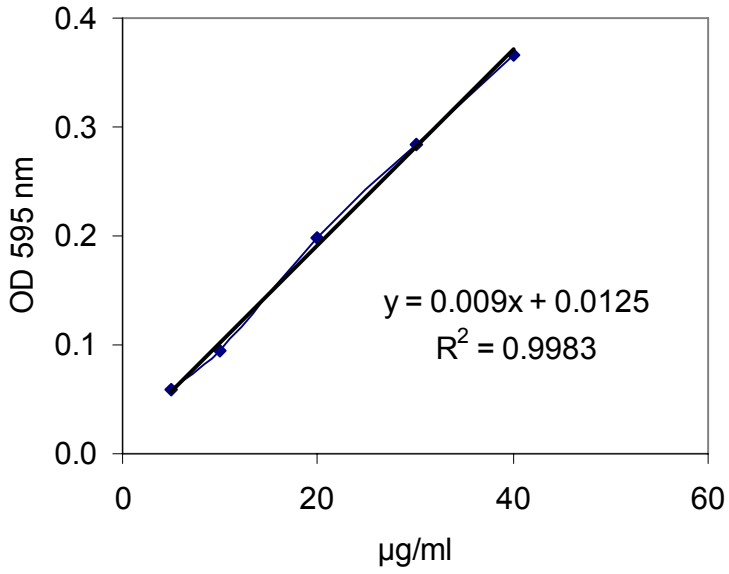

Appendix II. Sucrose gradient centrifugation analysis of pre-reassembled PC incubated with PSA (13–990 kDa) (a) or PAA (450 kDa) (b).

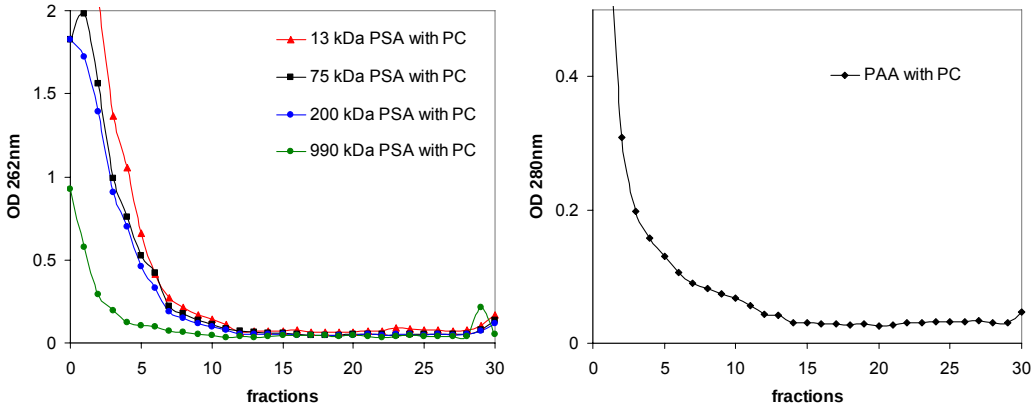

(a) (b)

Appendix III. Cytotoxicity of 100 µg/ml 200 kDa PSA to three cell lines (n = 8)